EXPERIMENTAL ANALYSIS OF ADSORPTION CAPACITIES AND BEHAVIORS OF SHALE SAMPLES

A THESIS SUBMITTED TO
THE GRADUATE SCHOOL OF NATURAL AND APPLIED SCIENCES
OF
MIDDLE EAST TECHNICAL UNIVERSITY

BY

ŞÜKRÜ MEREY

IN PARTIAL FULFILLMENT OF THE REQUIREMENTS
FOR
THE DEGREE OF MASTER OF SCIENCE
IN
PETROLEUM AND NATURAL GAS ENGINEERING

AUGUST 2013

Approval of the thesis

EXPERIMENTAL ANALYSIS OF ADSORPTION CAPACITIES AND BEHAVIORS OF SHALE SAMPLES

submitted by **ŞÜKRÜ MEREY** in partial fulfillment of the requirements for the degree of **Master of Science in Petroleum and Natural Gas Engineering Department, Middle East Technical University** by,

Prof. Dr. Canan Özgen
Dean, Graduate School of **Natural and Applied Sciences**

Prof. Dr. Mahmut Parlaktuna
Head of Department, **Petroleum and Natural Gas Engineering**

Asst. Prof. Dr. Çağlar Sınayuç
Supervisor, **Petroleum and Natural Gas Eng. Dept., METU**

Examining Committee Members

Prof. Dr. Mahmut Parlaktuna
Petroleum and Natural Gas Engineering Dept., METU

Asst. Prof. Dr. Çağlar Sınayuç
Petroleum and Natural Gas Engineering Dept., METU

Prof.Dr.Nurkan Karahanoğlu
Geological Engineering Dept., METU

Asst.Prof.Dr.İsmail Durgut
Petroleum and Natural Gas Engineering Dept., METU

Dr. Sevtaç Bülbül
METU Petroleum Research Center

Date: 05.08.2013

I hereby declare that all information in this document has been obtained and presented in accordance with academic rules and ethical conduct. I also declare that, as required by these rules and conduct, I have fully cited and referenced all material and results that are not original to this work.

Name, Last name: Şükrü MEREY

Signature:

ABSTRACT

EXPERIMENTAL ANALYSIS OF ADSORPTION CAPACITIES AND BEHAVIORS OF SHALE SAMPLES

Merey, Şükrü
M.Sc., Department of Petroleum and Natural Gas Engineering
Supervisor: Asst. Prof. Dr. Çağlar Sınayuç

August 2013, 173 pages

In recent years, unconventional reserves such as shale gas reservoirs have become a major alternative source of energy in the world. It is known that Turkey has shale gas potentials especially in the Southeastern and Thrace region.

In shale gas reservoirs, significant amounts of natural gas exist as conventional “free” gas in porous spaces as well as “adsorbed” gas on shale matrix. Understanding adsorption capacities and behaviors of shale gas reservoirs may help exploitation and resource evaluation.

In this study, experimental adsorption measurements for shale samples obtained from different shale gas reservoirs in Turkey were conducted at various pressures and temperatures by using pure methane and pure carbon dioxide. It was shown that the effects of temperature and pressure on adsorption are very important.

Matlab programs for Ono-Kondo monolayer model, Ono-Kondo three layer model and Ono-Kondo model for binary mixtures of methane and carbon dioxide were written in this study. By using Langmuir model and Matlab programs for Ono-Kondo models, experimental adsorption results were evaluated and adsorption isotherms were constructed. The advantages and disadvantages of these models were compared. It was concluded that Ono-Kondo monolayer model is thoroughly capable to fit adsorption isotherms of shale samples. By using Ono-Kondo monolayer model data, absolute adsorption values were calculated for all adsorption experiments.

By conducting carbon dioxide adsorption experiments on shale samples in this study, it was shown that carbon dioxide might be stored in depleted shale gas reservoirs.

In this study, initial shale gas-in place equation that uses Langmuir model were modified for Ono-Kondo monolayer model, and then initial-gas in place calculations for unit weight of shale deposits were done. It was shown that shale gas-in place equation proposed in this study is a good alternative for most accurate shale gas-in place calculations.

Keywords: Adsorption, methane adsorption, carbon dioxide adsorption, shale gas-in place calculations

ÖZ

ŞEYL ÖRNEKLERİNİN ADSORPSİYON KAPASİTELERİNİN VE DAVRANIŞLARININ DENEYSEL OLARAK ANALİZ EDİLMESİ

Merey, Şükrü
Yüksek Lisans, Petrol ve Doğal Gaz Mühendisliği Bölümü
Tez Yöneticisi: Yard. Doç. Dr. Çağlar Sınayuç

Ağustos 2013, 173 sayfa

Son yıllarda şeyl gaz rezervleri gibi alışılmadık rezervler dünyada önemli alternatif enerji kaynağı olmuştur. Türkiye’de özellikle Güneydoğu Anadolu ve Trakya bölgelerinde şeyl gaz rezerv potansiyeli olduğu bilinmektedir.

Şeyl rezervlerinde gaz gözeneklerde serbest ve adsorbe edilmiş şekilde bulunmaktadır. Şeyl gaz rezervlerinin adsorpsiyon kapasiteleri ve davranışları, bu rezervlerin araştırılması ve değerlendirilmesi için oldukça önemlidir.

Bu çalışmada, Türkiye’deki şeyl örneklerinin farklı sıcaklık ve basınçlarda adsorpsiyon kapasiteleri saf metan ve saf karbondioksit kulllanılarak ölçülmüştür. Sıcaklık ve basıncın adsorpsiyon üzerinde önemli etkileri olduğu gözlenmiştir.

Bu çalışmada tek katmanlı Ono-Kondo modeli için, üç katmanlı Ono-Kondo modeli için ve metan ve karbondioksit karışım Ono-Kondo modeli için Matlab programları yazılmıştır. Adsorpsiyon deney sonuçları Langmuir modeli ve Ono-Kondo modelleri ile analiz edilmiştir ve adsorpsiyon izotermleri elde edilmiştir. Bu modellerin olumlu ve olumsuz yönleri karşılaştırılmıştır. Tek katmanlı Ono-Kondo modeli ile şeyl örnekleri için iyi bir şekilde adsorpsiyon izotermleri oluşturulmuştur. Tek katmanlı Ono-Kondo model verileri kullanılarak net adsorpsiyon değerleri tüm deneyler için hesaplanmıştır.

Bu çalışmadaki şeyl örnekleri ile yapılan karbondioksit deney sonuçları kullanılarak şeyl gaz rezervlerinin karbondioksit depolama amacıyla kullanılabileceği sonucuna varılmıştır.

Bu çalışmada Langmuir modeli ile hesaplanan yerinde şeyl gaz rezerv denklemi, tek katmanlı Ono-Kondo modeli için uyarlanmıştır ve rezerv hesaplamaları yapılmıştır. Bu çalışmada kullanılan yerinde şeyl gaz rezerv denkleminin daha net rezerv çalışmaları için iyi bir alternatif olduğu gösterilmiştir.

Anahtar Kelimeler: Adsorpsiyon, metan adsorpsiyonu, karbondioksit adsorpsiyonu, şeyl gaz yerinde rezerv hesaplamaları

ACKNOWLEDGEMENTS

I would like to acknowledge and express my sincere gratitude to my thesis advisor Asst. Prof.Dr.Çağlar Sınayuç for his support, encouragement, advice, interesting conversations and supervision throughout the study. Without his invaluable insights, this study would not have been accomplished.

I would like to thank Prof.Dr.Mahmut Parlaktuna, the chairperson of Department of Petroleum and Natural Gas Engineering, for his supports during this study. I would also like to thank my thesis committee members for their valuable suggestions, comments and contributions.

I would like to thank Asst.Prof.Dr. Sayeed Ahmed Mohammad from School of Chemical Engineering, Oklahoma State University. Without his articles and invaluable suggestions, this study would not have been accomplished.

I would like to express my sincere thanks to Uğur Karabakal from TPAO Research Center for his support throughout the study.

I also wish to thank Emre Özgür and Oytun Örs for their helps during this study. I also want to thank my coworkers for their friendship.

I would like to thank technical staff of the department, namely; Naci Doğru and Murat Çalışkan for their help during the experiments.

Finally, I would like to extend my sincere thanks to my wife Ayşe and my family for their patience, understanding, and support during the long course of my graduate program.

This study was supported by Faculty Development Program (ÖYP - Batman University) and the Scientific and Technological Research Council of Turkey (TÜBİTAK) under National Scholarship Programme for MSc Students.

TABLE OF CONTENTS

CHAPTERS

APPENDICES

LIST OF TABLES

TABLES

LIST OF FIGURES

FIGURES

CHAPTER 1

INTRODUCTION

1.1 General Background

In recent years, natural gas has become an important energy source in the world because of its abundance and less pollution. Natural gas is composed of methane, ethane, propane, nitrogen, hydrogen sulfide, etc., but it is mostly composed of methane (87-96 mole percent). Moreover, its heating value is 50.1 MJ/kg, which is higher than other hydrocarbon fuels (Kumar, 2011).

Due to its abundance, less pollution and high heating value, natural gas is commonly used for house heating, industry, and production of electricity. However, conventional natural gas reserves in the world are not limitless. In Table 1.1, it is shown that the total amount of recoverable conventional natural gas is around 421 trillion cubic meters. However, the amount of these reserves has been declining with the high amount of natural gas consumption (EIA, 2011, Annual Energy Outlook).

Recently, unconventional natural gas reserves such as shale gas reservoirs have been considered as alternative natural gas sources. In the past, production of natural gas from shale gas reservoirs was not feasible because of extremely low permeability and low porosity values. However, with huge amount of natural gas consumption of conventional reserves, natural gas price has increased recently. Increased natural gas prices and advancement of technology have triggered production of natural gas from unconventional natural gas reservoirs such as shale gas, tight gas and coal-bed methane reserves (Sunjay and Kothari, 2011).

As seen in Table 1.1, the amount of recoverable shale gas in the world is around 208 trillion cubic meters (tcm), which is very high compared to other unconventional natural gas reservoirs. Hence, the world has focused on shale gas reservoirs (EIA, 2011, Annual Energy Outlook).

Table 1.1: Remaining technically recoverable natural gas resources by type and region, end 2011 (tcm) (EIA Analysis)

	Total		**Unconventional**		
	Conventional	*Unconventional*	*Tight Gas*	*Shale Gas*	*Coalbed Methane*
E.Europe/Eurasia	131	43	10	12	20
Middle East	125	12	8	4	-
Asia/Pacific	35	93	20	57	16
OECD Americas	45	77	12	56	9
Africa	37	37	7	30	0
Latin America	23	48	15	33	-
OECD Europe	24	21	3	16	2
World	**421**	**331**	**76**	**208**	**47**

As seen in Table 1.1, the amount of shale gas reservoirs is crucial to supply the world's natural gas demand in future. However, gas production from these reserves are quite difficult because of their low porosity and extremely low permeability values (Boyer *et al.*, 2011). With the advancement of technology in hydraulic fracturing and horizontal drilling, feasible gas production is possible from these reservoirs. These technologies are commonly used in USA recently. According to EIA (2011), USA shale gas production was 4.87 trillion cubic feet in 2010, which was 23 % of USA dry gas production. After successful applications about shale gas production in USA, many countries such as China, Turkey, etc. and companies have focused on the exploration and research activities about shale gas reservoirs.

For exploration and research activities about shale gas reservoirs, it is important to understand production mechanism and to determine initial gas in place. Contrary to conventional reservoirs, gas in shale reservoirs is stored as both free gas and adsorbed gas (Lu and Watson, 1993). Adsorption capacities of shale gas reservoirs range from 20 % to 85 % (Lancaster *et al.*, 1993). Hence, initial gas-in place calculations for conventional reserves cannot be used for shale gas reserves. Moreover, their gas production mechanism is quite different from conventional gas reserves. For this purpose, adsorption experiments were conducted in this study by using pure methane and pure carbon dioxide on shale samples at different temperatures.

The accumulation of gas molecules at the surface of a solid rather than in the bulk is called adsorption (Do, 1998). In order to determine adsorption in shale gas reservoirs, experimental study is necessary. Sudibandriyo *et al.* (2003), Mohammad *et al.* (2009) and Chareonsuppanimit *et al.* (2012) used volumetric method to measure adsorption. In this study, volumetric method was also preferred because it is cheap and practical. Volumetric method is based on molar balance principle and requires precise measurements of pressure, volume and temperature in both sample cell and reference cell.

Adsorption experiments on shale samples for pure methane and pure carbon dioxide in this study were conducted on shale samples at 25, 50 and 75 ^{o}C. Then, adsorption isotherms were constructed for each experiment. Isotherm is commonly used to present adsorption equilibrium. It is a plot of adsorption capacity versus adsorption equilibrium pressure at a constant temperature (Do, 1998).

By using Langmuir model and Ono-Kondo models, experimental adsorption results were evaluated and adsorption isotherms were constructed in this study. Langmuir model is for gases adsorbed on solids. It is generally considered as the simplest model (Ruthven, 1984). Experimental adsorption data in this study were evaluated for Langmuir model by using ISOFIT (Mattot, 2007) program. Although Langmuir model is widely used, it is not suitable for especially high pressure adsorption. In Langmuir model, the volume of adsorbed phase is ignored and there is no correction for adsorbed phase volume (Sudibandriyo *et al.*, 2010). Void volume of the sample cell is measured by using helium (non-adsorbing) before adsorption experiment starts. However, when adsorbate (gas) is adsorbed by adsorbent (sample), void volume decreases because of the volume of adsorbed layer. If void volume is not corrected, free gas amount in the void spaces of the sample cell is calculated excessively, but adsorption capacity is calculated less than its actual value called absolute adsorption. Adsorption capacity calculated without void volume correction is called excess(Gibbs) adsorption (Sudibandriyo *et al.*, 2003; Mohammad *et al.*, 2009a).

Ono-Kondo models have many advantages compared to Langmuir model. They are used to describe multilayer adsorption and to calculate absolute adsorption. Moreover, Ono-Kondo model is used to calculate surface area of adsorbent (sample) (Sudibandriyo *et al.*, 2010). In this study, matlab codes were written for Ono-Kondo monolayer and three-layer models, which are used for the evaluation of experimental adsorption data and layered structure of adsorption. Furthermore, Ono-Kondo monolayer model data of the experiments of pure methane and pure carbon dioxide were used to make a theoretical approach to binary mixtures of adsorption of methane and carbon dioxide.

After determining the adsorption data and model data, shale gas in place calculations were done. Ambrose *et al.* (2010) proposed a new technique for shale gas-in place calculations. However, in Ambrose *et al.* (2010)'s equation for shale gas in-place calculations, only Langmuir model parameters are used and also volume occupied by adsorbed molecules is ignored. In this study, in addition to Langmuir model, Ono-Kondo models were used to evaluate experimental adsorption data by considering void volume correction. Hence, simple modifications were done in Ambrose *et al.* (2010)'s shale gas-in place equation in this study and new formula was used to calculate initial gas in place for unit weight of shale deposits.

CHAPTER 2

SHALE GAS

2.1 General Information about Shale Gas Reservoirs

Shale gas reservoirs are defined as organic-rich and very fine grained sedimentary rocks. Shale gas reservoirs can also be composed of shale (fissile), mudstone (non-fissile), siltstone, fine-grained sandstone interlaminated with shale or mudstone, carbonate rocks, clay minerals and other minerals such as calcite and quartz (Crain, 2011). As seen in Figure 2.1, shale samples may have different colors due to their different clay contents, organic contents and other minerals.

Figure 2.1: Shale sample in different colors

Shale acts as source rock only or both source rock and reservoir rock. Organic materials deposited in shale were buried with time. With the increase of temperature and pressure, organic materials such as lipids from animal tissue and plant matter, or lignin from plant cells were transformed into kerogen. Depending on organic materials, pressure and temperature, kerogen was converted to oil, wet gas and dry gas. In some shales, gas migrated from shale through fractures, faults, etc. due to expansion. However, gas did not migrate in some shale rocks. In that case, shale is defined both as source rock and reservoir rock, which is the case of shale gas reservoirs (Boyer *et al.*, 2011).

Shale gas reservoirs consist of matrix and natural fracture systems. They have also layered structures (Figure 2.2). Gas in shale gas reservoirs is stored as free gas phase in the pore spaces of shale matrix and natural fractures. Moreover, gas is stored as adsorbed phase on the surface of shale matrix, especially on the organic materials (kerogen) and clay minerals, and also small amount of gas dissolves in water and/or oil (Pashin *et al.*, 2010). Adsorption capacities of shale gas reservoirs range from 20 % to 85 % (Lancaster *et al.*, 1993). These percentages show that adsorption is very important phenomena for shale gas reservoirs.

Figure 2.2: Layered structures of outcrop of Utica shale in Canada (National Energy Board, 2009)

Total organic carbon (TOC) content increases adsorption capacity. Moreover, Ross and Bustin (2008) stated that clay content of shale increases adsorption capacity. This means that even with low total organic carbon content, shale might have large adsorption capacity due to high clay content. In Figure 2.3, total organic carbon content range is not necessarily less than 5 % for shales and clay content ranges from 30 and 50 % (Heller and Zoback, 2011).

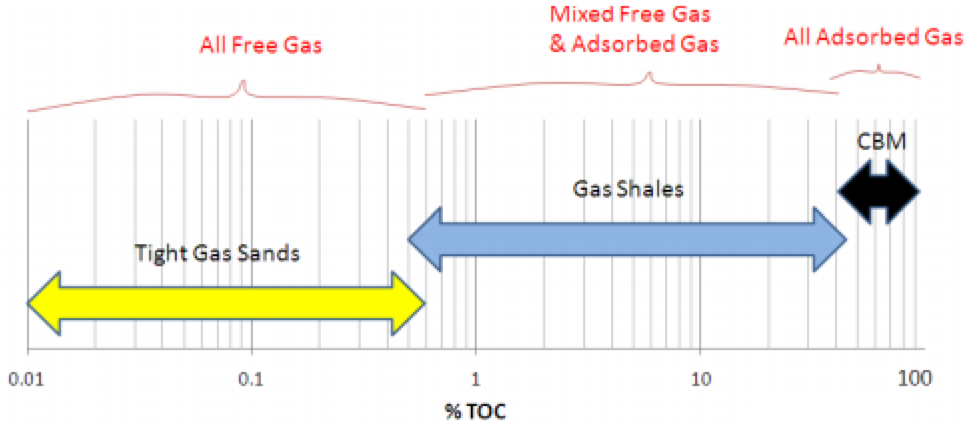

Figure 2.3: Ranges of TOC in coalbed methane, shale gas and tight gas sands (Promote UK, 2011)

Shale gas reservoirs have dual porosities; in the rock matrix and the natural fractures. Due to overburden pressure, natural fractures are generally closed (Sunjay and Kothari, 2011). Hence, shale gas reservoirs have low porosity values. At micron scale, it was shown by several authors that the shale organics are nanoporous materials (Kang, 2011). Shale matrix generally has micro (pores less than 2 nm diameter) to mesopores (pores with 2-50 nm diameters). These small pores on shale matrix are due to clay content and organic content (Kuila and Prasad, 2011). Moreover, shale gas reservoirs have extremely low matrix permeability values typically ranging from 10 to 100 nanodarcies (10^{-6} md) (Cipolla *et al.*, 2010). Reservoirs with permeability values greater than 0.1 md are defined as conventional reservoirs. Hence, shale gas reservoirs are in the classification of unconventional reservoirs (Boyer *et al.*, 2011).

Due to shale's extremely low permeability values, hydraulic fracturing and horizontal drilling operations are essential for gas production. With the advancement of technology in hydraulic fracturing and horizontal drilling, feasible gas production is possible from these reservoirs. Hydraulic fracturing is very effective to reactivate and reconnect natural fractures in shale, which increases permeability and gas production (Sunjay and Kothari, 2011).

Before conducting hydraulic fracturing and horizontal drilling activities, reservoir management studies are made to investigate the feasibility of operations. Hence, thermal maturity, reservoir thickness, total organic carbon content (TOC), adsorbed gas fraction, free gas fraction within pores and fractures and permeability are key parameters for the reservoir management studies in shale gas reservoirs (Arri *et al.*, 1992; Lewis *et al.*, 2004). The critical values of porosity, water saturation, oil saturation, permeability and TOC that shows whether shale gas reservoir is commercial or not are shown in Table 2.1.

Table 2.1: Critical values for different parameters to define a commercial shale gas play (Gutierrez *et al.*, 2009)

Parameters	**Minimum Value**
Porosity	> 4 %
Water Saturation	< 45 %
Oil Saturation	< 5 %
Permeability	> 100 nanodarcies
TOC	> 2 %

2.2 Shale Gas Production History

Shale gas reservoirs have become a major alternative source of energy in recent years (Salman *et al.*, 2011). Although shale gas reservoirs were known as a source of natural gas, their production generally was not feasible. However, Mitchell Energy and Development Corporation made detailed studies related to large scale shale gas production between 1980 and 1990 in the Barnett Shale in North-Central Texas, USA. This was the first commercial shale gas production in the world (EIA, 2011). Then, many companies focused on the production of natural gas from shale gas reservoirs such as Fayetteville Shale, Haynesville, Marcellus, Woodford, Eagle Ford and others. In Figure 2.4, shale gas production from different regions in USA is shown.

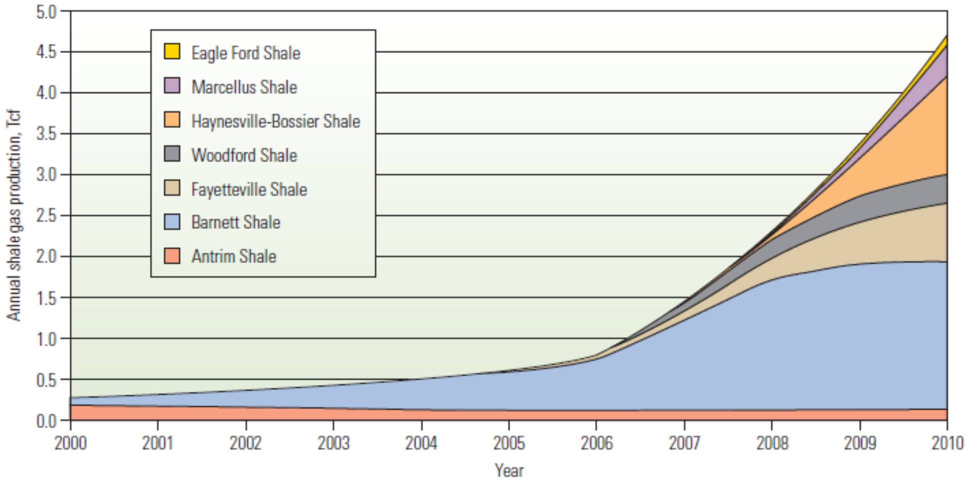

Figure 2.4: U.S.A. shale gas production from different shales (Boyer *et al.*, 2011)

With increased natural gas prices and the advancement of technology related to hydraulic fracturing and horizontal drilling in shale gas reservoirs, shale gas production has increased in USA (Cipolla *et al.*, 2010). With the production of natural gas from shale gas reservoirs, USA shale gas production increased from 0.39 trillion cubic feet in 2000 to 4.87 trillion cubic feet in 2010, which was 23 % of USA dry gas production. It is expected that by 2035, USA shale gas production will be 46 % of its total gas production (EIA, 2011).

With commercial shale gas production in USA, other countries and especially China have increased shale gas exploration activities and studies. Shale gas distributions in the world were determined as in Table 2.2 (EIA, 2011).

Table 2.2: Estimated shale gas technically recoverable resources for selected basins in 32 countries, compared to existing reported reserves, production and consumption during 2009 (EIA, 2011)

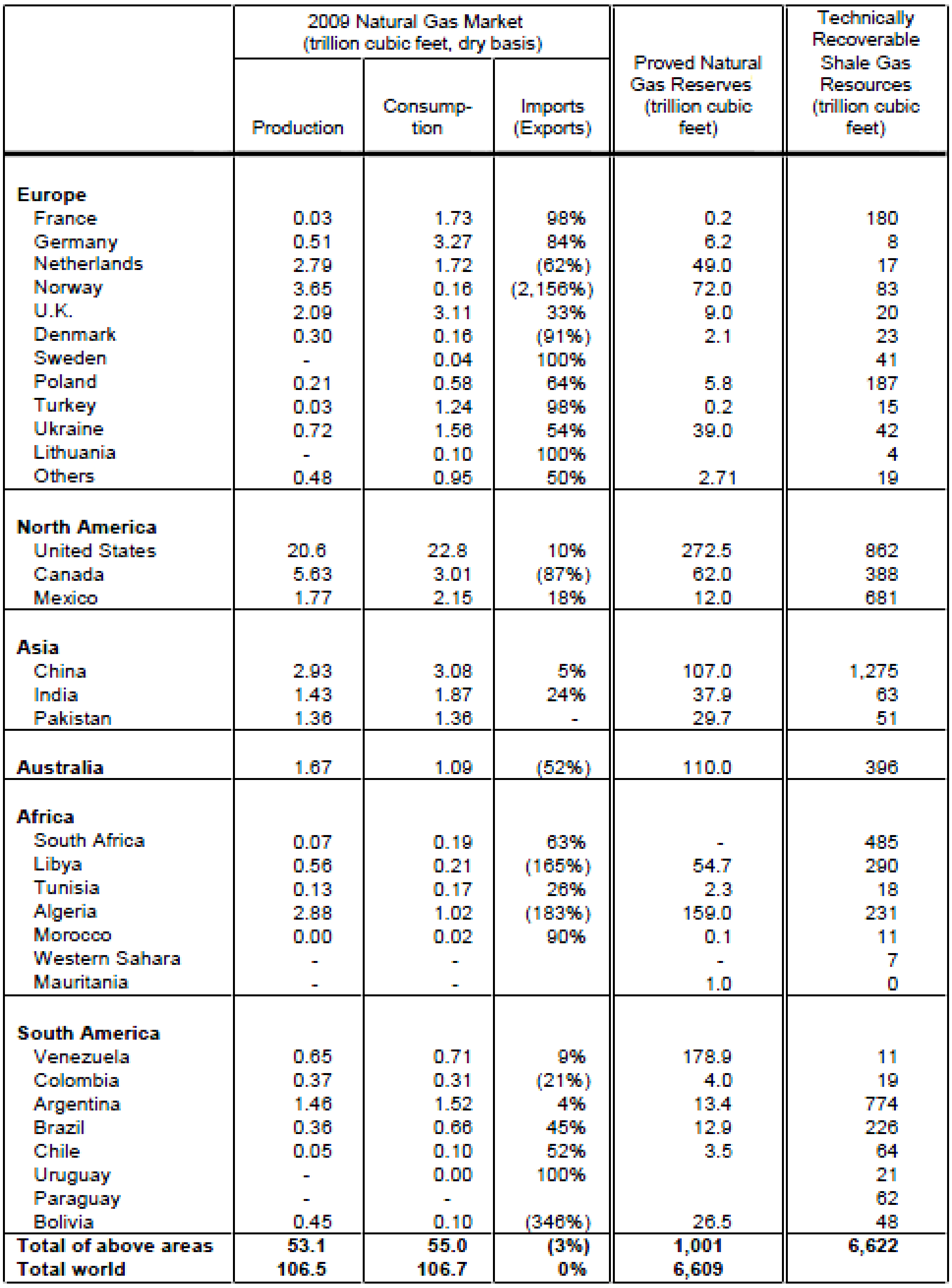

	2009 Natural Gas Market (trillion cubic feet, dry basis)			Proved Natural Gas Reserves (trillion cubic feet)	Technically Recoverable Shale Gas Resources (trillion cubic feet)
	Production	Consumption	Imports (Exports)		
Europe					
France	0.03	1.73	98%	0.2	180
Germany	0.51	3.27	84%	6.2	8
Netherlands	2.79	1.72	(62%)	49.0	17
Norway	3.65	0.16	(2,156%)	72.0	83
U.K.	2.09	3.11	33%	9.0	20
Denmark	0.30	0.16	(91%)	2.1	23
Sweden	-	0.04	100%		41
Poland	0.21	0.58	64%	5.8	187
Turkey	0.03	1.24	98%	0.2	15
Ukraine	0.72	1.56	54%	39.0	42
Lithuania	-	0.10	100%		4
Others	0.48	0.95	50%	2.71	19
North America					
United States	20.6	22.8	10%	272.5	862
Canada	5.63	3.01	(87%)	62.0	388
Mexico	1.77	2.15	18%	12.0	681
Asia					
China	2.93	3.08	5%	107.0	1,275
India	1.43	1.87	24%	37.9	63
Pakistan	1.36	1.36	-	29.7	51
Australia	1.67	1.09	(52%)	110.0	396
Africa					
South Africa	0.07	0.19	63%	-	485
Libya	0.56	0.21	(165%)	54.7	290
Tunisia	0.13	0.17	26%	2.3	18
Algeria	2.88	1.02	(183%)	159.0	231
Morocco	0.00	0.02	90%	0.1	11
Western Sahara	-	-		-	7
Mauritania	-	-		1.0	0
South America					
Venezuela	0.65	0.71	9%	178.9	11
Colombia	0.37	0.31	(21%)	4.0	19
Argentina	1.46	1.52	4%	13.4	774
Brazil	0.36	0.66	45%	12.9	226
Chile	0.05	0.10	52%	3.5	64
Uruguay	-	0.00	100%		21
Paraguay	-	-			62
Bolivia	0.45	0.10	(346%)	26.5	48
Total of above areas	**53.1**	**55.0**	**(3%)**	**1,001**	**6,622**
Total world	**106.5**	**106.7**	**0%**	**6,609**	

2.3 Shale Gas in Turkey

Turkey’s dependency to natural gas has been increasing recently. Turkey’s annual natural gas consumption have got closer to 40 billion cubic meters (1,412 billion cubic feet) (Yardimci, 2011). However, Turkey’s annual natural gas production in 2011 was 793 million cubic meters (TPAO, 2011), which supplied only 2 % of its natural gas consumption. Hence, the importance of unconventional energy sources such as shale gas and coalbed methane reserves has been increasing in Turkey as in the world. According to EIA (2011)’s report, Turkey has technically recoverable 15 trillion cubic feet of shale gas when Southeastern and Thrace regions’ potentials are considered. This amount is important for Turkey to reduce its natural gas dependency to foreign countries.

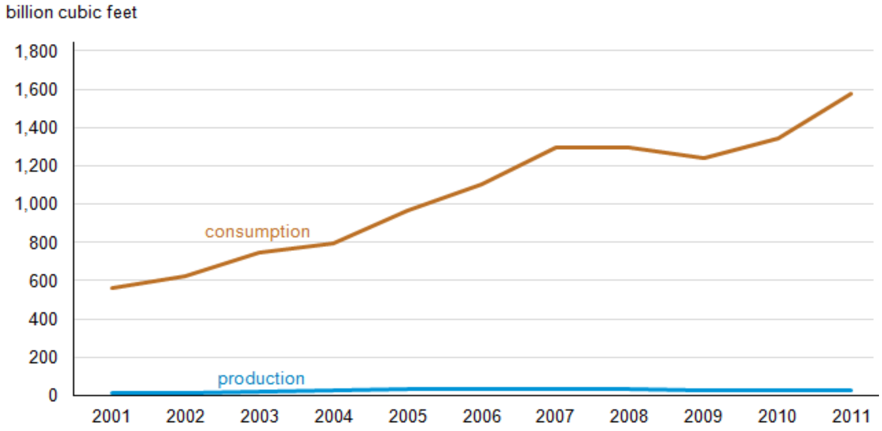

Figure 2.5: Turkey’s natural gas consumption and production (EIA, 2011)

Turkey has shale gas potentials in Southeast Anatolia Basin and Thrace Basin. Moreover, Turkey may have shale potentials in Taurus Basins and Black Sea Basin. However, about Blacklake, Taurus and Black Sea Basin, there are no detailed studies. In Figure 2.6, the locations of potential shale gas reserves in Turkey are shown (EIA, 2011).

Figure 2.6: Shale gas basins of Turkey (EIA, 2011)

2.3.1 Southeast Anatolia Basin

Southeast Anatolia Basin has 7640.5 km^2 area of Dadas shale. Depth of Dadas shale changes from 6,560 feet to 9,840 feet. Dadas shale has three members with the gross thickness of 1300 feet. In these three members, Dadas I is very rich with organic materials compared to other two members. Its thickness is around 150 feet. Total organic content (TOC) changes from 2 % to 16 % and also its thermal maturity is between 1 % and 1.2 % R_o. It is estimated that Dadas shale contains a risked gas in place of 43 trillion cubic feet and 9 trillion cubic feet of this gas is technically recoverable. In Table 2.3, detailed properties of Dadas shale in Southeast Anatolia Basin are shown (EIA, 2011).

Table 2.3: Shale properties of Southeast Anatolian Basin (EIA, 2011)

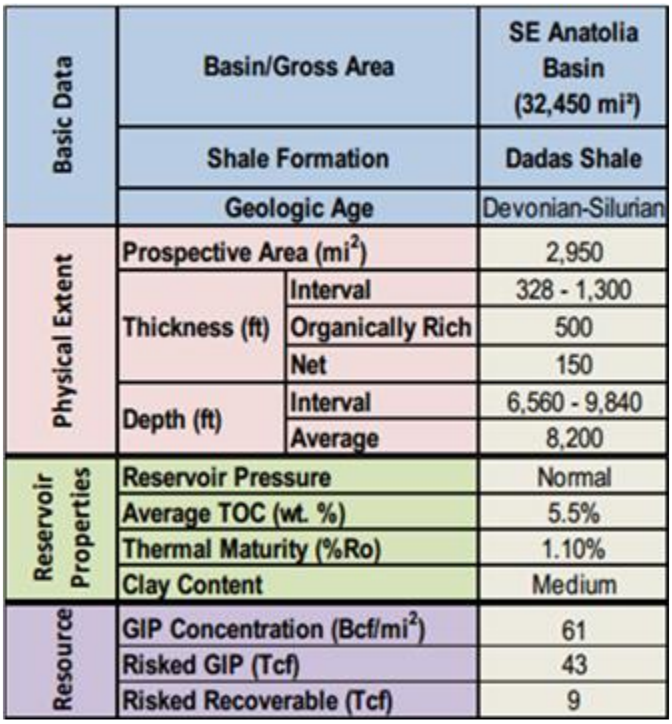

Basic Data	Basin/Gross Area		SE Anatolia Basin (32,450 mi^2)
	Shale Formation		Dadas Shale
	Geologic Age		Devonian-Silurian
Physical Extent	Prospective Area (mi^2)		2,950
	Thickness (ft)	Interval	328 - 1,300
		Organically Rich	500
		Net	150
	Depth (ft)	Interval	6,560 - 9,840
		Average	8,200
Reservoir Properties	Reservoir Pressure		Normal
	Average TOC (wt. %)		5.5%
	Thermal Maturity (%Ro)		1.10%
	Clay Content		Medium
Resource	GIP Concentration (Bcf/mi^2)		61
	Risked GIP (Tcf)		43
	Risked Recoverable (Tcf)		9

2.3.2 Thrace Basin

Thrace Basin has two formations with shale gas potential; Hamitabat formation (the Lower Mid-Eocene) and Mezardere formation (the Lower Oligocene).

Hamitabat formation consists of sandstone, shale, and marl deposited in shallow marine environment. Hamitabat shale has 808 km^2 prospective areas. Hamitabat shale depth changes from 12,100 to 16,400 feet. TOC ranges from 1.5 % to 6.4 %. The net shale thickness is 344 feet. Hamitabat shale contains a risked gas in place of 14 trillion cubic feet and 4 trillion cubic feet of this gas is technically recoverable.

Mezardere formation consists of sandstone, shale, marl deposited in a deltaic environment. Mezardere shale has 785 km^2 prospective areas. Mezardere shale depth changes from 8,200 to 10,168 feet. TOC ranges from 1% to 4%. The net shale thickness is 295 feet. Hamitabat shale contains a risked gas in place of 7 trillion cubic feet and 2 trillion cubic feet of this gas is technically recoverable. In Table 2.4, detailed shale properties of Thrace Basin are shown (EIA, 2011).

Table 2.4: Shale properties of Thrace Basin (EIA, 2011)

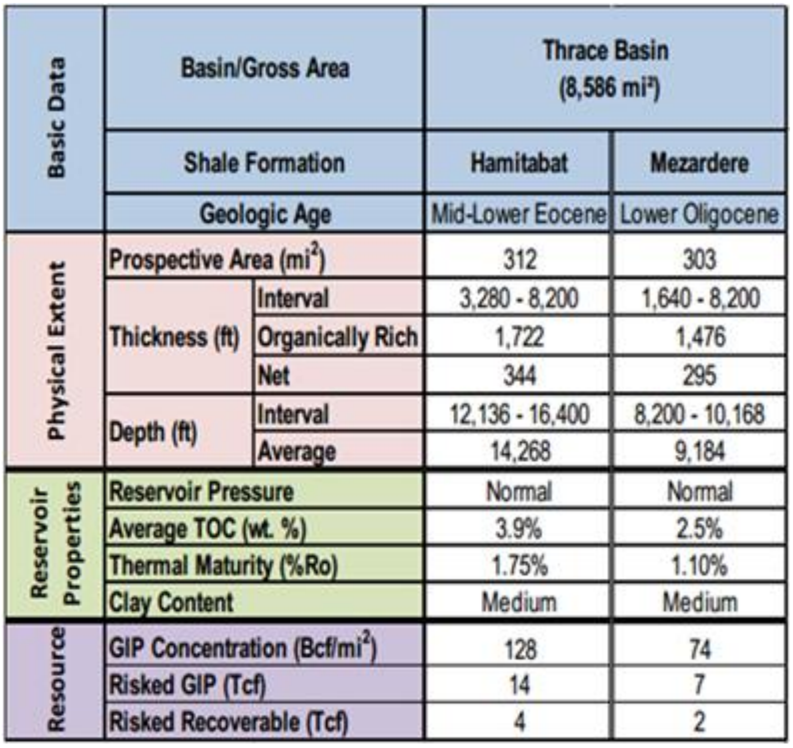

Basic Data	Basin/Gross Area		Thrace Basin ($8,586 mi^2$)	
	Shale Formation		Hamitabat	Mezardere
	Geologic Age		Mid-Lower Eocene	Lower Oligocene
Physical Extent	Prospective Area (mi^2)		312	303
	Thickness (ft)	Interval	3,280 - 8,200	1,640 - 8,200
		Organically Rich	1,722	1,476
		Net	344	295
	Depth (ft)	Interval	12,136 - 16,400	8,200 - 10,168
		Average	14,268	9,184
Reservoir Properties	Reservoir Pressure		Normal	Normal
	Average TOC (wt. %)		3.9%	2.5%
	Thermal Maturity (%Ro)		1.75%	1.10%
	Clay Content		Medium	Medium
Resource	GIP Concentration (Bcf/mi^2)		128	74
	Risked GIP (Tcf)		14	7
	Risked Recoverable (Tcf)		4	2

CHAPTER 3

ADSORPTION

3.1 General Information about Adsorption

Adsorption is defined as the change in the concentration of a substance at the interface as compared to the neighboring phases. Adsorption can occur between liquid-gas, liquid-liquid, solid-liquid and solid-gas (Thomas and Crittenden, 1998). However, in a shale gas reservoir system, solid-gas adsorption is the determining factor.

When a gas and a solid interact, there are intermolecular attractive forces between them. If these intermolecular attractive forces are greater than those existing between molecules of gas itself, gas accumulates on the surface of solid. This phenomenon is called adsorption of gas on solid (Vellanki, 1995).

Adsorption is generally mixed with the term absorption. In absorption, a fluid (gas or liquid) permeates or dissolved by a liquid or solid. However, adsorption occurs only on surface. Hence, adsorption is a surface phenomenon. The molecules adsorbed on the surface of solid is defined as “adsorbate” and the solid material upon which the adsorbate is adsorbed is defined as “adsorbent” (Condon, 2006; Luo *et al.*, 2011). As seen in Figure 3.1, adsorbate molecules diffuse into the porous spaces and channels of adsorbate.

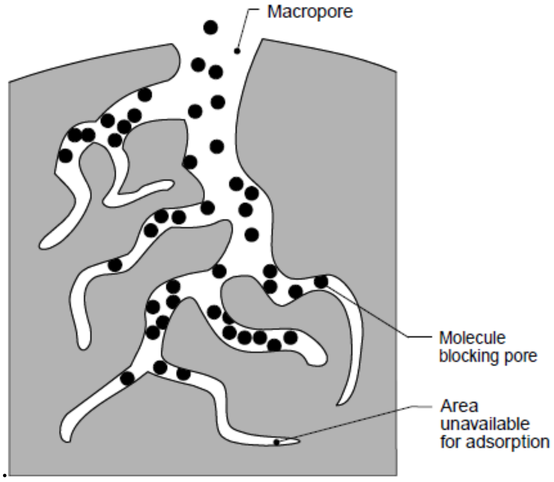

Figure 3.1: Gas adsorbed into pores of adsorbent (APTI, 2008)

3.2 Adsorption Forces

Solid-gas adsorption is a surface process that leads to the transfer of gas molecules from a fluid bulk to solid surface. Intermolecular attractive forces lead to adsorption. Hence, it is important to investigate adsorption forces to understand the general concept. Adsorption occurs in two ways: physical adsorption and chemical adsorption (Sherwin, 2011).

3.2.1 Physical Adsorption

Physical adsorption is also named as physisorption. In physical adsorption, intermolecular forces causing adsorption between adsorbate and adsorbent are due to Van der Waals forces. Hence, physical adsorption is also defined as Van der Waals' adsorption (Sherwin, 2011).

Physical adsorption is reversible due to weak forces. By heating or decreasing pressure, it can be reversed easily. The reverse of adsorption is defined as desorption (Thomas and Crittenden, 1998). Physical adsorption is an exothermic process and heat is always released when adsorption occurs in order to form new bonds (Dabrowski, 2001).

Van der Waals forces causing adsorption are due to dipole-dipole, dipole-induced dipole, London forces and possibly hydrogen bonding. These forces are relatively weak compared to chemical forces. Hence, it is a reversible process. (Condon, 2006).

In physical adsorption, the polarities of adsorbate and adsorbent play an important role. Due to their characteristics, molecules can be polar or nonpolar. Polar molecules have separated positive and negative charges, which is called permanent dipole (Figure 3.2.). For example, water is a polar substance. In contrast to polar substances, positive and negative charges of nonpolar substances are in one center, which means that they have no permanent dipole. Carbon dioxide and methane molecules are non-polar. Moreover, most organic compounds are nonpolar due to their symmetry (APTI, 2008).

Orientation, dispersion, or induction may cause physical adsorption. Between polar-polar molecules, attraction occurs because of the orientation effect. As seen in Figure 3.2, the positive charge of polar adsorbent molecule attracts the negative charge of polar adsorbate molecule (APTI, 2008).

In dispersion effect, a nonpolar adsorbate molecule is adsorbed by a nonpolar adsorbent. Although nonpolar molecules do not have a permanent dipole, they have a fluctuating or oscillating dipole. Fluctuating dipoles form due to the momentary changes in electron distribution round the atomic nuclei, which causes physical adsorption by dispersion effect (APTI, 2008).

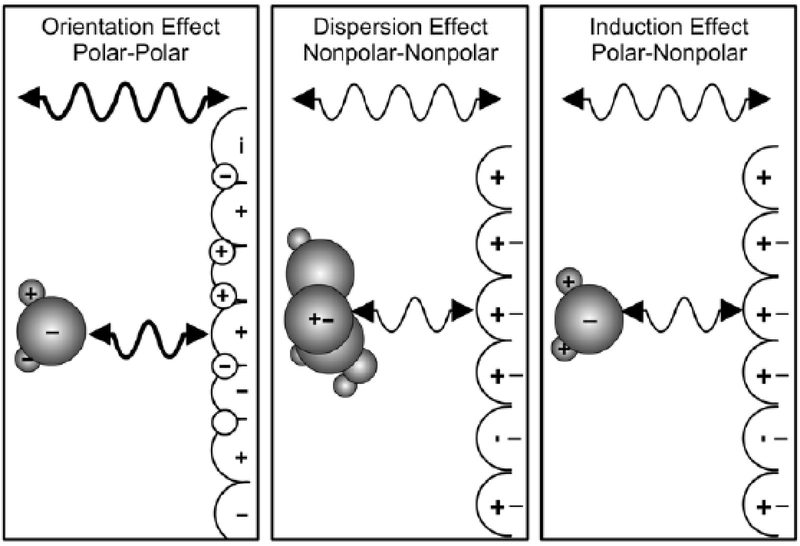

Figure 3.2: Physical forces causing adsorption (APTI, 2008)

A polar adsorbate molecule is attracted by a nonpolar adsorbent molecule, called the induction effect. When a polar adsorbate molecule with a permanent dipole comes in close to a nonpolar adsorbent molecule, the polarity can be induced into adsorbent. The polarizability of nonpolar molecules determines the energy of this effect. The induction effect is the attraction between a polar molecule and a non-polar molecule. However, the induction effect is relatively small compared to the orientation or dispersion effects (APTI, 2008).

3.2.2 Chemical Adsorption

Chemical adsorption is also named as chemisorption or Langmuir adsorption. Chemical adsorption occurs when there is a chemical interaction between adsorbate and adsorbent (Ruthven, 1984).

Chemical adsorption involves the formation of strong chemical bond between adsorbate and adsorbent. Physical adsorption forces are relatively small compared to chemical adsorption. Chemical adsorption is almost irreversible process because it is very difficult to remove adsorbate molecules from adsorbent’s surface (Dabrowski, 2001).

Due to strong chemical bonds, chemical adsorption occurs only as a monolayer structure on adsorbent because chemical adsorption stops when all the active sites on the surface of adsorbent have reacted. However, multilayers of adsorbed molecules can often be formed in physical adsorption. Similar to physical adsorption, chemical adsorption is also exothermic process (Ruthven, 1984). Hence, there are both differences and similarities between chemical and physical adsorption. A comparison of physical and chemical adsorption is shown in Table 3.1 (Ruthven, 1984).

Table 3.1: A comparison of physical adsorption and chemical adsorption (Ruthven, 1984)

Physical Adsorption	Chemical Adsorption
Low heat of adsorption usually in range of 20-40 kJ/mole, which is two or three times less than latent heat of evaporation.	High heat of adsorption in the range of 50-400 kJ/mole, which is two or three times larger than latent heat of evaporation.
Forces of attraction are Van der Waals' forces.	Forces of attraction are chemical bond forces.
It is reversible.	It is irreversible.
It usually takes place at low temperature and decreases with increasing temperature.	It takes place at high temperature.
It is related to the case of liquefaction of the gas.	It is not related to the case of liquefaction of the gas.
It forms multi-molecular layers.	It forms monomolecular layers
It does not require any activation energy.	It requires high activation energy.
High pressure is favorable. Decrease of pressure causes desorption.	High pressure is favorable. Decrease of pressure does not cause desorption.

3.3 Adsorption in Shale Gas Reservoirs

Gas in shale reservoirs is stored as both free gas and adsorbed gas. Significant amount of gas in shale gas reservoirs is stored as adsorbed or condensed phase; even more than 50 % of gas in these reservoirs might be stored as adsorbed state. The amount of gas adsorbed depends on reservoir temperature, pressure, particle size and type. Total organic carbon content (TOC) and clay content of shales are also important parameters for adsorption (Lu and Watson, 1993).

As seen in Figure 3.3, shale gas reservoirs have naturally fractured systems. Shale matrix are layered structures. Gas is adsorbed on the surface of micro-porous shale matrix. Some gas is stored as free phase in the fractures and porous spaces of shale matrix. In adsorption, Van der Waals type gas-shale interactions at the shale-gas interface increase the concentrations of gas molecules near shale surface, where densities become high comparable to those of liquids. Thus, shale gas reservoirs can actually hold more gas than conventional gas reservoirs of comparable volumes (Song *et al.*, 2011).

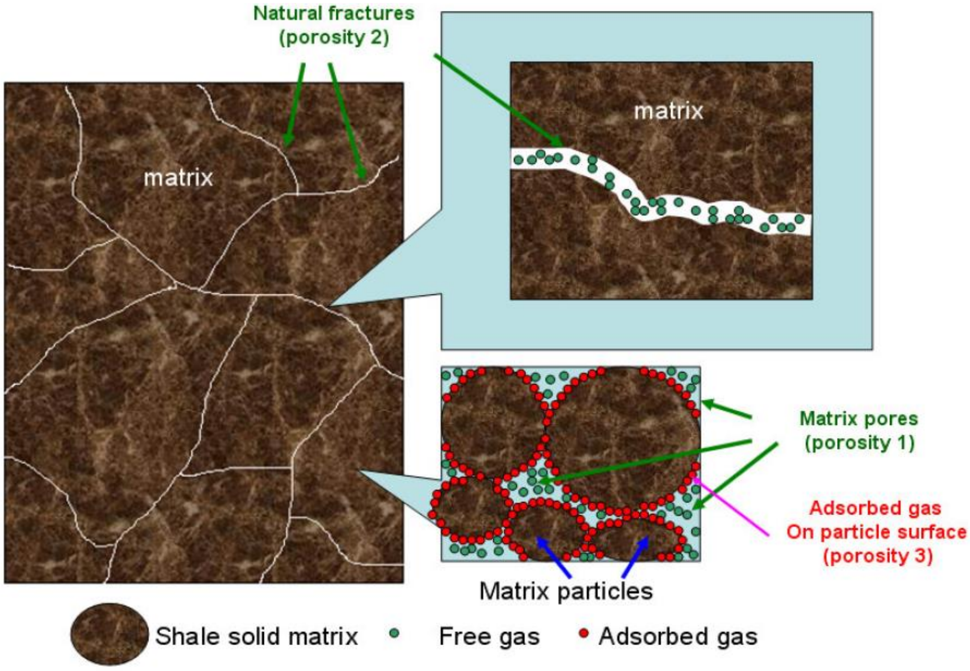

Figure 3.3: Adsorption mechanisms of gas in shale gas reservoirs (Song *et al.*, 2011)

3.4 Desorption in Shale Gas Reservoirs

Gas adsorption is a surface phenomenon and is mainly a physical bond caused by inter-molecular attractive forces (Van der Waals forces). Desorption is the reverse process of adsorption. Desorption from shale gas reservoirs occur when reservoir pressure decreases due to the production of free gas and/or water (Song *et al.*, 2011).

In shale gas reservoirs, desorption mechanism is very important for production. To provide desorption, pressure is an important parameter for shale gas systems. By lowering reservoir pressure, desorption occurs in shale gas reservoirs (Velanki, 1995). In order to decrease reservoir pressure, much free gas and/or water is produced from shale gas reservoir and then, adsorbed gas in pore spaces starts to desorb in a significant amount (Salman *et al.*, 2011).

As shown in Figure 3.4, when production starts in shale gas reservoirs, free gas in matrix porous system and fracture system is produced (Song *et al.*, 2011). This production causes decrease in pressure. Decreasing pressure causes gas desorption in matrix pores. Then, desorbed gas and free gas is produced through fracture systems. However, for this mechanism, successful hydraulic fracturing operations are essential to provide the diffusivity of desorbed gas from shale matrix through fractures.

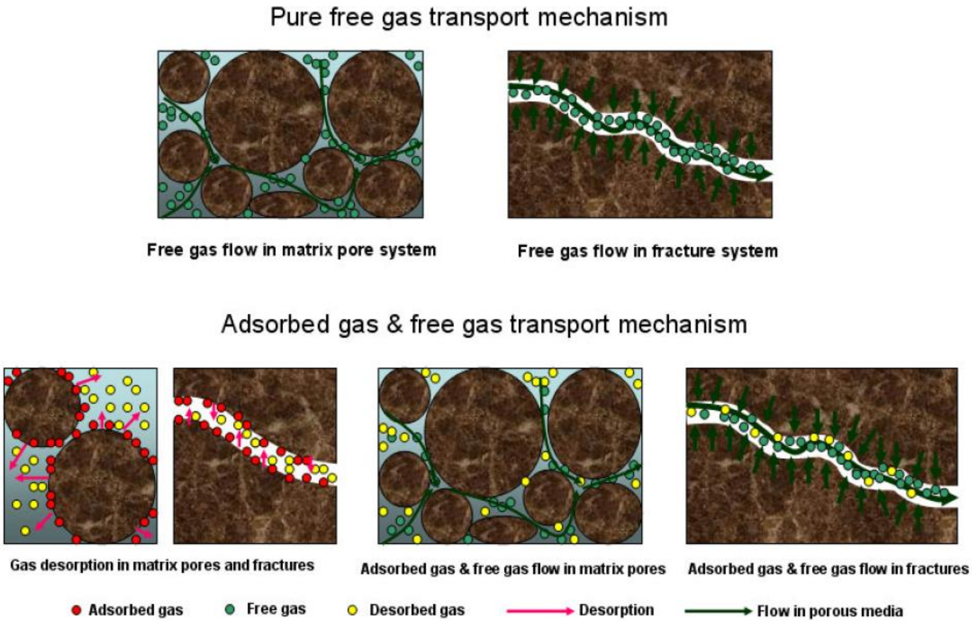

Figure 3.4: Flow mechanism of shale gas reservoirs (Song *et al.*, 2011)

3.5 Adsorption in Coalbed Methane Reservoirs

Similar to shale gas reservoirs, coalbed methane reservoirs are also unconventional energy sources. In coalbed methane reservoirs, almost all gas is stored as an adsorbed state. However, in shale gas reservoirs, there is also significant amount of free gas in porous spaces and fractures. Therefore, in coalbed methane reservoirs, significant amount of methane is stored. In recent years, in USA, gas production from coalbed methane reservoirs is quite high. Coal seam thickness, desorption isotherm, desorption pressure, static coalbed pressure, absolute permeability, directional permeability, relative permeability, porosity, pore compressibility, capillary pressure, irreducible water saturation, diffusion are key parameters for coalbed methane reserve analysis (Hall *et al.*, 1994).

3.6 Adsorption in Activated Carbons

In recent years, the transports of natural gas with LNG and CNG methods are common. However, these kinds of transports are very dangerous because of high working pressures. There is an idea to store gas in activated carbons as an adsorbed phase. In this case, much gas is stored at low pressures compared to CNG and LNG (Wang *et al.*, 2011). Moreover, activated carbons are used for separation processes in industry.

Activated carbon is generally produced from coal, wood, petroleum based products, nutshells, lignite, synthetic high polymers, etc. In activation process, first, the material is heated at high temperatures (around 600-900 ^{o}C) to evaporate all volatile materials. Then, only carbon and small amount of ash are left. Secondly, carbon dioxide, air and steam are injected into the system to activate the carbon and to increase surface area. When surface area and porous spaces increase, adsorption amounts also increase (Suzuki, 1990). Hence, by using some activated carbons, gas can be stored at low pressures compared to LNG and CNG.

3.6.1 BPL Granular Activated Carbon

BPL is a virgin granular activated carbon designed for use in gas phase applications. It is a bituminous coal-based product activated at a high temperature in a steam atmosphere. Because of its surface area, density and strength characteristics, BPL can be reactivated for reusing and eliminating disposal problems (Calgon Carbon, 2012). BPL activated carbon was used in this study to prove the reliability of adsorption experiments and calculation procedures. In Table 3.2, the specifications of BPL activated carbon are listed.

Table 3.2: BPL activated carbon specifications (Calgon Carbon, 2012)

Iodine Number	1000 mg/g (min.)
Butane Activity, by weight	23.3 % (min.)
Moisture, as packed by weight	2 % (max.)
Hardness Number	95 (min.)
Apparent Density	0.43 g/cc
Mean Particle Diameter	3.7 mm (min.)
Screen Size by weight, U.S.Sieve Series:	
On mesh	15 % (max.)
Through 7 mesh	8.0 % (max.)

CHAPTER 4

ADSORPTION ISOTHERMS AND MODELS

4.1 Adsorption Equilibrium

Adsorption occurs when an adsorbent comes in contact with adsorbate. After adsorption starts, adsorbent and adsorbate reach at equilibrium, which is called adsorption equilibrium. Adsorption equilibrium data is represented by isotherm, isobar and isostere (Do, 1998):

4.1.1 Isotherm

Isotherm is commonly used to present adsorption equilibrium. At a constant temperature, a plot of adsorption capacity versus adsorption equilibrium pressure represents adsorption. The shape of isotherm plot is important to make analysis about adsorption type and porous structure of adsorbate.

4.1.2 Isobar

Although isobar representation is not common, isobar is a plot of adsorption capacity versus temperature at a constant partial pressure of adsorbate.

4.1.3 Isostere

Isostere is also used to present adsorption equilibrium. It is a plot of the natural log of the pressure versus the reciprocal of absolute temperature at a constant amount of gas adsorbed. Generally, isostere lines are straight.

4.2 Classification of Adsorbent

Adsorbent’s type, porous structure, and surface area affect the adsorption capacity of adsorbate. For high amount of adsorption capacity (Gregg and Sing, 1982);

- ✓ Adsorbent must have reasonably high surface area or micropore volume.
- ✓ Solid (adsorbent) must have relatively large pore network for the transport of molecules to the interior.

To satisfy first requirement, porous solid must have small pore size with a reasonable porosity. This suggests that a good solid must have a combination of two pore ranges: the micropore range and the macropore range.

International Union of Pure and Applied Chemistry (IUPAC) classified pore sizes as (Bantraj, 2011)

Micropores: d < 2 nanometers
Mesopores: 2 < d < 50 nanometers
Macropores: d > 50 nanometers

4.3 Types of Adsorption Isotherm

Isotherms are commonly used to represent adsorption. At a constant temperature, the change in equilibrium uptake against pressure is called adsorption isotherm. Six types of adsorption isotherms are shown in Figure 4.1 (Gregg and Sing, 1982):

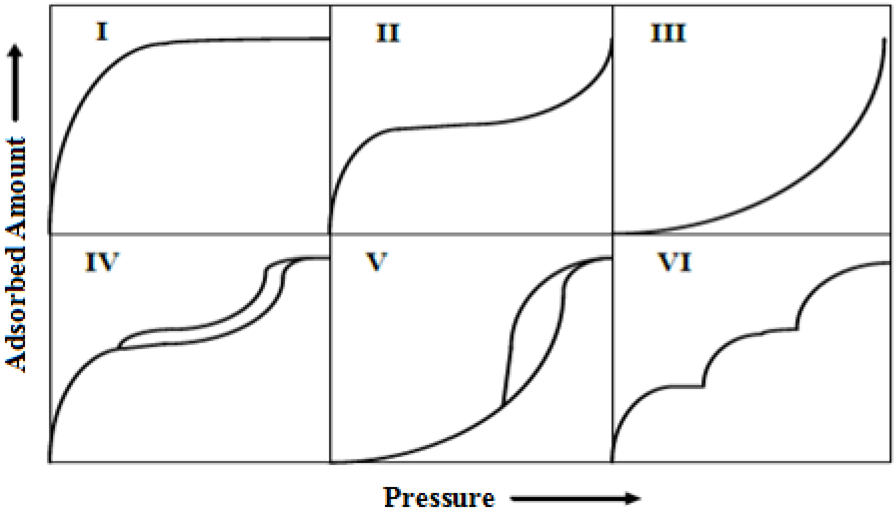

Figure 4.1: Type of adsorption isotherms (Gregg and Sing, 1982)

4.3.1 Type I Isotherm

An adsorbent containing very fine molecules has only few molecular diameters of pore dimensions. There are potential forces from the neighboring walls of the pores. These forces increase interaction energy between adsorbent surface and gas molecules. Hence, this causes an increase in adsorption and may cause complete filling of pores at low pressure. Generally, monolayer is formed on the surface of adsorbent in Type I (Gregg and Sing, 1982).

4.3.2 Type II Isotherm

Type II is very common in the case of physical adsorption with multilayer formation. At low relative pressure, it is concave, and then linear for a small pressure range where monolayer coverage is complete. Then, it becomes convex to the relative pressure axis. Convex behavior shows that the formation of multilayer. Multilayer's thickness increases progressively with increase in relative pressure. An example is the adsorption of water vapor on carbon black at 30 ^{o}C (Gregg and Sing, 1982).

4.3.3 Type III and Type V Isotherm

Both Type III and Type V isotherms are characterized by being convex to the relative pressure axis. As seen in Figure 4.1, Type III isotherm's convexity continues throughout the isotherm. However, Type V isotherm reaches a plateau at high relative pressure. The convexity of the isotherm indicates that the already adsorbed molecules have tendency to enhance the adsorption of other molecules. In nonporous or highly microporous adsorbents, Type III isotherms are common. On the other hand, Type V isotherms are observed in the case of mesoporous or microporous adsorbents for the adsorption of both polar and non-polar adsorbent (Gregg and Sing, 1982).

4.3.4 Type IV Isotherm

Type IV isotherms are observed in the case of mesoporous adsorbents. At low relative pressures, the shape of isotherms follows as the same path as Type II. Then, the slope starts decreasing at higher pressure. At saturation vapor pressure, the isotherm levels off to constant value of adsorption. The portion of isotherm which is parallel to the pressure axis is attributed to pores filling by the capillary condensation (Gregg and Sing, 1982).

4.3.5 Type VI Isotherm

Type VI isotherms show discrete steps which may be caused by multilayer formation in different ranges of micropores (Gregg and Sing, 1982).

4.4 Adsorption Isotherms

Adsorption is generally expressed by using adsorption isotherms. Hence, the amount of adsorbed gas is measured by conducting adsorption experiments at constant temperature. By using raw experimental adsorption data, the graph of the amount adsorbed versus equilibrium pressure is drawn. A line is fitted on the points on the graph by using different adsorption isotherms and models (Sherwin, 2011).

4.4.1 Freundlich Isotherm

The first mathematical fit to an isotherm was published by Freundlich and Kuster (1894) and is a purely empirical formula (Matott, 2007; Sherwin, 2011).

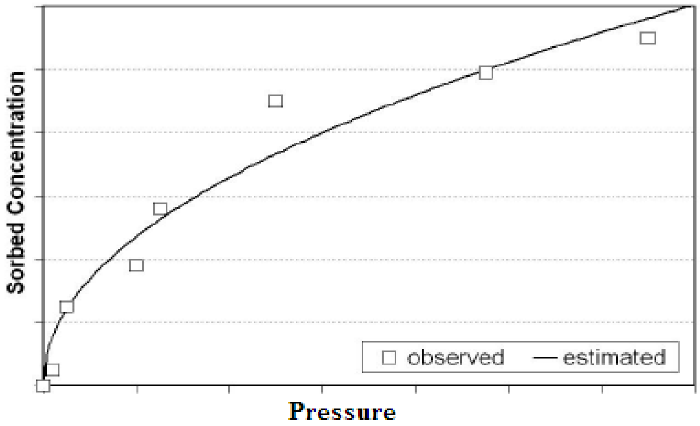

Figure 4.2: Example Freundlich isotherm fit (Matott, 2007)

$$\frac{x}{m} = kP^{1/n} \tag{4.1}$$

where x: the amount of adsorbed, g, m: mass of adsorbent, g, P: pressure of adsorbate, psia, k and n: are empirical constant (changing with temperature).

For a good adsorbent, 1<n<10, and a higher value of n indicates better adsorption and formation of rather strong bond between the adsorbate and adsorbent.

4.4.2 Langmuir Model

Langmuir model was proposed by Irving Langmuir in 1918. It is for gases adsorbed on solids. It is generally considered as the simplest model. Langmuir made some assumptions to propose this model (Ruthven, 1984; Matott, 2007):

1) The surface of an adsorbent is homogenous. This means that all the adsorption sites are energetically equivalent.
2) Adsorbed molecules do not interact with neighboring adsorbed molecules.
3) Each site can hold one adsorbate molecule.
4) At the maximum adsorption, only a monolayer is formed.

Langmuir isotherms are commonly used, because it is easy to apply. However, four assumptions above are not valid for most cases because there are always imperfections on the surface of adsorbent. Moreover, molecules are not necessarily inert and adsorption mechanism is not same for the first molecule adsorbed as for the last. Molecules can form multilayered adsorption on the surface of adsorbent instead of monolayer. In spite of these problems, Langmuir isotherm is the first choice in many adsorption models and it has many applications in industry, because it is easy to apply and practical (Czepirski, 2000).

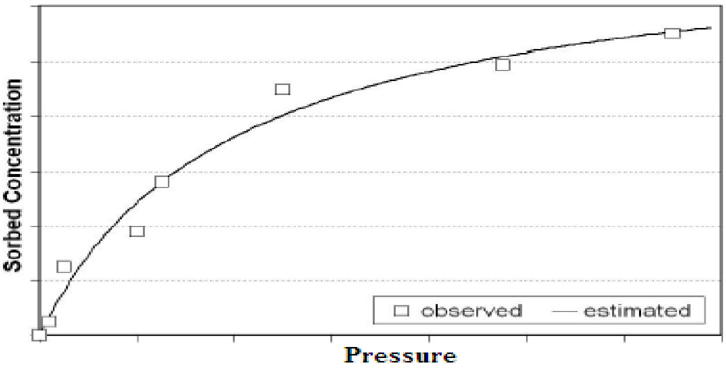

Figure 4.3: Example Langmuir isotherm fit (Matott, 2007)

Langmuir adsorption models are explained by different expressions:

Langmuir Model Expression 1:

$$\theta = \frac{bP}{1+bP} = \frac{q}{q_s} \tag{4.2}$$

where θ: surface coverage, P: pressure of adsorbate, psia, b is constant, q: amount adsorbed, scf/ton, q_s: the maximum amount that can be adsorbed, scf/ton (For very low pressures θ=bP and for high pressures θ=1) (Matott, 2007).

Langmuir Model Expression 2:

Langmuir model is also expressed as (Siemons and Busch, 2007)

$$\frac{n_L^{sorb}}{n_L} = \frac{P}{P+P_L} \tag{4.3}$$

where n_L^{sorb}:adsorbed amount, mmol/g, P: pressure of adsorbate, psia, n_L: the Langmuir parameters for molar mass, mmol/g, P_L : Langmuir pressure, psia

Langmuir Model Expression 3:

Langmuir Model is expressed as in equation 4.4 (Song *et al.*, 2011). Equation 4.4 is Langmuir equation, which describes the adsorption capacity of rock as pressure changes under isothermal conditions.

$$V_{ads} = \frac{V_L P}{P_L + P} \tag{4.4}$$

where

V_{ads} is the gas volume that can be adsorbed by a rock of unit mass in scf/ton,

V_L is the Langmuir volume, scf/ton (the maximum gas volume can be adsorbed), P_L is Langmuir pressure, psia, at which half of Langmuir volume gas can be adsorbed (Figure 4.4), P is the pore pressure, psia

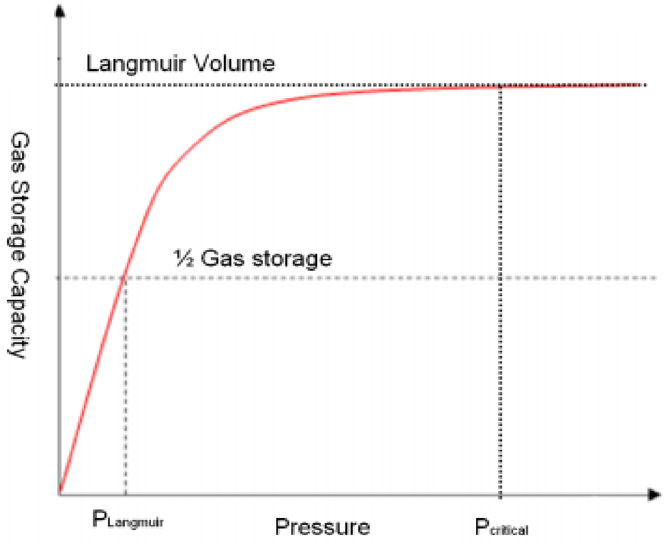

Figure 4.4: Langmuir isotherm curve (Song *et al.*, 2011)

As seen in Figure 4.4, Langmuir volume is the adsorbed volume when pressure is infinite. Langmuir pressure is defined as half of Langmuir volume gas can be adsorbed.

4.4.3 Extended Langmuir Isotherm

For mixtures, Langmuir isotherm formula in equation 4.2 was extended by Ruthven and Yang (Arri *et al.*, 1992). The isotherm can be expressed as

$$q_i = \frac{(q_s)_i b_i P_i}{1 + \sum_{i=1}^{n} b_i P_i} \tag{4.5}$$

where $(q_s)_i$ and b_i are the Langmuir constants for pure gas sorption, P_i: pressure of adsorbate i, psia. The partial pressure is related to

$$P_i = P y_i \tag{4.6}$$

With the extended Langmuir isotherm, the gas content of each component (y_i) can be directly calculated from its partial pressure (P_i). Only the Langmuir constants from pure gas sorption are used and no binary sorption constants are needed. The extended Langmuir isotherm is a very simple form making it quite easy to use in mathematical calculations.

4.4.4 BET Isotherms

The assumptions of Langmuir isotherm are not often valid, especially for relatively flat and non-porous surfaces. BET isotherm was developed by Stephen Brunauer, Paul Emmett, and Edward Teller in 1938 to solve these problems. Their theory is called BET theory, after the initials in their last names (Czepirski, 2000).

For BET isotherm, there are several assumptions. The key one of these assumptions is that the successive heats of adsorption for all layers except the first are equal to the heat of condensation of adsorbate. Moreover, this model assumes that the surface of adsorbent is energetically homogeneous with no interaction between adsorbed molecules. At saturated vapor pressure, adsorbate condenses to liquid on the surface of the solid leading to infinite layers (Ruthven, 1984; Matott, 2007).

Langmuir isotherm is usually better for chemisorption and BET isotherm works better for physisorption for non-microporous surface. BET isotherm equation is given as:

$$\frac{1}{V(P_o/P-1)}=\frac{1}{V_mC}+\frac{C-1}{V_mC}\frac{P}{P_o} \tag{4.7}$$

where V_m is the monolayer volume, scf/ton, C is a constant, P_o is the saturation vapor pressure, psia and P: pressure of adsorbate, psia.

Although BET equation does not entirely fit into experimental data, it is a useful tool that provides a theoretical foundation for the various isotherms shapes. Moreover, BET equations are important to calculate the surface area of adsorbent. By using nitrogen and special equipment, surface area measurements are made. BET equations are used for the evaluation of these measurements and calculations of surface area (Gregg and Sing, 1982). In Figure 4.5, a typical BET isotherm's fitting to laboratory data is shown (Matott, 2007).

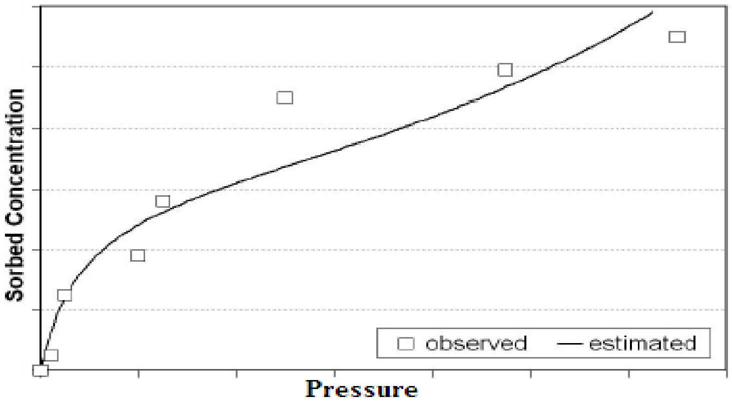

Figure 4.5: Example BET isotherm curve (Matott, 2007)

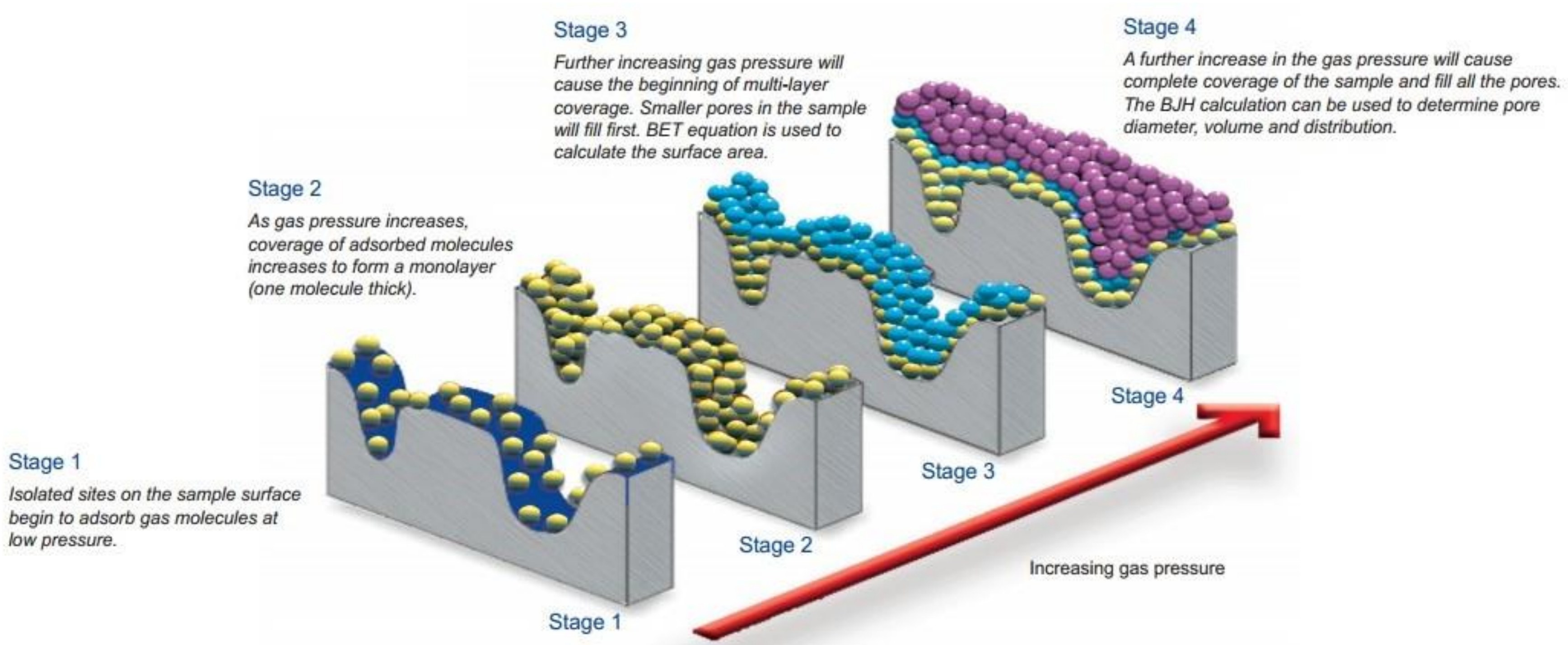

Figure 4.6: Adsorption procedure according to BET theory (Micromeritics, 2012)

In Figure 4.6, adsorption is illustrated by four stages according to BET theory (Micromeritics, 2012). As seen in Figure 4.6, at stage 1, at low pressures, adsorption starts on the surface of adsorbent. As pressure increases, coverage of adsorbed molecules increases to form a monolayer. Further increasing pressure causes to form multilayered adsorption .

4.5 Ono-Kondo Lattice Model

Adsorption occurs in gas separation, gas storage, shale gas and coalbed methane reservoirs at high pressures. However, there are not enough studies and models to represent adsorption at high pressures, especially for shales. Langmuir model is widely used but it is not suitable for especially high pressure adsorption. In Langmuir model, the volume of adsorbed phase is ignored and there is no correction for adsorbed phase volume (Sudibandriyo *et al.*, 2010).

With increasing pressure, excess (Gibbs) adsorption reaches peak and then starts decreasing especially for carbon dioxide. This indicates that the contribution of adsorption at high pressures is diminished as compared to the compression of bulk gas. At high pressures, bulk densities approach liquid or liquid-like densities. Therefore, excess (Gibbs) adsorption cannot generally be fitted especially for carbon dioxide by Langmuir model except at low pressures. (Leahy-Dios *et al.*, 2011).

By considering the drawbacks of adsorption models such as Langmuir model and other traditional methods, Ono-Kondo lattice model is based on lattice theory and was proposed originally by Ono and Kondo in 1960 and recently developed by Sudibandriyo. In this model, adsorption system is composed of layers of lattice cells that contain fluid molecules and vacancies. For the case of adsorption, more fluid molecules reside in the cells of the adsorbed-phase layers than in the cells of the bulk-phase layers (Sudibandriyo *et al.*, 2010).

Ono-Kondo model has several advantages (Sudibandriyo *et al.*, 2010):

1) It is used to describe multilayer adsorption (some molecules are adsorbed on already adsorbed molecules).
2) It has ability to describe the adsorption behavior based on the physical properties of adsorbate and adsorbent.
3) It is used to estimate adsorbed-phase densities, which provides calculation of absolute gas adsorption.
4) It was modeled to incorporate accurate density calculations from equation-of-state models, which reduce the correlative burden on the adsorption model.

In Ono-Kondo model, fluid system consists of lattice cells occupied by fluid molecules or just empty cells. When adsorption occurs, more molecules will occupy cells in adsorbed phase layer than gas phase (bulk) (Figure 4.7) (Sudibandriyo *et al.*, 2010).

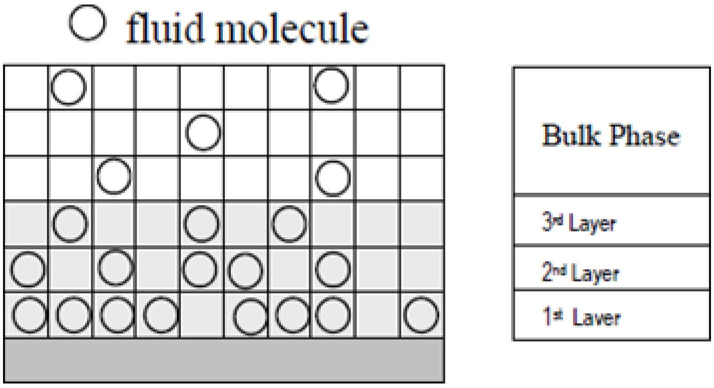

Figure 4.7: Approximation of Ono-Kondo lattice model to adsorption (Sudibandriyo *et al.*, 2010)

When equilibrium exists between gas-phase and multilayer adsorbed phase, the expression for thermodynamic equilibrium for pure-component adsorption under the mean-field approximation can be written as (Sudibandriyo *et al.*, 2010):

$$\ln\left[\frac{x_t(1-x_b)}{x_b(1-x_t)}\right]+\frac{z_0(x_t-x_b)\varepsilon_{ii}}{kT}+\frac{z_2(x_{t+1}-2x_t+x_{t-1})\varepsilon_{ii}}{kT}=0 \qquad (4.8)$$

For t = 2,3,..,m, number of the layer, and for 1st adsorbed layer:

$$\ln\left[\frac{x_1(1-x_b)}{x_b(1-x_1)}\right]+\frac{(z_1x_1+z_2x_2-z_0x_b)\varepsilon_{ii}}{kT}+\frac{\varepsilon_{is}}{kT}=0 \qquad (4.9)$$

where x_t is the reduced density or fraction of sites occupied by adsorbed molecules in layer t, x_b is the fraction of sites occupied by fluid molecules in the bulk. The fluid–fluid interaction energy is expressed by ε_{ii}/kT and the fluid–solid surface interaction energy is expressed by ε_{is}/kT, where k is Boltzman’s constant, and T is the absolute temperature.

For a hexagonal configuration of lattice cells, the coordination numbers z_0 and z_1 are 8 and 6, respectively; and by definition, $z_2 = (z_0 - z_1)/2$.

The analytical expression for the excess (Gibbs) adsorption from this model is:

$$\Gamma = C\sum_{t}^{m}(x_t - x_b) \qquad (4.10)$$

where C is a prefactor related to the capacity of the adsorbent for a specific gas, m is the maximum number of adsorbed layers in an adsorption isotherm. The reduced densities x_t and x_b are expressed as $x_t = \rho_t/\rho_{mc}$ and $x_b = \rho_b/\rho_{mc}$, where ρ_t and ρ_b are the adsorbed and the bulk density of the adsorbate at layer t, respectively, and ρ_{mc} is the adsorbed phase density at maximum capacity.

For simplicity, it was modeled as the adsorption as occurring within a slit. For monolayer adsorption inside a slit, the equilibrium expression is written as:

$$\ln\left[\frac{x_{ads}(1-x_b)}{x_b(1-x_{ads})}\right]+\frac{((z_1+1)x_{ads}-z_0x_b)\varepsilon_{ii}}{kT}+\frac{\varepsilon_{is}}{kT}=0 \qquad (4.11)$$

where $z_1 = 6$ and $z_0 = 8$ for the hexagonal lattice cell.

Excess (Gibbs) adsorption then simplifies to:

$$\Gamma = 2C(x_{ads}-x_b)=2C\left(\frac{\rho_{ads}}{\rho_{mc}}-\frac{\rho_b}{\rho_{mc}}\right) \qquad (4.12)$$

The parameters of the model: ρ_{mc}, ε_{ii}/k, ε_{is}/k and C, are obtained by fitting the model with experimental adsorption isotherm data. The parameters are fit when the average absolute percent deviation (AAD) in each isotherm is minimum. The AAD is calculated using the following equation.

$$ADD=\sum_{i}^{N}\left|\frac{n_{\exp}-n_{\mathrm{mod}el}}{n_{\exp}}\right|\times 100\% \qquad (4.13)$$

where n_{exp} and n_{model} are the adsorption capacity of the experimental data and the one calculated from the model, respectively.

4.5.1 Fluid-Fluid Energy Parameter Estimate

The fluid–fluid energy parameter, ε_{ii}/k, is estimated as being proportional to the Lennard–Jones well depth energy parameter (Sudibandriyo *et al.*, 2010).

The following estimate for the fluid–fluid energy parameter is used in Ono-Kondo model:

$$\varepsilon_{ii}=0.432\varepsilon^* \qquad (4.14)$$

where, ε^* is the well depth of the potential (Positive fluid-fluid enery parameters represent a repulsive energy potential. Negative fluid-fluid energy parameters represent an attraction energy potential).

In order to calculate the fluid-fluid energy parameter, the well depth of the potential is needed. In Table 4.1, the well depths of the potential of gases are listed.

Table 4.1: Physical properties of adsorbates and adsorbents (Reid *et al.*, 1987)

Adsorbate/Adsorbent	**Normal Boiling Point (K)**	**Reciprocal van der Waals co-volume (mol/L)**	**ε*/k (K)**
H_2	20.4	38.16	59.7
N_2	77.3	25.89	71.4
H_2S	212.8	23.08	301.1
CO_2	216.6	23.34	195.2
CH_4	111.7	23.37	148.6
C_2H_4	169.4	17.39	224.7
C_2H_6	184.6	15.41	215.7
C_3H_8	231.1	11.07	237.1
i-C_4H_{10}	261.4	8.60	330.1
Carbon	-	3.4	28
O (zeolite)	-	3.04	139.96

4.6 Two-parameter Ono-Kondo Model

Adsorbed phase densities and the fluid–fluid energy parameter can be estimated from the reciprocal van der Waals co-volume and from a proportional relation to the well depth of the Lennard–Jones 12-6 potential, respectively, as listed in Table 4.1.

In this study, it was preferred that ρ_{mc} (the adsorbed phase density at maximum capacity) is equal to reciprocal van der Waals co-volume (Table 4.1) because Sudibandriyo *et al.* (2010) found that maximum adsorbed density is close to reciprocal van der Waals co-volume of adsorbate. For two-parameter Ono-Kondo model, the fluid–solid energy parameter, ε_{is}/k, is regressed on each specific adsorption system and the parameter C is regressed on each adsorption isotherm. Hence, it is called two-parameter Ono-Kondo model. In this study, two-parameter Ono-Kondo model was preferred to evaluate experimental adsorption data (Appendix B).

4.7 Surface Area Estimation by using Ono-Kondo Lattice Model

Adsorption experimental data are also used to calculate surface area of adsorbent. Different adsorption isotherms such as BET are used to estimate surface area. Although commercial systems are available to measure surface area by the help of BET model, their cost is expensive. Hence, adsorption experiments with volumetric method are cheap compared to commercial systems for surface area determination.

Ono-Kondo lattice model is used to correlate high-pressure, supercritical adsorption isotherms. This model and its temperature dependence of the parameters are used to make the model capable of consistently calculating the surface area of any porous materials at any experimentally generated adsorption isotherm (Sudibandriyo, 2010).

Based on the evaluation of the regressed parameter C, it appears that the value of C increases as the surface area of the adsorbent increases. This suggests that the maximum adsorption capacity, C, can be divided into two contributions; the contribution from the adsorbent characteristic, represented by surface area (A, m^2/g), and the contribution from the adsorbate characteristic(s). The following simple relation is for the maximum adsorption capacity, C (Sudibandriyo, 2010):

$$C(T) = \frac{AC_a(T)}{2} \tag{4.15}$$

where, C_a is the surface adsorbed-phase density ($mmol/m^2$), with its value depending only on the adsorbate.

Furthermore, the maximum adsorption capacity, C can be expressed in term of the following equation 4.16:

$$\ln(1/C) = \delta T - \left[\ln C_{a,o} + \delta T_o + \ln(A/2)\right] \tag{4.16}$$

where T_o (K) is chosen at the normal boiling point of the adsorbate (triple point for carbon dioxide), T(K) is the absolute temperature, $C_{a,o}$ is the maximum surface adsorbed phase density at T_o, and δ is the thermal expansion coefficient of the adsorbed phase.

For all components studies, except carbon dioxide (CO_2), the mean thermal expansion coefficient of the adsorbed phase, δ, is approximately 0.0024 K^{-1}. For CO_2, δ is equal to 0.0039 K^{-1} and $C_{a,o}$ is equal to 0.0142 $mmol/m^2$. General equations for $C_{a,o}$ for each adsorbate is in term of following equation 4.17:

$$C_{a,o} = \frac{0.102}{\sigma^2} + 0.0034 \tag{4.17}$$

where σ: molecule diameter of adsorbate, angstrom

4.8 Ono-Kondo Lattice Model for Mixtures

Adsorption of mixtures of gases is complicated compared to adsorption of pure gases. Traditional adsorption models such as Langmuir model cannot be used for mixtures of gases. Ono-Kondo model for mixtures was developed by Sudibandriyo *et al.* (2011):

1) It has ability to derive a general equation for monolayer, random mixed-gas adsorption.

2) It is useful to predict mixture adsorption for selected multicomponent adsorption systems.

The equality of the chemical potential in the adsorbed and the bulk phases for each component leads to the following equilibrium equations for the binary mixed gas-adsorption for component A and B:

$$\ln\frac{x_A\left(1-x_{A,b}-x_{B,b}\right)}{x_{A,b}\left(1-x_A-x_B\right)}+\frac{\varepsilon_{AA}}{kT}\left(\left(z_1+1\right)x_A-z_0x_{A,b}\right)+\frac{\varepsilon_{AB}}{kT}\left(\left(z_1+1\right)x_B-z_0x_{B,b}\right)+\frac{\varepsilon_{As}}{kT}=0$$
(4.18)

$$\ln\frac{x_B\left(1-x_{A,b}-x_{B,b}\right)}{x_{B,b}\left(1-x_A-x_B\right)}+\frac{\varepsilon_{BB}}{kT}\left(\left(z_1+1\right)x_B-z_0x_{B,b}\right)+\frac{\varepsilon_{AB}}{kT}\left(\left(z_1+1\right)x_A-z_0x_{A,b}\right)+\frac{\varepsilon_{Bs}}{kT}=0$$
(4.19)

Thus, a general equilibrium equation for monolayer, random mixed-gas adsorption for each component can be written as:

$$\ln\frac{x_i\left(1-\sum_{j=1}^{n}x_j,b\right)}{x_{i,b}\left(1-\sum_{j=1}^{n}x_j\right)}+\sum_{j=1}^{n}\frac{\varepsilon_{ij}}{kT}\left(\left(z_1+1\right)x_j-z_0x_{j,b}\right)+\frac{\varepsilon_{is}}{kT}=0 \qquad (4.20)$$

Where the summation n is over all the components.

Further, a geometric combination rule is used to evaluate the interaction energy between molecules i and j,

$$\varepsilon_{ij}=\left(1+C_{ij}\right)\sqrt{\varepsilon_{ii}\varepsilon_{jj}} \qquad (4.21)$$

Where a binary interaction C_{ij} is introduced to facilitate calculation of the unlike-molecule interaction energy in cases where it may deviate from the geometric mean relation. In such case, the value of C_{ij} is determined by regression of the available adsorption data.

Excess (Gibbs) adsorption for each component is calculated using the following expression:

$$\Gamma_i = 2C_i^{pure}\left(x_i - x_{i,b}\right) \tag{4.22}$$

Where C_i^{pure} is the maximum adsorption capacity of the pure component.

The fractional coverage in the bulk phase, $x_{i,b}$ is obtained from the following equation:

$$x_{i,b} = \frac{y_i \rho_b}{\rho_{mc}} \tag{4.23}$$

where the bulk density, ρ_b, is calculated by using Peng-Robinson equation of state because the mixture adsorbed phase density is generally not available experimentally, the maximum density, ρ_{mc}, is estimated using the following ideal mixing rules:

$$\frac{1}{\rho_{mc}} = \frac{x_A^{Abs}}{\rho_{mc,A}} + \frac{x_B^{Abs}}{\rho_{mc,B}} \tag{4.24}$$

The absolute adsorbed-phase mole fractions, x_A^{Abs} and x_B^{Abs} are used in this equation. These mole fractions are calculated on the basis of absolute adsorbed amounts of each adsorbate rather than the excess (Gibbs) amounts adsorbed because the maximum adsorption capacity of a component may well be different in pure and mixture adsorption, a modification can also be introduced to calculate the Gibbs adsorption for each component. In this case, equation 4.21 becomes

$$\Gamma_i = 2\beta C_i^{pure}\left(x_i - x_{i,b}\right) \tag{4.25}$$

Where β is evaluated as follows

$$\beta = \sum_i^n \sum_j^n x_i^{Abs} x_j^{Abs} E_{ij} \tag{4.26}$$

where an additional binary interaction parameter, E_{ij}, is introduced in this expression in which E_{ii}=E_{ij}=1. E_{ij} is only used to test correlative capabilities of the model and is not needed when Ono-Kondo model is used in an entirely predictive model.

If z_i^{feed} represents the mole fraction of each component i in the feed, then, by molar balance, z_i^{feed} can be expressed terms of the other experimentally accessible variables as

$$z_i^{feed} = \frac{(n_{Gibbs})_i + \overline{V}_{void}\rho_b y_i}{n_{Gibbs}^{Total} + \overline{V}_{void}\rho_b} \tag{4.27}$$

where $(n_{Gibbs})_i$ is the Gibbs adsorption of component i, V_{void} is the void volume, ρ_b is the bulk density and y_i is the gas phase composition of component i.

In calculation process, equation 4.27 should be evaluated and satisfied for each component. If equation 4.27 is not satisfied for each component and each trial, then a new set of equilibrium mole fractions is used to calculate the next trial adsorbed amount. A matlab program was written in this study for binary mixtures of adsorption (Appendix B).

4.9 Equations of States

Peng and Robinson equations of states (EOS) and other traditional equations of states are not highly accurate. When pressure increases, errors in density values due to EOS calculations increase. Hence, more accurate equations of states, Span & Wagner for carbon dioxide and Angus for methane were used in this study in order to analyze experimental adsorption data. These equations of states are considered as most reliable equations of states (Angus *et al.*, 1978; Span and Wagner, 1996; Busch *et al.*, 2003). An online program on the website of NIST, USA was used to calculate the bulk densities for experimental excess adsorption calculations in this study. All equations of states on this website are highly accurate for each fluid (NIST, 2012).

CHAPTER 5

STATEMENT OF PROBLEM

In shale gas reservoirs, significant amounts of natural gas exist as conventional "free" gas in porous spaces as well as "adsorbed" gas on shale matrix. Before hydraulic fracturing and horizontal drilling operations, adsorption capacities and behaviors of shale gas reservoirs are needed to be investigated properly. Understanding adsorption capacities and behaviors of shale gas reservoirs may help exploitation and resource evaluation. In order to calculate shale gas-in place, the determination of adsorption capacity of a shale gas reservoir is very crucial because it is important both for feasibility and reservoir management studies.

The aim of this study is to determine initial gas-in place in shale gas reservoirs after conducting pure methane adsorption experiments with shale samples in Turkey because conventional initial gas-in place equations are not valid for these reservoirs due to the existence of free phase and adsorbed phase together.

Contrary to conventional gas reservoirs, in shale gas reservoirs, gas is both stored as adsorbed and free gas phases. In order to understand production mechanisms of these reservoirs, it is very important to understand adsorption phonemona. Adsorption experiments were conducted at different temperatures (25, 50, and 75 ^oC) to understand the effect of temperature on adsorption behaviors. Moreover, the effect of surface area on adsorption was investigated.

Additionally to pure methane adsorption experiments, pure carbon dioxide adsorption experiments on shale samples were conducted to understand the effect of carbon dioxide on adsorption behaviors of shale samples. The aim of carbon dioxide adsorption experiments is to investigate possible storage of carbon dioxide in shale gas reservoirs after depletion or as a recovery technique.

It is also aimed to evaluate raw experimental adsorption data by using Langmuir model and Ono-Kondo models. By using Ono-Kondo monolayer model and three-layer model, layered structure of adsorption on shale samples were investigated. Moreover, by using Ono-Kondo monolayer model data of the experiments of pure methane and pure carbon dioxide, a theoretical approach to binary mixtures of adsorption of methane and carbon dioxide was investigated.

CHAPTER 6

EXPERIMENTAL SET-UP AND PROCEDURE

6.1 Type of Adsorption Experiments

Adsorption experiments are conducted by different methods. However, volumetric method and gravimetric method are widely used for adsorption measurements:

6.1.1 Gravimetric Method

In gravimetric method, adsorption capacity is determined by monitoring the weight of sample in a gas phase at well-defined pressure and temperature conditions (Humayun and Tomasko, 2000).

In gravimetric method, the weight change of adsorbent sample in the gravity field due to adsorption from gas phase is recorded. Various types of sensitive microbalance were developed for this purpose. A continuous-flow gravimetric technique coupled with wavelet rectification allows for higher precision, especially in the near-critical region (Ming, 2009). In Figure 6.1, schematic diagram of gravimetric apparatus is shown (Saghafia et al., 2007).

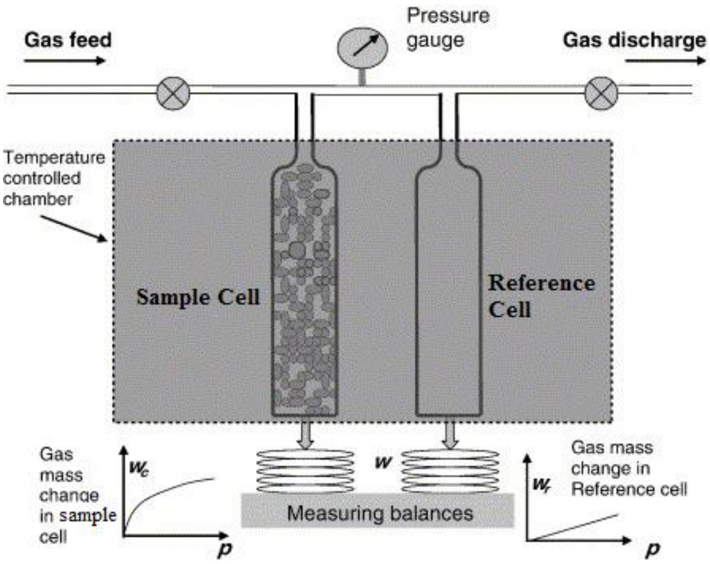

Figure 6.1: Schematic diagram of gravimetric apparatus (Saghafia *et al.*, 2007)

6.1.2 Volumetric Method

Volumetric method is one of the most common methods for adsorption experiments. In volumetric method, adsorption capacity is determined by measuring pressure changes in reference cell and sample cell (Mavor *et al.*, 1990). In this study, volumetric method was used to measure adsorption because it is cheap and easy to apply compared to gravimetric method.

6.2 Experimental Equipment and Procedure

In this study, a volumetric adsorption apparatus was designed and constructed for BPL activated carbon and shale samples' adsorption measurements. Accurate measurements of adsorption in shales are difficult because of the relatively small adsorptive capacities compared to coalbed methane and the relatively small volumes of samples that are available. Hence, it is very important to have careful attention to experimental accuracy in design of cell volumes, temperature control, and experimental procedures.

6.2.1 Reliability of Adsorption Experiments

In order to prove the reliability of the experiments conducted in this study, adsorption capacities of pure methane and pure carbon dioxide on BPL activated carbon were investigated. The results of these experiments were compared with Reich *et al.* (1980)'s experimental adsorption data. Moreover, some experiments with shale samples were reconducted to show the repeatability of adsorption experiments in this study.

6.2.2 Sample Preparation

Adsorption experiments were performed on powdered samples such as BPL activated carbon and shale samples that were ground and sieved different mesh sizes. Sample A and B, obtained from different shale gas reservoirs in Turkey, were used in this study. Shale and BPL samples were dried by placing in a vacuum oven at 120 ^{o}C for 24 hours until constant mass was achieved before each isotherm measurement. This procedure was used to ensure that samples were completely dry and that any adsorbed gas was completely removed from the samples.

6.2.3 Experimental Procedure

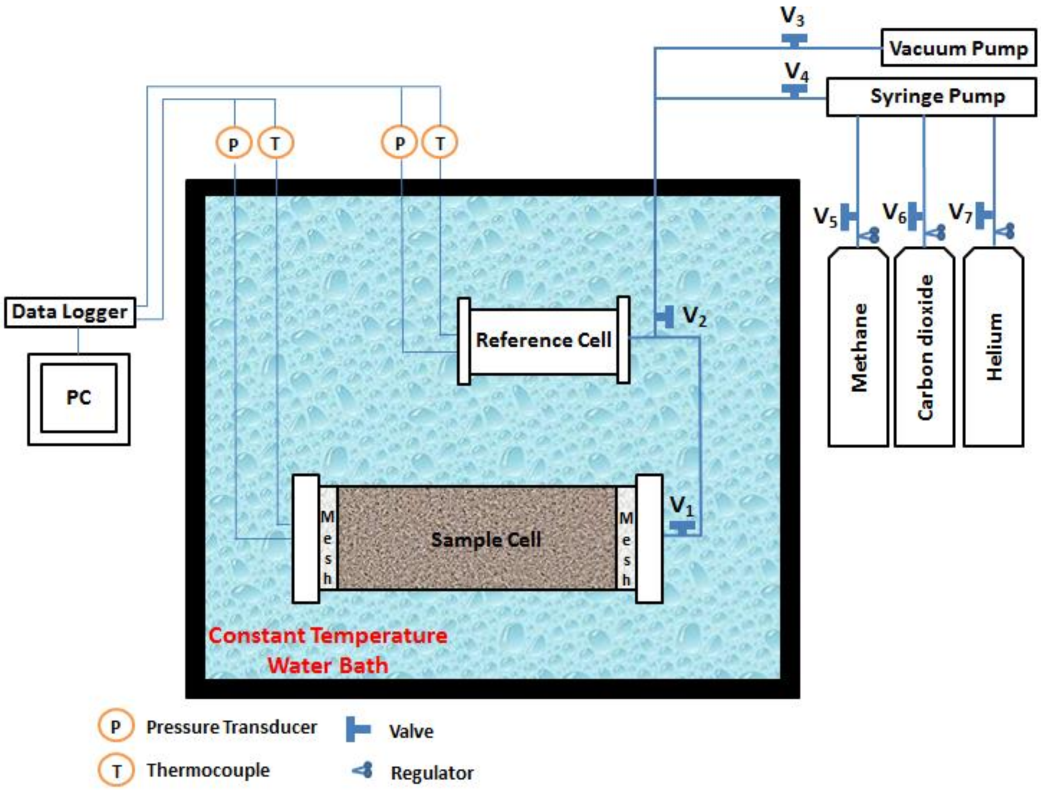

Figure 6.2: Schematic of volumetric experimental setup used in this study

As shown in Figure 6.2, Figure 6.3 and Figure 6.4, the equipment used in this study are listed:

1) Constant Temperature Water Bath
2) Sample cell
3) Reference cell
4) Pressure Transducers
5) Thermocouples
6) PC
7) Data Logger
8) Helium Bottle (99.99% Purity)
9) Methane Bottle (99.99% Purity)
10) Carbon dioxide Bottle (99.99% Purity)
11) Syringe Pump
12) Weighing Balance
13) Screens
14) Lines, fittings, and valves

Figure 6.3: General view of volumetric experimental set-up used in this study

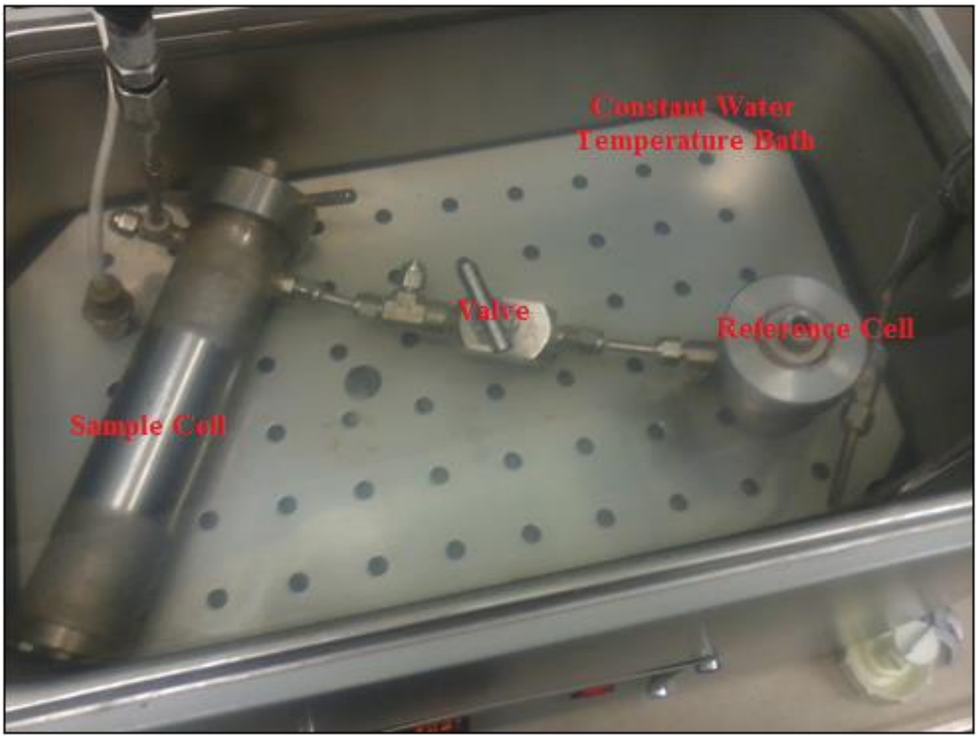

Figure 6.4: Sample cell and reference cell in constant temperature water bath

Before the start of an adsorption experiment, the void volume of the sample cell is determined volumetrically using helium because helium is non-adsorbing and inert gas. For void volume calculations and adsorption experiments, almost same experimental procedure is used. Helium void volume measurements were done at room temperature (25 ^{o}C).

For the experiments conducted in this study, the following experimental procedure was used (Figure 6.5):

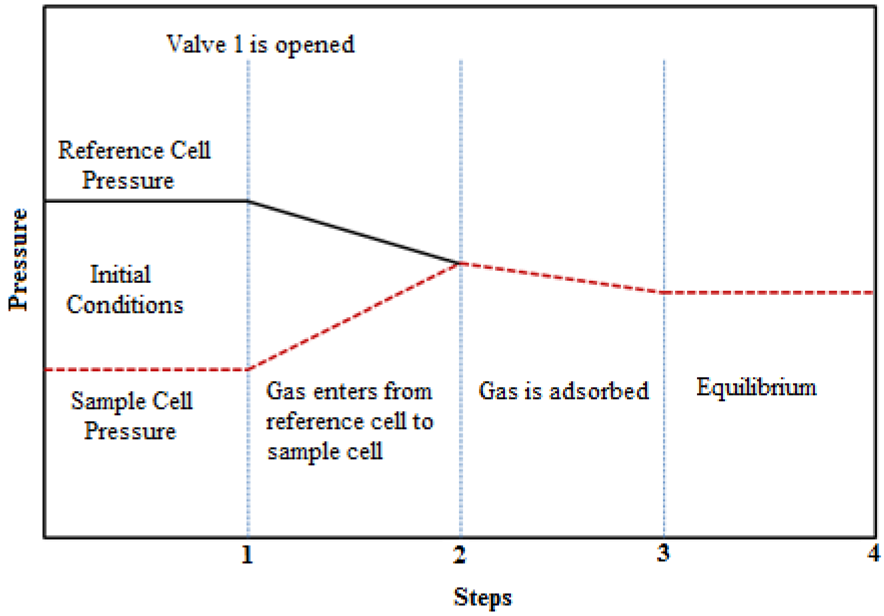

Figure 6.5: Procedure for gas injection by using volumetric experimental set-up

1) The entire apparatus is maintained in a constant temperature water bath.
2) The sample cell is filled with adsorbent to be studied. The weight of adsorbent is recorded in the sample cell. Then, after making connections between the sample cell and the reference cell, the whole system is put into the constant temperature water bath.
3) At the beginning of the experiment, the sample cell, the reference cell and connections such as lines, fittings, valve, etc. are evacuated from air by a vacuum pump to establish defined starting conditions.
4) After vacuuming, all valves in the system are closed. As seen in Figure 6.2 and Figure 6.4, the sample cell and the reference cell are separated by closing the shut-off valve V_1.
5) In the next step, a certain amount of gas is admitted to the reference cell by opening the gas access valves V_2 and V_4. Desired pressure values in the reference cell are supplied by syringe pump. After desired pressure is satisfied in the reference cell, the valve V_2 is closed, a certain time is allowed for pressure and temperature equilibration in the reference cell. Using Angus *et al.* (1978) equation of state (EOS) for methane and Span & Wagner (1996) EOS for carbon dioxide, the amount of substance (moles of gas) in the reference cell can be computed from the pressure, the temperature and the volume of the reference cell.

6) Then, the valve V_1 between the reference cell and the sample cell is opened. Gas (adsorbate) is admitted to the sample cell from the reference cell. Then, adsorption starts.

7) Until pressure equilibrium in the sample cell is satisfied, pressure and temperature values are recorded in every 10 seconds both in the sample cell and the reference cell.

8) By measuring pressure values before and after expansion both in the sample cell and the reference cell, gas molar densities at different stages are calculated using an appropriate equation of state (EOS) and the amount of gas adsorbed at one pressure level is calculated.

9) Adsorption isotherm is constructed by repeating these procedures until the measurement at the highest desired gas pressure is achieved (200 psia increments are preferred generally for adsorption at high pressures).

6.2.4 The Key Points for Adsorption Experiments of Shale Samples

In shale gas reservoirs, adsorption capacity is very low compared to coal and activated carbon's adsorption capacities. Hence, experimental uncertainties are very important for most accurate adsorption experiments in shale gas reservoirs.

In this study, some key points suggested by Mohammad *et al.* (2009) to decrease experimental uncertainties in adsorption experiments were used:

- ✓ Before starting to adsorption experiments, pressure transducers and thermocouples are calibrated.
- ✓ Prior to measuring adsorption isotherms, apparatus is checked for pressure leaks. Adsorption isotherms are measured only when no leaks are observed in the system over a period of 24 hours.
- ✓ Equilibrium pressure in sample cell is indicated by the constancy of recorded pressure (usually within 6 to 12 hours for shale samples).
- ✓ Experimental adsorption measurement accuracy increases when the ratio of reference cell volume to sample cell volume decreases. It is advised that the ratio of volumes of sample cell to reference cell should be at least 2.0 (This ratio in this study is around 2.76).
- ✓ Void volume is minimized by filling sample cell with as much of shale sample is possible and minimizing the remaining dead space within apparatus (in lines, fittings, etc.).
- ✓ The particular EOS for each gas is chosen based on the National Institute for Standards and Technology (NIST) recommendation (0.1 % errors in density calculations). The reason is that as pressure increases, error in density increases in traditional EOS.

✓ Unit conversions are very important because different units are used in the evaluation of adsorption. The amount of adsorbed gas is presented as mmol/g of shale on a dry basis (1 mmol/g=759 scf/ton).

The properties of the equipment used in this study are listed in Table 6.1:

Table 6.1: Specifications of the equipment used in the experimental set-up

Pressure Transducers	
Trademark	Keller Sensors
Pressure Range	0 – 250 bar G
Output	4 - 20 mA
Supply	12 to 35 V
Precision	± 1 psig
Thermocouples	
Trademark	Elimko
Model	PT - 100
Temperature Range °C	5 to +99.9
Precision	± 0.2 °C
Data Logger and Controller	
Trademark	Elimko
Model	E-680-08-2-0-16-1-0
Voltage	220 V
Data Transfer	RS485 Mod Bus
Data Analysis	A package program of Elimko, Turkey
High Pressure Syringe Pump	
Trademark	Teledyne Isco
Model	500D Pump Module
Capacity	507 ml
Flow Range ml/min	0. 001 - 204
Flow Accuracy	0.5% of setpoint
Vacuum Pump	
Trademark	Javac, England
Model	DS40
Voltage	220 V/ 50 Hz
Type	Single Stage High Vacuum
Weighing Balance	
Trademark	Avery Berkel
Weighing Range	0-6 kg
Weighing Accuracy	6 kg x 0.1 g & 600 g x 0.01 g

Table 6.1 (Continued): Specifications of the equipment used in the experimental set-up

Constant Temperature Water Bath	
Trademark	Kocintok Constant Temperature Water Bath
Model	Standard
Capacity	30 lt
Powers	230 V, 50 Hz
Temperature range	+5 ^{o}C to 99.9 ^{o}C
Temperature accuracy	± 0.1 °C
Temperature sensor	Fe-Const

CHAPTER 7

EVALUATION OF EXPERIMENTAL ADSORPTION DATA

7.1 Evaluation of Adsorption Experiments' Raw Data

The reference cell and the sample cell are placed into the constant water temperature bath. The sample cell is filled completely with adsorbent. Then, the sample cell, the reference cell and all the connections in the system are evacuated from air by the vacuum pump. After that, void volume in the sample cell is determined by injecting helium. Helium is an inert gas and its adsorption is considered to be zero (McCarthy and Arp, 1990; Arri *et al.*, 1992; Mohammad *et al.*, 2009a; Chareonsuppanimit *et al.*, 2012).

By using measured pressure values during injection of helium gas from the reference cell to the sample cell, void volume is calculated as in Equation 7.1:

$$V_{void} = \frac{V_{ref}\left(\frac{P_{ref1}}{z_{ref1}} - \frac{P_{ref2}}{z_{ref2}}\right)}{\frac{P_{void2}}{z_{void2}} - \frac{P_{void1}}{z_{void1}}} \tag{7.1}$$

where V_{void}: is the void volume of the sample cell, V_{ref}: is the volume of the reference cell, P_{ref1}: pressure of the reference cell before expansion, Z_{ref1}: compressibility factor of gas in the reference cell before expansion, P_{ref2}: pressure of the reference cell after expansion, Z_{ref2}: compressibility factor of gas in the reference cell after expansion, P_{void1}: pressure in the void volume of the sample cell before expansion, Z_{void1}: compressibility factor of gas in the void spaces of the sample cell before expansion, P_{void2}: pressure in the void volume of the sample cell after expansion, Z_{void2}: compressibility factor of gas in the void spaces of the sample cell after expansion

Helium void volume measurements were performed at room temperature (25 ^{o}C) as gas adsorption isotherms and over a range of pressures from atmospheric to about 2000 psi in intervals of 200 psia for shale samples.

In this study, after gas was expanded from the reference cell to the sample cell, adsorption equilibrium pressure values were recorded when the pressures of the sample cell were constant (6 to 12 hours for shales).

Injected gas amounts from the reference cell to the sample cell were calculated by using the appropriate EOS (NIST, 2012). Then, adsorption capacities were calculated. Moreover, a Matlab program was written in this study for adsorption calculations to analyze experimental data (Appendix B).

Excess (Gibbs) adsorption is expressed as in Equation 7.2:

$$n_{ads}^{Gibbs} = \left(n_{inj} - n_{unads}^{Gibbs}\right) \big/ W \qquad (7.2)$$

where n_{ads}^{Gibbs}: Excess (Gibbs) adsorption, mmol/g, n_{inj}: injected gas amount from reference cell to sample cell, mmol, n_{unads}^{Gibbs}: amount of free gas in the sample, mmol, W: weight of sample in the sample cell, g.

The amount of gas injected from the reference cell to the sample cell can be determined from pressure, temperature:

$$n_{inj} = \frac{V_{ref}}{RT}\left(\frac{P_{ref1}}{z_{ref1}} - \frac{P_{ref2}}{z_{ref2}}\right) \qquad (7.3)$$

The amount of unadsorbed gas (free gas) in the sample cell at equilibrium pressure is calculated by using the following formula:

$$n_{unads}^{Gibbs} = \frac{V_{void}}{RT}\left(\frac{P_{void2}}{z_{void2}}\right) \qquad (7.4)$$

7.1.1 Gas Compressibility Factor for Helium

The compressibility factor of helium is calculated by using Equation 7.5. For the calculation of helium compressibility factor, there is a general formula of the National Bureau of Standards Technical Note 631 for Helium (Sudibandriyo *et al.*, 2003).

$$Z_{He} = 1 + \frac{\left(0.001471 - 0.000004779T + 0.00000000492T^{2}\right)}{P} \qquad (7.5)$$

Where T: temperature, K and P: pressure, atm

7.1.2 Gas Solubility in Water

If a shale gas reservoir has high water content in fractures and/or porous spaces, solubility of gas in water becomes important for adsorption experiments. Hence, for the most accurate adsorption capacity, the amount of gas dissolved in water should be subtracted from adsorbed amount (Hall *et al.*, 1994; Mohammad *et al.*, 2009a);

$$n_{ads}^{Gibbs} = n_{inj} - n_{unads}^{Gibbs} - n_{sol} \tag{7.6}$$

where n_{sol}: the amount of gas solved in water

To calculate the gas solubility in water as a function of pressure, an empirical equation is used for temperatures around 318 ^{o}K (Mohammad *et al.*, 2009a),

$$x_{gas} = \frac{P}{a + bP + cP^2} \tag{7.7}$$

Table 7.1: Parameters for CH_4 and N_2 solubility in water at temperatures around 318 ^{o}K (Mohammad et al., 2009a)

Constant	Units of constant	Methane	Nitrogen
a	MPa	5302.07	10204.24
b	-	150.4	127.3
c	1/MPa	-0.78	-0.09

The solubility of methane and nitrogen in water are small compared to carbon dioxide's solubility in water. Hence, the parameters in Table 7.1 can be used for methane and nitrogen at different temperatures. However, the solubility of carbon dioxide (CO_2) is high in water. For carbon dioxide, between 313.2 ^{o}K and 348.2 ^{o}K, the empirical formula is shown in equation 7.8 (Chareonsuppanimit *et al.*, 2012). Thus, the mole fraction of CO_2 present in water (x_{CO2}) at temperature T (in ^{o}K) and pressure P (in MPa) is given as

$$x_{CO_2} = \frac{P}{a + (b_1 + b_0 T)P + (c_1 + c_o T)P^2} \tag{7.8}$$

Table 7.2: Parameters for CO_2 solubility in water at multiple temperatures (Chareonsuppanimit et al., 2012)

Constant	Value	Units
a	272.21	MPa
b_1	-332.64	-
b_0	1.06683	1/K
c_1	19.18	1/MPa
c_0	-0.0561	1/(MPa K)

The amount of CO_2 dissolved in water (n_{sol}) can be given as

$$n_{sol} = \frac{x_{CO_2} n_{water}}{\left(1 - x_{CO_2}\right)} \tag{7.9}$$

The amount of gas dissolved in water (n_{water}) is taken as the product of mole fraction of CO_2 and the amount of water in moles in the system. Thus, the amount of CO_2 dissolved in water per unit mass of sample is expressed as

$$n_{sol} \cong \frac{x_{CO_2} n_{water}}{m_{sample}} \tag{7.10}$$

where n_{water} is the amount of water in moles and m_{sample} is the mass of adsorbent in the system.

7.2 Adsorbed Phase Density

The volume of gas adsorbed on the surface of adsorbent is ignored in excess (Gibbs) adsorption calculations. However, the volume of gas adsorbed on the surface of adsorbent is important, especially at high pressures. The volume of adsorbed gas cannot be calculated directly by using experimental data. For the calculation of the volume of adsorbed gas, it is essential to determine adsorbed phase density.

Bulk density of gas is very low compared to density of adsorbed gas. For example, for methane, adsorbed methane forms a 0.38 nm thickness of monolayer and the adsorbed phase density is 1.8-2.5 times larger than the density of bulk methane (Ambrose *et al.*, 2010).

There are different approaches for the calculation of adsorbed phase density. Adsorbed density is considered to be almost equal to reciprocal value of the Van der Waals co-volume (b) (Dubinin, 1960; Haydel *et al.*, 1967; Sudibandriyo *et al.*, 2010). Menon (1968) and Arri *et al.* (1992) stated that adsorbed density is equal to liquid density of gas at the atmospheric pressure boiling point.

The volume of adsorbed gas depends on temperature, pressure, and pore size. For example, 100 nm pore, the volume of adsorbed phase is insignificant, but, for 1 nm pore, the volume of adsorbed phase is quite important (Ambrose *et al.*, 2010). Therefore, the volume of adsorbed phase is very important for absolute adsorption calculations.

7.3 Absolute Adsorption Calculations

In order to calculate absolute adsorption, the adsorbed density of gas is needed. When adsorption equilibrium pressure in the sample cell increases, the volume occupied by adsorbed gas increases. Hence, this reduces void volume in the sample cell.

Void volume of the sample cell is measured by using helim (non-adsorbing) before adsorption experiment starts. However, when adsorbate (gas) is adsorbed by adsorbent (sample), void volume decreases because of the volume of adsorbed layer. If void volume is not corrected, free gas amount in the void spaces of the sample cell is calculated excessively, but adsorption capacity is calculated less than its actual value called absolute adsorption. Adsorption capacity calculated without void volume correction is called excess(Gibbs) adsorption (Sudibandriyo *et al.*, 2003; Mohammad *et al.*, 2009b).

Figure 7.1: Helium void volume correction after adsorption

At lower pressures, the volume of adsorbed phase is negligible. Hence,

$$V_{void}^{He} \approx V_{unads} \tag{7.11}$$

$$n_{ads}^{abs} = n_{ads}^{Gibbs} = n_{inj} - \rho_{gas} V_{void}^{He} \tag{7.12}$$

At higher pressures, the volume of adsorbed phase is significant (Figure 7.1).

$$V_{void}^{He} = V_{unads} - V_{ads} \tag{7.13}$$

$$n_{ads}^{abs} = n_{inj} - \rho_{gas} V_{void}^{He} - \rho_{ads} V_{ads} \tag{7.14}$$

By combining Equation 7.13 and Equation 7.14, Equation 7.15 is obtained for absolute adsorption (Sudibandriyo *et al.*, 2003):

$$n_{ads}^{abs} = \frac{n_{ads}^{Gibbs}}{\left(1 - \dfrac{\rho_{gas}}{\rho_{ads}}\right)} \tag{7.15}$$

where V_{void}^{He}: void volume in sample cell, V_{unads}: volume of unadsorbed gas in sample cell, n_{ads}^{abs}:absolute adsorption, n_{ads}^{Gibbs}: excess (Gibbs) adsorption, n_{inj}: moles of injected gas from reference cell to sample cell, ρ_{gas}: density of gas (Bulk phase), ρ_{ads}: density of adsorbed gas

7.4 Swelling of Shales

In adsorption experiments, swelling of shales is generally ignored. However, Kumar *et al.* (2010) studied the change in permeability in Marcellus shale due to swelling when exposed to methane and carbon dioxide. At first, for carbon dioxide, they observed that the permeability of shale was reduced to half of its original value. However, after a sufficient interaction, they observed that the permeability of sample returned to its original value. Hence, it cannot be concluded that there is no swelling in shales. In many adsorption experiments conducted by Sudibandriyo *et al.* (2003), Mohammad *et al.* (2009a) and Chareonsuppanimit *et al.* (2012), the swelling properties of shale samples were ignored. Thus, no swelling corrections were done in the data reduction of this study.

7.5 Initial Gas in Place Calculations in Shale Gas Reservoirs

For gas reservoirs, the calculation of initial gas in place is very important for the future decisions about gas field. However, initial gas in place calculation in shale gas reservoirs is quite different from other conventional gas reservoirs. Initial gas in place calculations in shale gas reservoirs are difficult to calculate because gas is stored both as free phase and adsorbed phase. Ambrose *et al.* (2010) suggested a new technique for initial shale gas in place calculations (Figure 7.2):

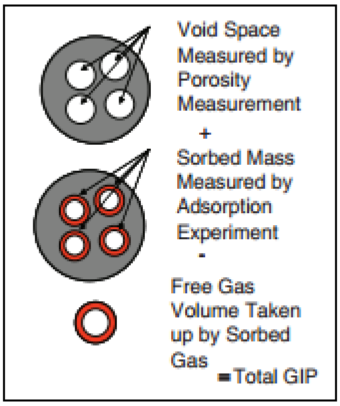

Figure 7.2: A method in predicting shale gas in-place; for simplicity, oil and water volumes are not shown (Ambrose *et al.*, 2010)

Shale gas in-place is calculated in the following (Ambrose *et al.*, 2010):

$$G_{st} = G_f + G_a + G_{so} + G_{sw} \tag{7.16}$$

where G_{st}: total gas in place, scf/ton, G_f: free gas in the pore space scf/ton, G_a: gas adsorbed on the surface, scf/ton, G_{so}: gas dissolved into the liquid hydrocarbon, scf/ton, G_{sw}: gas dissolved into the formation water, scf/ton.

Where the components of storage on the right side are defined as

$$G_f = 32.0368 \frac{\phi(1 - S_w - S_o)}{\rho_b B_g} \tag{7.17}$$

$$G_a = G_{sL} \frac{P}{P + P_L} \tag{7.18}$$

$$G_{so} = 5.706 \frac{\phi S_o R_{so}}{\rho B_o} \tag{7.19}$$

$$G_{sw} = 5.706 \frac{\phi S_w R_{sw}}{\rho B_w} \tag{7.20}$$

where P: pressure, psia, P_L: Langmuir pressure, psia, G_{sL}: Langmuir Volume, scf/ton , R_{so}: solution-gas/oil ratio, scf/STB, R_{sw}: solution-gas/water ratio, scf/STB, B_g: gas formation factor, rcf/scf, B_o: oil formation factor, rbbl/stb, B_w: water formation volume, rbbl/stb, S_o: oil saturation, dimensionless, S_w: water saturation, dimensionless, ρ_b: bulk-rock density, g/cm^3, ϕ: total porosity fraction, dimensionless

In industry generally, G_{so} and G_{sw} are ignored. Then, Equation 7.21 is used (Ambrose *et al.*, 2010).

$$G_{st} = G_f + G_a \tag{7.21}$$

Then, total gas-in place is calculated for shale gas reservoirs by using Equation 7.22:

$$G_T = 32.0368 \frac{\phi(1 - S_w - S_o)}{\rho_b B_g} + \left(G_{sL} \frac{P}{P + P_L} \right) \tag{7.22}$$

The free gas volume G_f corrected for the fraction of porosity consumed by adsorbed gas volume in shale gas reservoir, ϕ_a , can be expressed as:

$$G_f = 32.0368 \frac{\phi(1 - S_w - S_o) - \phi_a}{\rho_b B_g} \tag{7.23}$$

where ϕ_a , for a single-component fluid system, can be written as:

$$\phi_a = 1.318 \times 10^{-6} \hat{M} \frac{\rho_b}{\rho_s} (G_a) \tag{7.24}$$

which, in the case of organic-rich shale with nanopores, is expected to occupy a significant pore volume thus reduce porosity available for the free gas storage under live, in-situ, reservoir conditions (Ambrose *et al.*, 2010). Then, equation 7.16 (total shale gas-in place), for a reservoir consisting of pure gas species, can be expressed as follows:

$$G_T = \frac{32.0368}{B_g} \left[\frac{\phi(1 - S_w)}{\rho_b} - \frac{1.318 \times 10^{-6} \hat{M}}{\rho_s} \left(G_{sL} \frac{P}{P + P_L} \right) \right] + \left(G_{sL} \frac{P}{P + P_L} \right)$$

(7.25)

where G_T: total gas in place, scf/ton, $\hat{M}$: apparent natural-gas molecular weight, lbm/lbmole, P: pressure, psia, P_L : Langmuir pressure, psi, S_w: water saturation, dimensionless, ρ_b: bulk-rock density, g/cm^3, ρ_f: free-gas-phase density, g/cm^3, ρ_s : sorbed-phase density, g/cm^3, ϕ: total porosity fraction, dimensionless, ϕ_a: sorbed-phase porosity fraction, dimensionless

Sorbed-phase density of methane equals to 0.34 g/cm^3 according to molecular modeling and simulation of methane adsorption in organic slit-pores (Ambrose *et al.*, 2010).

CHAPTER 8

RESULTS & DISCUSSION

In this study, adsorption experiments were conducted by using BPL activated carbon, shale sample A and shale sample B. The aim of the experiments conducted by using BPL was to show the reliability of the adsorption experiments in this study. Shale sample A and B were used to construct the adsorption isotherms of pure methane and pure carbon dioxide. By using these isotherms, shale gas-in place calculations were done for the cases in this study. In the following parts, the details of all the adsorption experiments in this study are shown. Table 8.1 summarizes the experiments that were conducted.

Table 8.1: Experiments conducted throughout this study

Run#	Explanation
1	Methane adsorption experiment with BPL at 28.3 ^{o}C to show the reliability of the experiments in this study.
2	Methane adsorption experiment with BPL at 28.3 ^{o}C to show the repeatability of the experiments in this study.
3	Carbon dioxide adsorption experiment with BPL at 28.3 ^{o}C to show the reliability of the experiments in this study.
4	Methane adsorption experiment with shale sample A at 25 ^{o}C to construct adsorption isotherm.
5	Methane adsorption experiment with shale sample A at 50 ^{o}C to construct adsorption isotherm.
6	Methane adsorption experiment with shale sample A at 75 ^{o}C to construct adsorption isotherm.
7	Carbon dioxide adsorption experiment with shale sample A at 25 ^{o}C to construct adsorption isotherm.
8	Carbon dioxide adsorption experiment with shale sample A at 50 ^{o}C to construct adsorption isotherm.
9	Carbon dioxide adsorption experiment with shale sample A at 75 ^{o}C to construct adsorption isotherm.
10	Methane adsorption experiment with shale sample B at 25 ^{o}C to construct adsorption isotherm.
11	Methane adsorption experiment with shale sample B at 25 ^{o}C to show the repeatability of the experiments in this study.
12	Methane adsorption experiment with shale sample B at 50 ^{o}C to construct adsorption isotherm.

Table 8.1 (Continued): Experiments conducted throughout this study

Run#	Explanation
13	Methane adsorption experiment with shale sample B at 75 °C to construct adsorption isotherm.
14	Carbon dioxide adsorption experiment with shale sample B at 25 °C to construct adsorption isotherm.
15	Carbon dioxide adsorption experiment with shale sample B at 50 °C to construct adsorption isotherm.
16	Carbon dioxide adsorption experiment with shale sample B at 75 °C to construct adsorption isotherm.
17	Methane adsorption experiment with shale sample B at 25 °C to show the effect of mesh size on adsorption.

8.1 Adsorption Experiments Results of BPL Activated Carbon

Adsorption experiments on BPL activated carbon were conducted by Reich *et al.* (1980) at 28.3 °C. Before starting to conduct adsorption experiments with shale samples, it is very important to show the reliability of adsorption experiments and calculation procedures. Hence, in these experiments, adsorption experiments of pure methane and pure carbon dioxide on BPL activated carbon at 28.3 °C were conducted by using the same procedure with Reich *et al.* (1980)'s experiments. Moreover, in order to show the repeatability of adsorption experiments in this study, Run#1 was repeated with Run#2. In Figure 8.1, a picture of BPL activated carbon used in this study is shown.

Figure 8.1: A picture of BPL activated carbon used in this study

8.1.1 Run#1 & Run#2: Methane Adsorption on BPL at 28.3 °C

In these experiments, 20/85 mesh size and 20 mesh size BPL samples were used. Moreover, before starting the experiments, BPL samples were heated at 120 °C for 24 hours to avoid any moisture and its effects. Samples were filled into the sample cell for Run#1 and Run#2 (Table 8.2).

Table 8.2: Run#1 & Run#2's experimental data

		Run#1	**Run#2**
Reference Cell Volume	**:**	40.5 cm^3	40.5 cm^3
Temperature	**:**	28.3 °C	28.3 °C
Sample Weight	**:**	46.7 g	46.5 g
Sample Cell Volume	**:**	122.4 cm^3	122.4 cm^3
Mesh Size	**:**	20/85	20
Average Void Volume	**:**	84.13 cm^3	82.92 cm^3

After placing the sample cell into the constant temperature water bath, void volumes of the sample cell were measured by using helium because helium is an inert gas and its adsorption is negligible. Void volumes of the sample cell were measured at different pressures both for Run#1 and Run#2 at room temperature (25 °C). Average values of void volumes at different pressures were used in calculations both for Run#1 and Run#2 (Figure 8.2 and Figure 8.3). Although samples were squeezed well into the sample cell, void volumes of both Run#1 and Run#2 are quite high. This is due to high porous structure of BPL activated carbon.

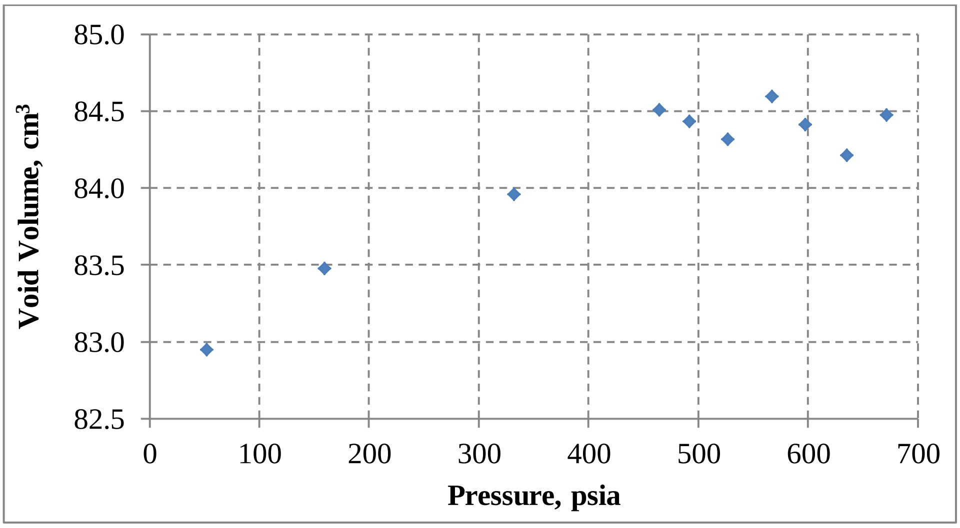

Figure 8.2: Run#1- Helium void volume of the sample cell filled with BPL

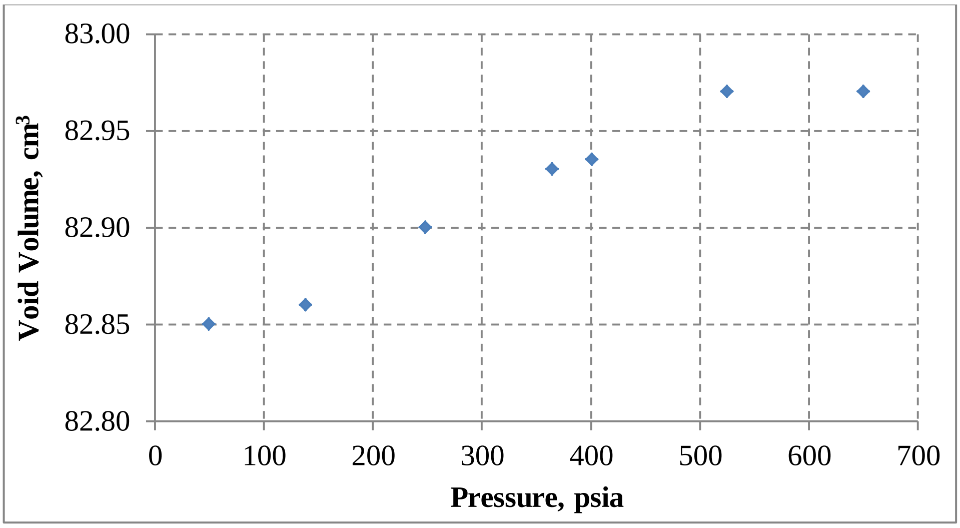

Figure 8.3: Run#2- Helium void volume of the sample cell filled with BPL

Before starting to inject methane into the system, leakage tests were conducted by using helium at 700 psia for 24 hours. When there was no leakage in the system for 24 hours, adsorption experiments with methane on BPL at different pressure stages were conducted at 28.3 ^{o}C. For every pressure increments, after expansion of methane from the reference cell into the sample cell, it was waited for the equilibrium of pressure. Furthermore, by using a matlab program written in this study, excess (Gibbs) adsorption values and absolute uncertainties in excess (Gibbs) adsorption capacities due to uncertainties in pressure transducers, thermocouples, volumes of cells, etc. were calculated for each pressure stages and listed in Table 8.3 (Appendix A and B).

Table 8.3: Run#1 & Run#2's methane adsorption on BPL at 28.3 ^{o}C

Run#1			**Run#2**		
Pressure ,psia	*Excess (Gibbs) Adsorption, mmol/g*	*Absolute Uncertainty in Excess Adsorption, mmol/g*	*Pressure ,psia*	*Excess (Gibbs) Adsorption, mmol/g*	*Absolute Uncertainty in Excess Adsorption, mmol/g*
23	0.946	0.032	13	0.523	0.021
58	1.603	0.033	31	1.113	0.035
128	2.496	0.032	73	1.892	0.036
229	3.284	0.031	160	2.804	0.033
303	3.663	0.033	261	3.426	0.033
380	3.936	0.034	341	3.768	0.034
443	4.015	0.035	-	-	-

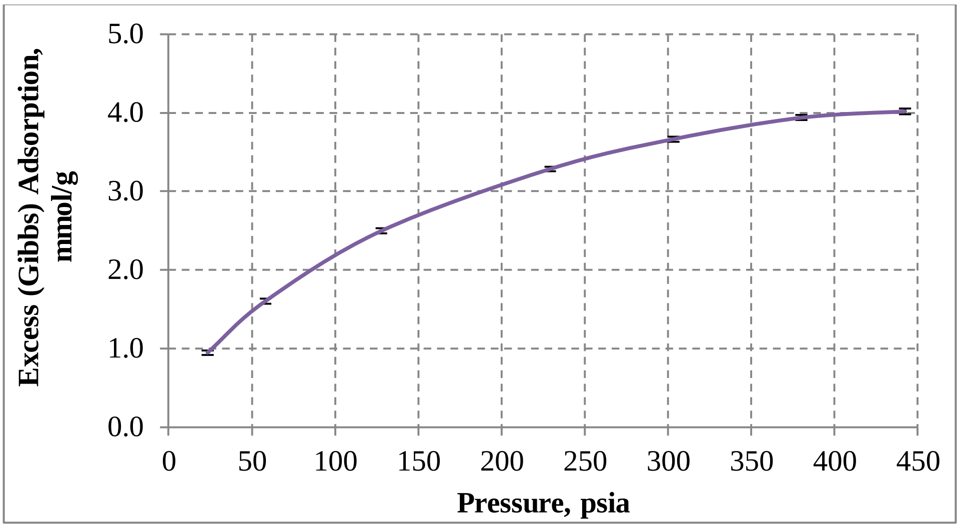

Figure 8.4: Run#1- Methane adsorption isotherm of BPL at 28.3 ^{o}C

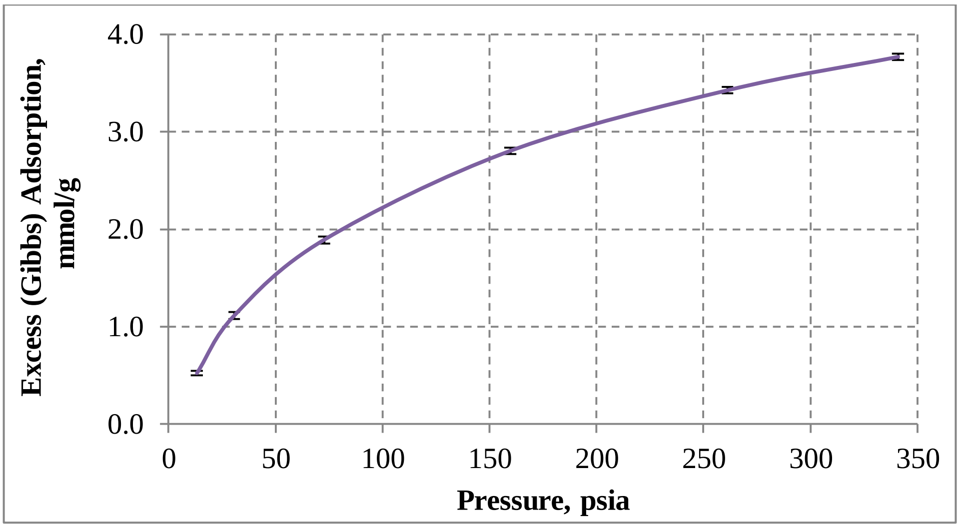

Figure 8.5: Run#2- Methane adsorption isotherm of BPL at 28.3 ^{o}C

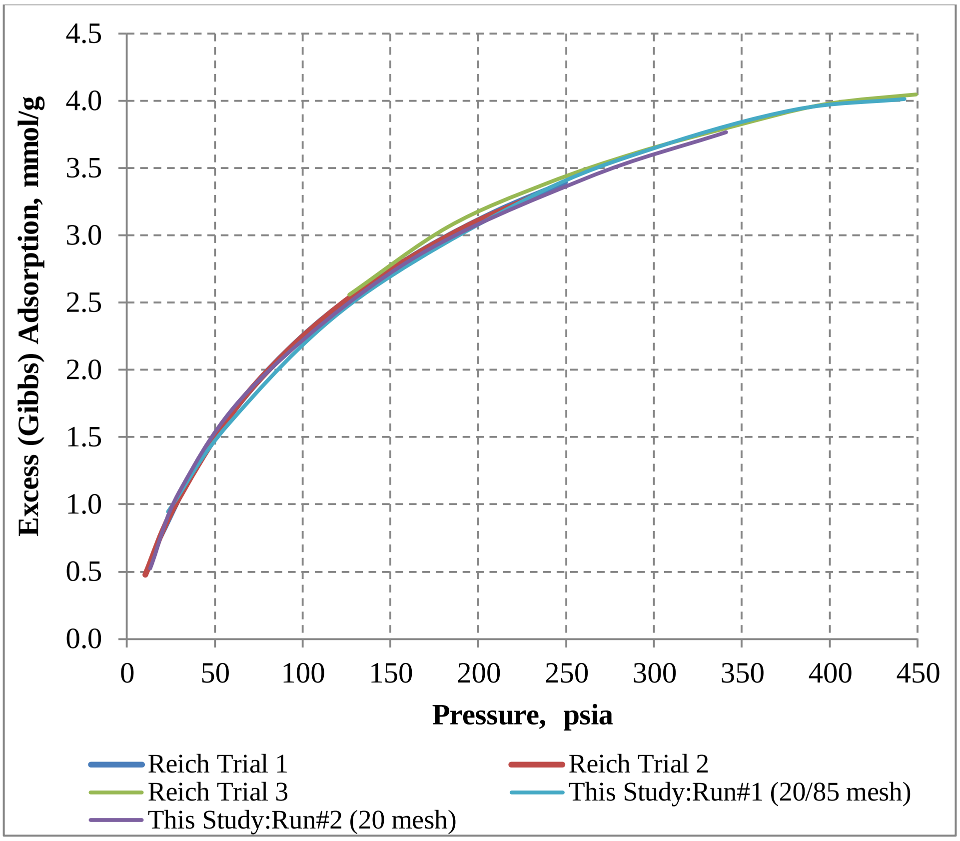

Figure 8.6: Comparison of Reich *et al.*(1980)'s adsorption experiments and Run#1 & Run#2

Figure 8.6 shows the experimental results of Run#1 & Run#2 and Reich *et al.* (1980)'s results. As seen in Figure 8.6, there is a good agreement in all adsorption isotherms. Therefore, it can be concluded that experimental set-up and calculation procedure used in this study are capable to adsorption experiments.

Additionally, for Run#1, 20/85 mesh size BPL was used. However, for Run#2, 20 mesh size BPL was used. As seen in Figure 8.6, Run#1 and Run#2's adsorption values are very close to each other, which indicates that mesh size is not important for adsorption capacities, but mesh size might affect only equilibrium times. Moreover, BPL has highly porous structure and gas molecules contact easily with the surface of BPL because of its high surface area, causing high adsorption.

8.1.1.2 Langmuir Model Analysis for Run#1: Methane Adsorption on BPL at 28.3 °C

Langmuir isotherm is generally preferred to analyze experimental adsorption data, because it is practical. Experimental adsorption data in this study were evaluated by using ISOFIT computer program written by Matott (2007) for Langmuir isotherms (Figure 8.8).

By ISOFIT program, the experimental data of Run#1 was evaluated with Langmuir model. In Table 8.4 and Table 8.5, results are shown for Run#1. Langmuir parameters, P_L (Langmuir pressure) and n_L (Langmuir molar mass) are used to calculate adsorption capacity at any pressure (See Equation 4.3). Hence, in shale gas reservoirs, at different reservoir pressures, adsorption capacity is easily calculated by using Langmuir parameters.

As seen in Table 8.4 and Figure 8.8, calculated excess adsorption and experimental excess adsorption values for Run#1 are close to each other. Therefore, Langmuir model has good fitting results for Run#1. In Table 8.4, excess (Gibbs) adsorption represents experimental adsorption data and calculated excess (Gibbs) adsorption represents the adsorption data calculated after regressing excess (Gibbs) adsorption data by using adsorption models.

Table 8.4: Langmuir isotherm results for Run#1

Pressure, psia	Excess (Gibbs) Adsorption, mmol/g	Calculated Excess (Gibbs) Adsorption, mmol/g
23	0.946	0.795
58	1.603	1.611
128	2.496	2.582
229	3.284	3.324
303	3.663	3.645
380	3.936	3.880
443	4.015	4.025

Table 8.5: Langmuir isotherm parameters for Run#1

Model Parameters	Results
n_L	5.205 mmol/g
P_L	130 psia
R^2	0.997

8.1.1.3 Ono-Kondo Monolayer Model Analysis for Run#1: Methane Adsorption on BPL at 28.3 ^{o}C

In this study, additionally to Langmuir model, Ono-Kondo model was preferred to evaluate experimental adsorption data (Figure 8.8). In this model, it was assumed that adsorption occurs as a monolayer structure. A matlab computer program written in this study was used to evaluate experimental adsorption data with Ono-Kondo monolayer model (See Appendix B).

In order to check the matlab program written for Ono-Kondo monolayer model in this study, Sudibandriyo *et al.* (2003)'s experimental methane adsorption results for BPL were used in the matlab program. Then, model results in this study and Sudibandriyo *et al.* (2003)'s study were compared. Model results are quite equal to each other (Table 8.6). Small differences in the results are due to different initial guesses and different regression methods used.

Table 8.6: Comparisions of Ono-Kondo monolayer model results

Model in This Study	**AAD (%)**	0.8
	ε_{fs}/k (K)	-1381
	C, mmol/g	3.14
Model in Sudibandriyo *et al.* (2003)'s Study	**AAD (%)**	0.6
	ε_{fs}/k (K)	-1385
	C, mmol/g	3.26

As seen in Table 8.7 and Figure 8.8, calculated excess adsorption values by the matlab program and experimental excess adsorption values for Run#1 are close to each other. Hence, Ono-Kondo monolayer model has good fitting results for Run#1.

Table 8.7: Ono-Kondo monolayer model results for Run#1

Pressure, psia	Excess (Gibbs) Adsorption, mmol/g	Calculated Excess (Gibbs) Adsorption, mmol/g
23	0.946	0.887
58	1.603	1.659
128	2.496	2.550
229	3.284	3.287
303	3.663	3.641
380	3.936	3.919
443	4.015	4.098

In adsorption, adsorbed molecules form a layer on adsorbent. At low pressures, the volume of adsorbed layer is negligible. However, with increasing pressure, the volume of adsorbed layer becomes important. Langmuir model is not capable to calculate the volume of adsorbed layer by using adsorbed phase densities. For Run#1, by using Ono-Kondo monolayer model, adsorbed gas phase densities were calculated at each pressure values. Then, absolute adsorption values were calculated by using equation 7.15 (Table 8.8). As seen in Figure 8.7, between 0 and 75 psia, absolute adsorption and excess adsorption capacities are almost equal. However, after 75 psia, the gap between absolute and excess adsorption increases due to the increase in the volume of adsorbed layer.

Table 8.8: Ono-Kondo monolayer model parameters for Run#1

Pressure, psia	$x_a = \rho_{adsorbed}/\rho_{mc}$	$\rho_{adsorbed}$**, mol/l**	**Absolute Adsorption, mmol/g**
23	0.122	2.862	0.968
58	0.231	5.392	1.652
128	0.359	8.396	2.607
229	0.471	11.013	3.489
303	0.528	12.345	3.939
380	0.575	13.449	4.284
443	0.608	14.201	4.411

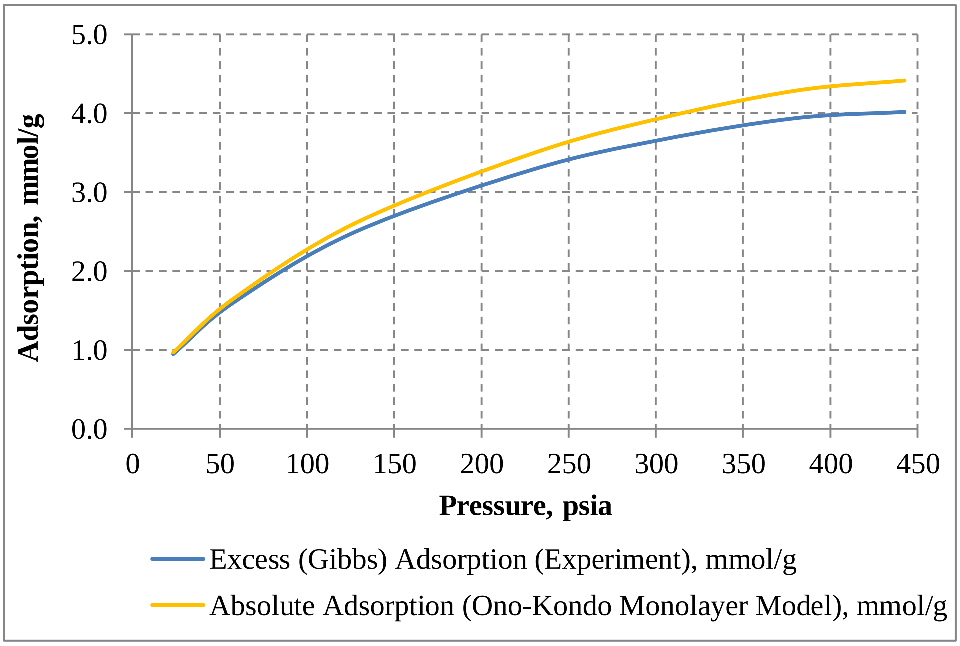

Figure 8.7: Ono-Kondo monolayer model isotherm and absolute adsorption for Run#1-Methane adsorption isotherm of BPL at 28.3 ^{o}C

By using the matlab code for Ono Kondo monolayer model, model parameters were calculated for Run#1. As seen in Table 8.9, surface area was calculated with this model, which is 1101 m^2/g for BPL. Reich *et al.* (1980) found the surface area of BPL activated carbon as 988 ±15 m^2/g using the conventional nitrogen BET surface area method. Hence, Ono-Kondo monolayer model has also good approximation for surface area.

Table 8.9: Ono-Kondo monolayer regression parameters for Run#1

AAD (%)	2.152
ε_{fs}/k, (K)	-1235
C, mmol/g	3.706
Surface Area, m^2/g	1101

8.1.1.4 Ono-Kondo Three-layer Model Analysis for Run#1: Methane Adsorption on BPL at 28.3 °C

Adsorption can form as monolayer or multilayered (some molecules are adsorbed on already adsorbed molecules). Ono-Kondo three-layer model was used in this study to check the layered structure of adsorption and to make comparison with Ono-Kondo monolayer model (Figure 8.8). A matlab computer program written in this study was used to evaluate experimental adsorption data for this model (See Appendix B).

In order to check the matlab program written for Ono-Kondo three-layer model in this study, Sudibandriyo *et al.* (2003)'s experimental methane adsorption results for BPL were used in the program. Then, model results in this study and Sudibandriyo *et al.* (2003)'s study were compared. Model results are quite equal to each other (Table 8.10). Small differences in the results are due to different initial guesses and different regression methods used.

Table 8.10: Comparisions of Ono-Kondo three-layer model results

Model in This Study	**AAD (%)**	2.9
	ε_{fs}/k (K)	-1721
	C, mmol/g	4.34
Model in Sudibandriyo *et al.* (2003)'s Study	**AAD (%)**	2.8
	ε_{fs}/k (K)	-1690
	C, mmol/g	4.53

Table 8.11: Ono-Kondo three-layer model results for Run#1

Pressure, psia	Excess (Gibbs) Adsorption, mmol/g	Calculated Excess (Gibbs) Adsorption, mmol/g
23	0.946	0.896
58	1.603	1.675
128	2.496	2.566
229	3.284	3.287
303	3.663	3.625
380	3.936	3.884
443	4.015	4.047

Table 8.12: Ono-Kondo three-layer model results for Run#1

Pressure (psia)	Bulk Phase	1st Layer	2nd Layer	3rd Layer
	$x_b=\rho_b/\rho_{mc}$	$x_1=\rho_{adsorbed1}/\rho_{mc}$	$x_2=\rho_{adsorbed2}/\rho_{mc}$	$x_3=\rho_{adsorbed3}/\rho_{mc}$
23	0.003	0.132	0.003	0.003
58	0.007	0.248	0.007	0.007
128	0.015	0.384	0.014	0.015
229	0.028	0.502	0.025	0.028
303	0.037	0.561	0.033	0.037
380	0.047	0.609	0.042	0.047
443	0.055	0.641	0.049	0.055

In Table 8.12, bulk phase densities, first layer adsorbed phase densities, second layer adsorbed phase densities, and third layer adsorbed phases densities divided by reciprocal van der Waals co-volume of methane preferred as the adsorbed phase density of methane at maximum capacity are listed respectively. First layer's fractions are higher than bulk (gas) phase's fractions. This is due to adsorption on the first layer because adsorbed phase density is higher than bulk density. However, second and third layer's fractions are very close to bulk phase's fractions. This means that adsorption occurred as monolayer in Run#1.

As seen in Table 8.10 and Table 8.13, model parameters of Ono-Kondo three-layer model are close to the parameters of Ono-Kondo monolayer model. This is also an indication of monolayer adsorption.

Table 8.13: Ono-Kondo three-layer model regression parameters for Run#1

AAD (%)	2.264
ε_{fs}/k, (K)	-1255
C, mmol/g	3.486
Surface Area, m^2/g	1035

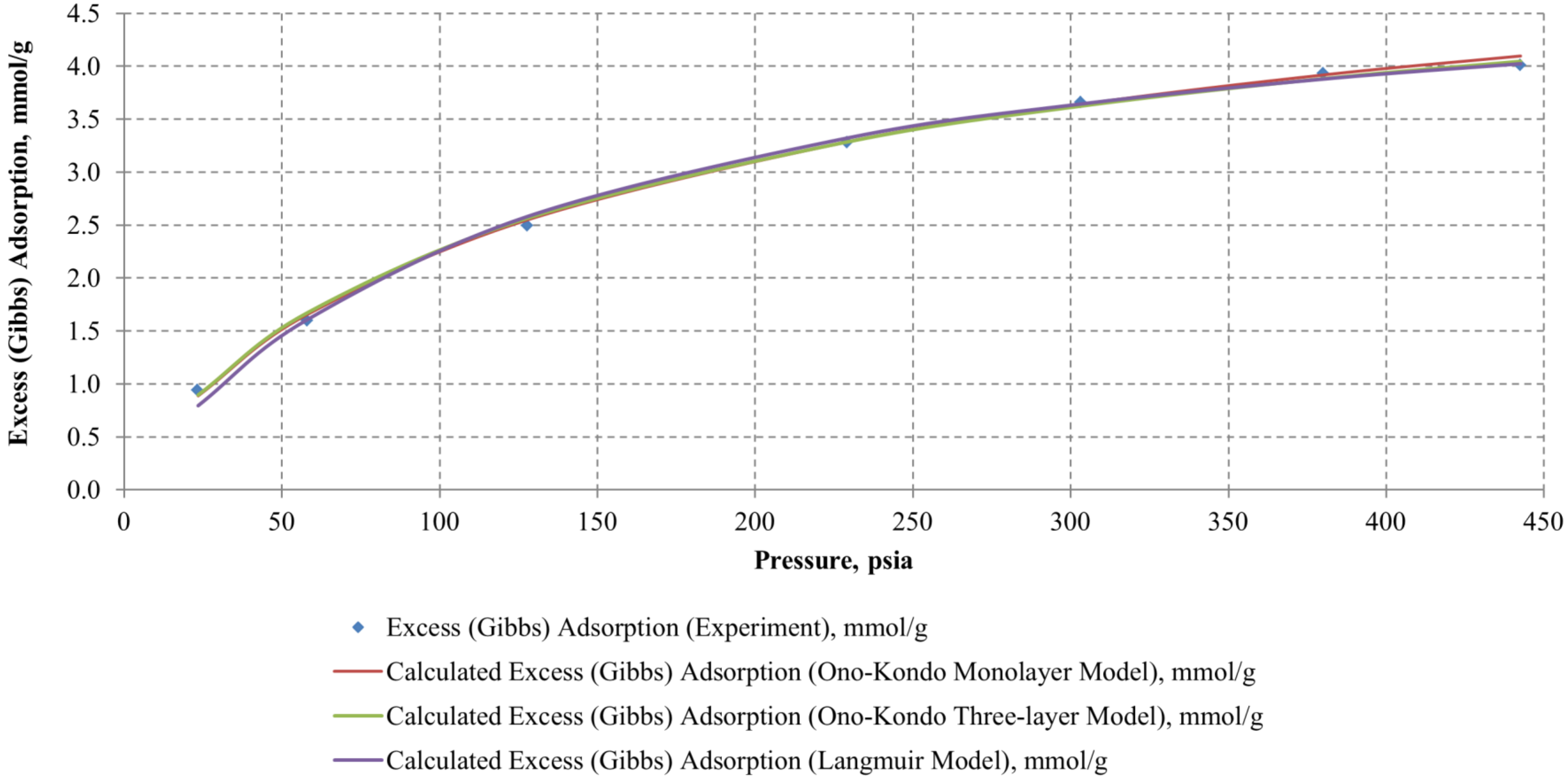

Figure 8.8: Adsorption models for Run#1- Methane adsorption isotherm of BPL at 28.3 °C

8.1.2 Run#3: Carbon dioxide Adsorption on BPL at 28.3 °C

In this experiment, 20 mesh size BPL activated carbon was used for carbon dioxide adsorption. Moreover, before starting to the experiment, BPL samples were heated at 120 °C for 24 hours to avoid any moisture and its effects. Samples were filled into the sample cell for Run#3 (Table 8.14).

Table 8.14: Run#3's experimental data

		Run#1
Reference Cell Volume	**:**	44.5 cm^3
Temperature	**:**	28.3 °C
Sample Weight	**:**	39.6 g
Sample Cell Volume	**:**	122.4 cm^3
Mesh Size	**:**	20
Average Void Volume	**:**	85.22 cm^3

In Run#3 and other experiments, the procedures for Run#1 & Run#2 were followed.

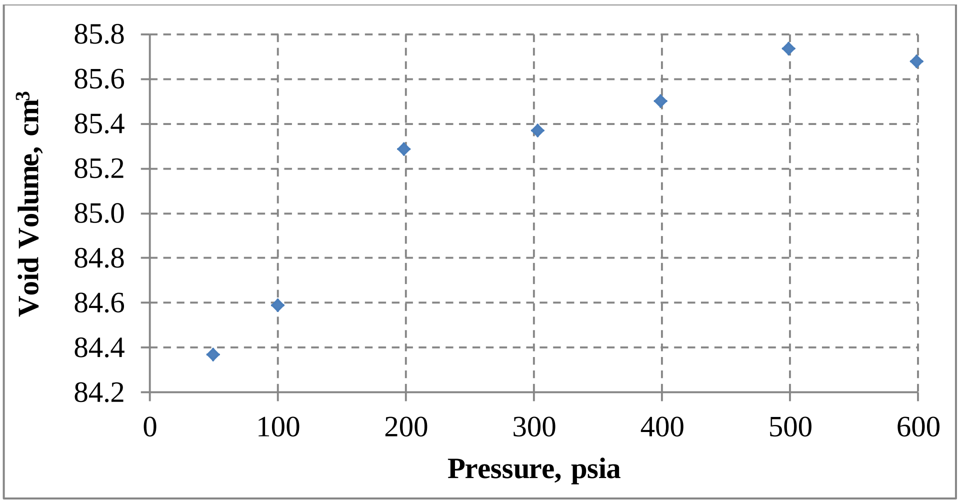

Figure 8.9: Run#3-Helium void volume of the sample cell filled with BPL

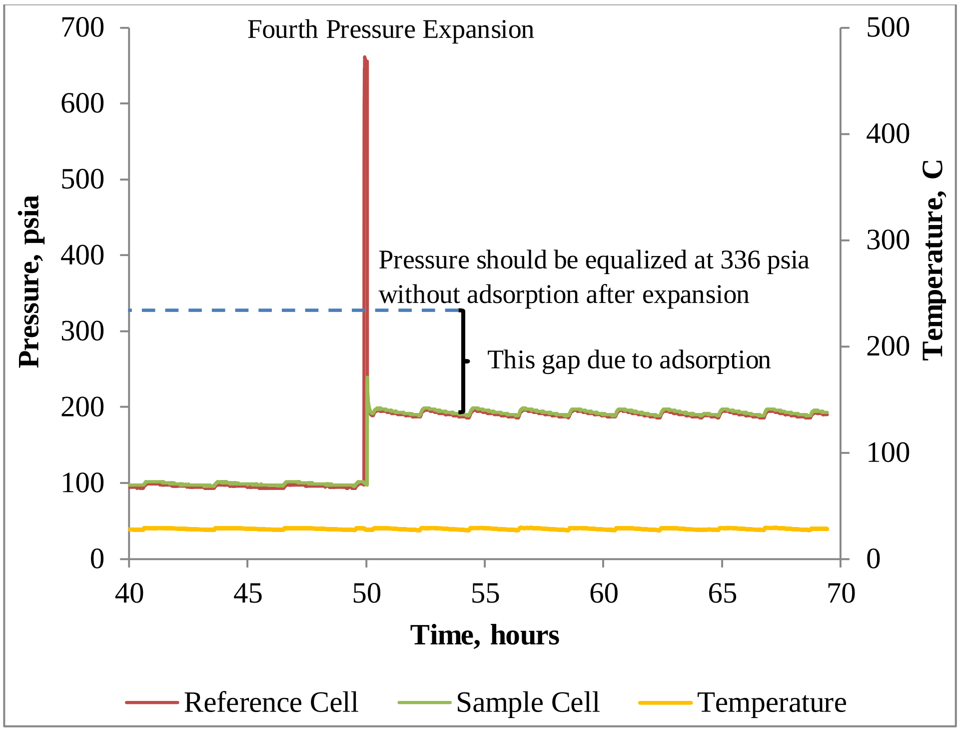

Figure 8.10: Fourth pressure expansion stage for Run#3

In Figure 8.10, before and after the fourth pressure expansion, pressure versus time graph is shown for Run#3. As seen in Figure 8.10, temperature values changed in a range ±1°C because constant temperature water bath tries to keep temperature at desired value (28.3°C for Run#3) in a range ±1°C. This causes small fluctuations in pressure values. For the fourth expansion, the valve between the sample cell and the reference cell was closed. Then, carbon dioxide was injected into the reference cell for next stage. It was essential to wait for equilibrium pressure in the reference cell for 15 minutes (656 psia). After opening the valve between the cells, carbon dioxide was expanded from the reference cell to the sample cell. Without adsorption, pressure was expected to be equalized in both cells at around 336 psia after expansion. However, after opening the valve, adsorption started immediately and this caused decrease in pressure. Although most of adsorption occured after opening the valve, it is important to wait equilibrium pressure for 6 or 12 hours.

Table 8.15: Run#3 carbon dioxide adsorption on BPL at 28.3 °C

Pressure , psia	Excess(Gibbs) Adsorption, mmol/g	Absolute Uncertainty in Excess Adsorption, mmol/g
5	0.773	0.056
34	2.418	0.057
89	4.182	0.060
187	5.672	0.071
293	6.600	0.083
419	7.124	0.131

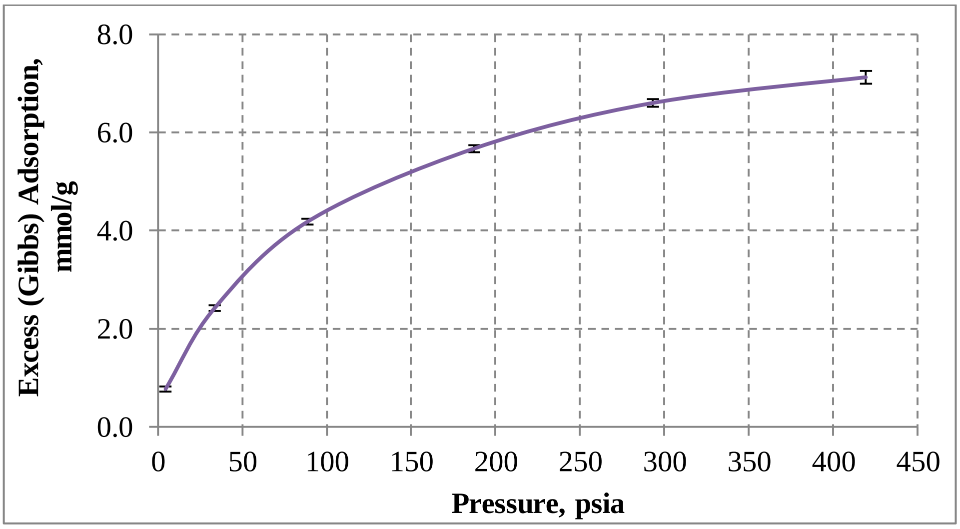

Figure 8.11: Run#3-Carbon dioxide adsorption isotherm of BPL at 28.3 °C

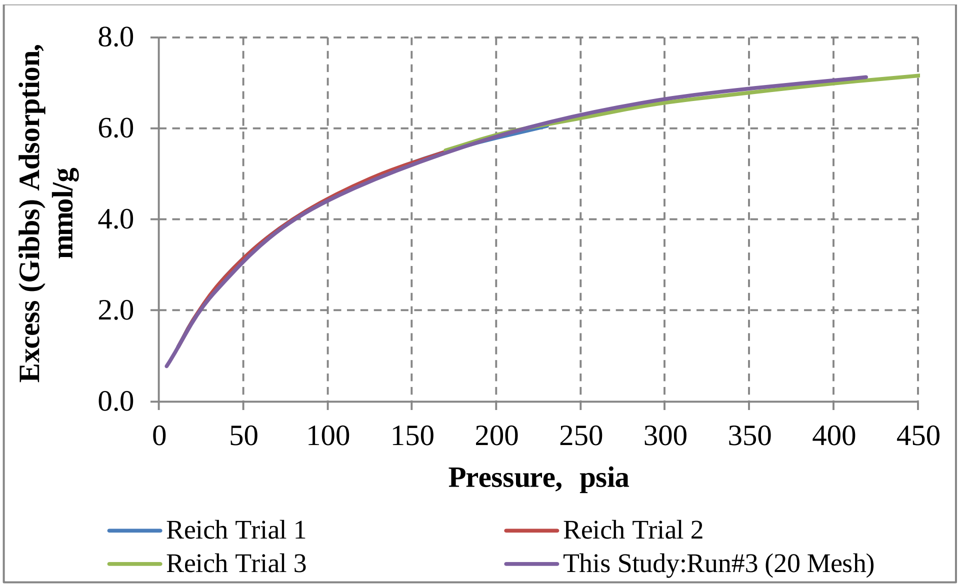

Figure 8.12: Comparison of Reich *et al.* (1980)'s adsorption experiments and Run#3

Figure 8.12 shows the experimental results of Run#3 and Reich *et al.* (1980)'s results. It can be concluded that experimental set-up and calculation procedures used in this study are capable for adsorption experiments.

When carbon dioxide (Run#3) and methane adsorption (Run#1) on BPL at 28.3 ^{o}C are compared, between 0 and 450 psia, as an average, carbon dioxide adsorption on BPL is around 1.9 times higher than methane adsorption on BPL. It is known that carbon dioxide and methane molecules are non-polar. Hence, adsorption of these gases on the surface of BPL and shales is mainly due to dispersion effect (nonpolar-nonpolar attraction). Methane has 10 electrons, but carbon dioxide has 16 electrons. The more electrons that are present in the molecule, the stronger the dispersion forces will be (Chapter 3.2). Therefore, carbon dioxide adsorption is higher than methane adsorption.

8.1.2.1 Adsorption Models for Run#3: Carbon dioxide Adsorption on BPL at 28.3 ^{o}C

- ✓ After conducting Run#3 experiment, results were evaluated by using Langmuir model and Ono-Kondo models. The results of Langmuir model's fitting to experimental data are listed in Table 8.16 and Table 8.17

Table 8.16: Langmuir isotherm results for Run#3

Pressure, psia	**Excess (Gibbs) Adsorption, mmol/g**	**Calculated Excess (Gibbs) Adsorption, mmol/g**
5	0.773	0.412
34	2.418	2.344
89	4.182	4.268
187	5.672	5.796
293	6.600	6.559
419	7.124	7.053

Table 8.17: Langmuir isotherm parameters for Run#3

Model Parameters	**Results**
$\mathbf{n_L}$	8.549 mmol/g
$\mathbf{P_L}$	89 psia
$\mathbf{R^2}$	0.999

As seen in Table 8.17 and Figure 8.14, experimental carbon dioxide adsorption data on BPL at 28.3 ^{o}C were fitted fairly by Langmuir Model.

- ✓ The results of Ono-Kondo monolayer model's fitting to experimental data are listed in Table 8.18, Table 8.19 and Table 8.20.

Table 8.18: Ono-Kondo monolayer model results for Run#3

Pressure, psia	**Excess (Gibbs) Adsorption, mmol/g**	**Calculated Excess (Gibbs) Adsorption, mmol/g**
5	0.773	0.683
34	2.418	2.760
89	4.182	4.354
187	5.672	5.686
293	6.600	6.463
419	7.124	7.030

Table 8.19: Ono-Kondo monolayer model parameters for Run#3

Pressure, psia	$x_a=\rho_{adsorbed}/\rho_{mc}$	$\rho_{adsorbed}$**, mol/l**	**Absolute Adsorption, mmol/g**
5	0.065	1.509	0.779
34	0.263	6.142	2.455
89	0.420	9.792	4.292
187	0.557	13.001	5.923
293	0.645	15.062	7.020
419	0.719	16.770	7.755

As seen in Table 8.18 and Figure 8.14, experimental carbon dioxide adsorption data on BPL at 28.3 ^{o}C were fitted fairly by Ono-Kondo monolayer model. Excess adsorption values were corrected by Ono-Kondo monolayer model in order to calculate absolute adsorption. In Figure 8.13, after around 90 psia, the gap between absolute adsorption and excess adsorption increases.

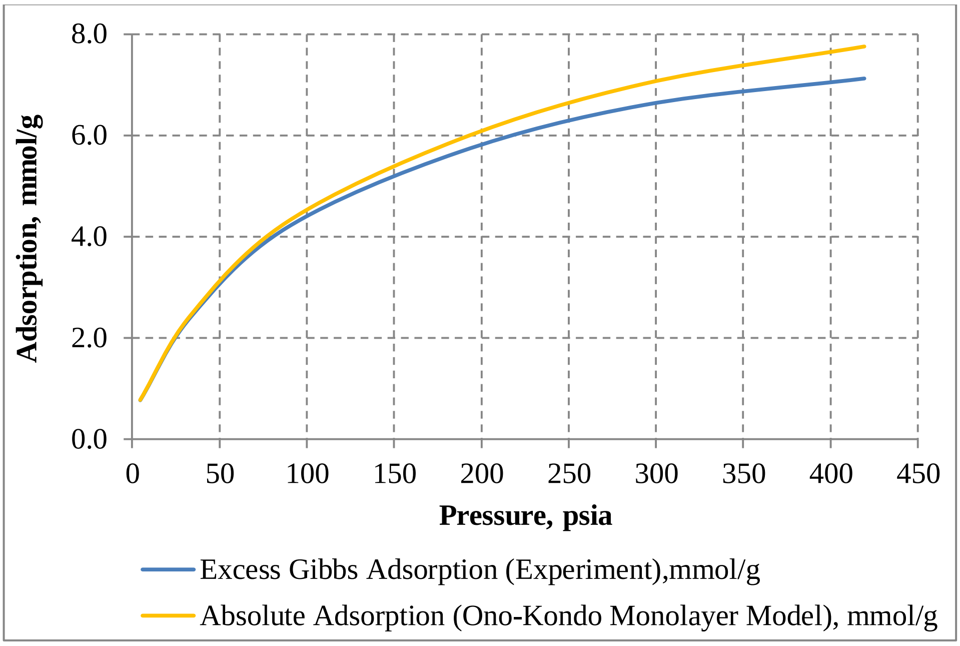

Figure 8.13: Ono-Kondo monolayer model isotherm and absolute adsorption for Run#3-Carbon dioxide adsorption isotherm of BPL at 28.3 ^{o}C

By using the matlab code for Ono Kondo monolayer model, model parameters were calculated for Run#3. As seen in Table 8.20, surface area was calculated, which is 1044 m^2/g. Reich *et al.* (1980) found the surface area of BPL activated carbon as 988 ±15 m^2/g by using the conventional nitrogen BET surface area method. Hence, Ono-Kondo monolayer model has good approximation for surface area.

Table 8.20: Ono-Kondo monolayer model regression parameters for Run#3

AAD (%)	5.589
ε_{fs}/k, (K)	-1505
C, mmol/g	5.326
Surface Area, m^2/g	1044

- ✓ The results of Ono-Kondo three-layer model's fitting to experimental data are listed in Table 8.21, Table 8.22 and Table 8.23.

Table 8.21: Ono-Kondo three-layer model results for Run#3

Pressure, psia	Excess (Gibbs) Adsorption, mmol/g	Calculated Excess (Gibbs) Adsorption, mmol/g
5	0.773	0.689
34	2.418	2.798
89	4.182	4.394
187	5.672	5.685
293	6.600	6.400
419	7.124	6.886

Table 8.22: Ono-Kondo three-layer model results for Run#3

Pressure (psia)	Bulk Phase	1st Layer	2nd Layer	3rd Layer
	$x_b=\rho_b/\rho_{mc}$	$x_1=\rho_{adsorbed1}/\rho_{mc}$	$x_2=\rho_{adsorbed2}/\rho_{mc}$	$x_3=\rho_{adsorbed3}/\rho_{mc}$
5	0.001	0.069	0.001	0.001
34	0.004	0.284	0.004	0.004
89	0.011	0.451	0.010	0.011
187	0.024	0.595	0.020	0.024
293	0.039	0.684	0.033	0.039
419	0.059	0.756	0.049	0.059

As seen in Table 8.21 and Figure 8.14, experimental carbon dioxide adsorption data on BPL at 28.3 ^{o}C were fitted fairly by Ono-Kondo three-layer model. In Table 8.22, bulk phase densities, first layer adsorbed phase densities, second layer adsorbed phase densities, and third layer adsorbed phase densities divided by reciprocal van der Waals co-volume of carbon dioxide preferred as the adsorbed phase density of carbon dioxide at maximum capacity are listed respectively. First layer's fractions are higher than bulk phase's fractions. This is due to adsorption on the first layer. However, second and third layer's fractions are very close to bulk phase's fraction. This means that adsorption occurred as monolayer in Run#3. As seen in Table 8.23, model parameters of Ono-Kondo three-layer model are close to the parameters of Ono-Kondo monolayer model. This also indicates monolayer adsorption.

Table 8.23: Ono-Kondo three-layer model regression parameters for Run#3

AAD (%)	6.363
ε_{fs}/k, (K)	-1525
C, mmol/g	5.004
Surface Area, m^2/g	981

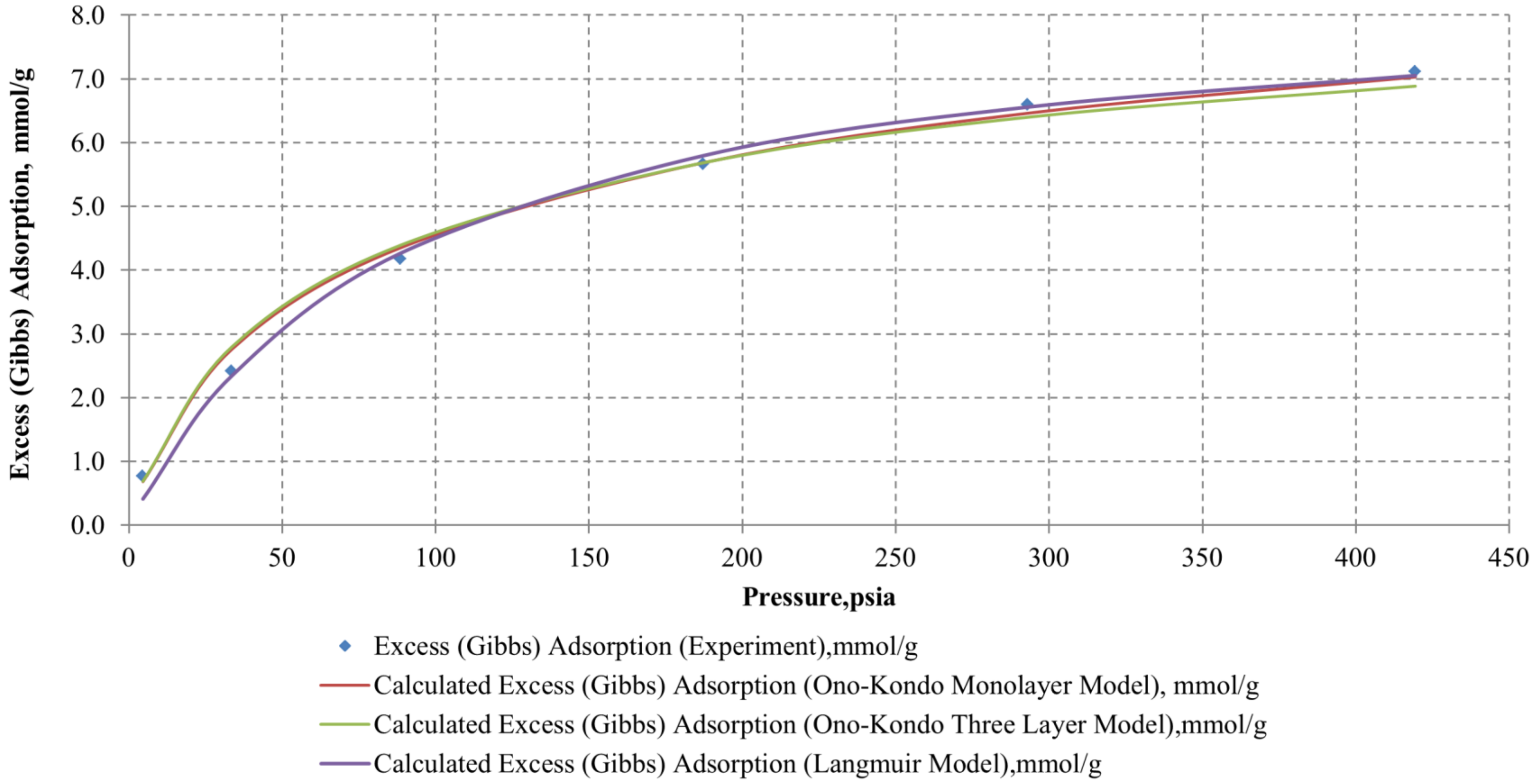

Figure 8.14: Adsorption Models for Run#3-Carbon dioxide adsorption isotherm of BPL at 28.3 °C

8.2 Adsorption Experiments Results of Shale Sample A

Shale samples of A field were used for adsorption experiments at different temperatures for both pure methane and pure carbon dioxide. Before using the samples, they were crushed to 50/85 mesh size. Then, shale samples were heated at 120 ^{o}C to avoid any moisture effects. The sample cell (122.4 cm^3) was filled by 94.6 g of shale sample A. Void volumes of the sample cell were measured at different pressure stages by using non-adsorbing gas helium.

Figure 8.15: A picture of shale sample A

After placing the cells into the constant temperature water bath, the following data were obtained:

Table 8.24: Experimental data for adsorption experiments with shale sample A

Reference Cell Volume :	44.3 cm^3
Sample Weight :	94.6 g
Sample Cell Volume :	122.4 cm^3
Mesh Size :	50/85
Average Void Volume :	76.07 cm^3

The figure below shows void volumes at different pressure values:

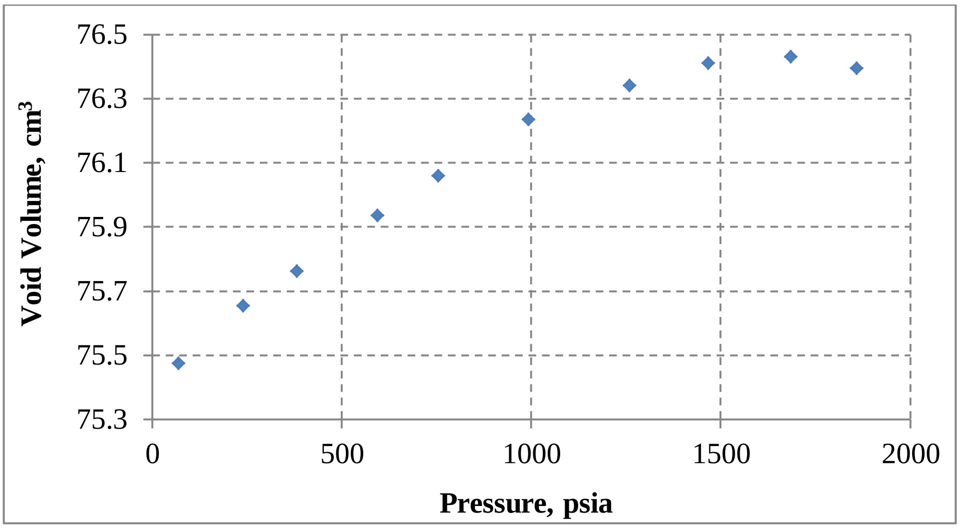

Figure 8.16: Run#4, 5, 6-Helium void volume of the sample cell filled with shale sample A

After determining void volume, leakage test was conducted at 2500 psia for 24 hours. Then, adsorption experiments on shale sample A were conducted for pure methane and pure carbon dioxide at 25, 50, and 75 ^{o}C.

8.2.1 Run#4 & Run#4 & Run#6: Methane Adsorption on Shale Sample A at 25 ^{o}C, 50 ^{o}C, and 75 ^{o}C

After placing the cells into the constant temperature water bath and void volume calculations (Table 8.24 and Figure 8.16), methane adsorption experiments were conducted at 25, 50, and 75 ^{o}C. It is known that as pressure increases, adsorption capacity increases. Temperature has also effects on adsorption. In order to show these effects, in this study, adsorption experiments were conducted at different temperatures.

According to the results of Run#4, Run#5 and Run#6, methane adsorption capacities of shale sample A are very small compared to BPL's adsorption and coalbed methane adsorption because methane adsorption capacities of shale gas reservoirs are very small due to their low TOC % and high ash content.

As seen in Figure 8.17, 8.18, and 8.19, absolute uncertainties in excess adsorption of shale sample A become very important compared to BPL's absolute uncertainties in excess adsorption, because shale sample A has very low adsorption capacities. Hence, more attentions were taken for shale samples' adsorption experiments in this study to reduce experimental uncertainties (See Chapter 6.2.4). Errors are shown as bars in the figures of adsorption isotherms.

Table 8.25: Run#4- Methane adsorption on shale sample A at 25 ^oC

Pressure , psia	**Excess(Gibbs) Adsorption, mmol/g**	**Absolute Uncertainty in Excess Adsorption, mmol/g**
196	0.0162	0.0037
412	0.0197	0.0056
607	0.0224	0.0077
807	0.0256	0.0099
1010	0.0283	0.0122
1201	0.0297	0.0145
1393	0.0310	0.0169
1619	0.0313	0.0198
1791	0.0314	0.0220
1951	0.0315	0.0240

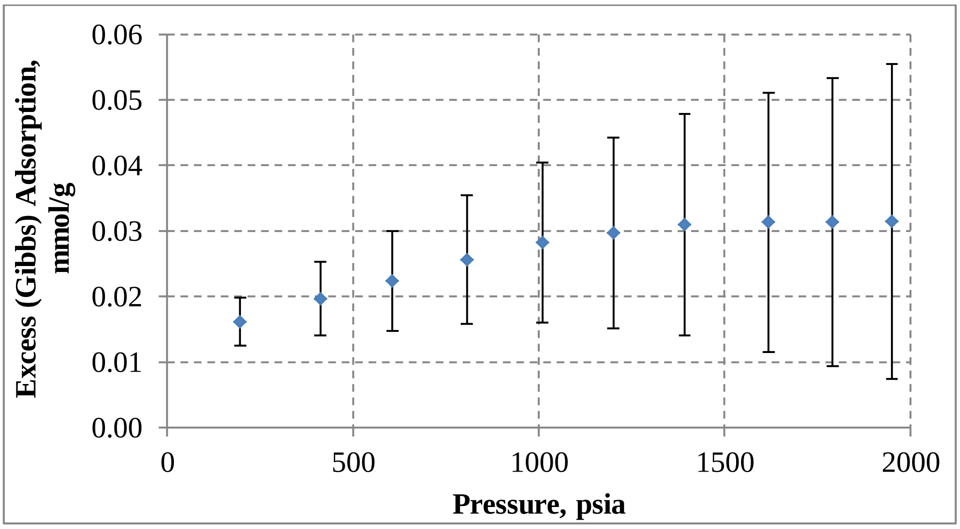

Figure 8.17: Run#4-Methane adsorption isotherm of shale sample A at 25 ^oC

Table 8.26: Run#5- Methane adsorption on shale sample A at 50 ^{o}C

Pressure , psia	**Excess(Gibbs) Adsorption, mmol/g**	**Absolute Uncertainty in Excess Adsorption, mmol/g**
196	0.0091	0.0033
409	0.0138	0.0051
609	0.0174	0.0069
811	0.0191	0.0088
1014	0.0204	0.0109
1201	0.0210	0.0128
1406	0.0209	0.0149
1603	0.0215	0.0170
1800	0.0212	0.0191
1987	0.0210	0.0223

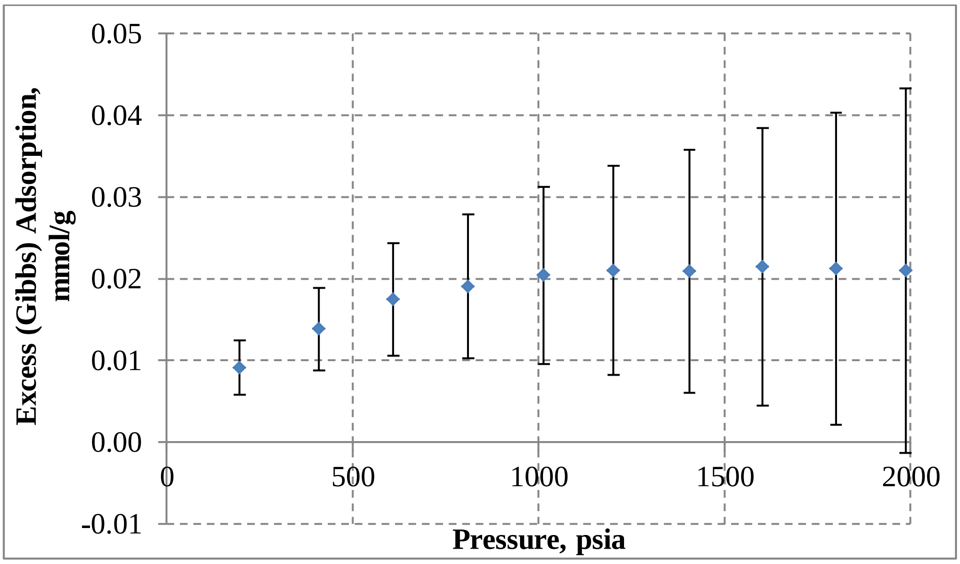

Figure 8.18: Run#5-Methane adsorption isotherm of shale sample A at 50 ^{o}C

Table 8.27: Run#6- Methane adsorption on shale sample A at 75 °C

Pressure, psia	Excess(Gibbs) Adsorption, mmol/g	Absolute Uncertainty in Excess Adsorption, mmol/g
203	0.0033	0.0031
415	0.0062	0.0047
611	0.0042	0.0063
811	0.0084	0.0080
1004	0.0086	0.0097
1211	0.0087	0.0116
1400	0.0083	0.0133
1603	0.0088	0.0157
1800	0.0086	0.0178
1987	0.0104	0.0204

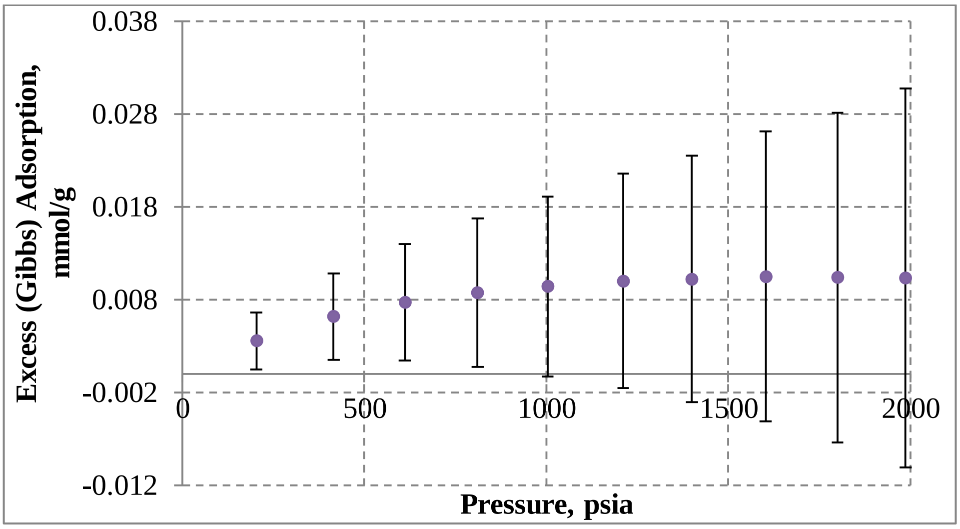

Figure 8.19: Run#6-Methane adsorption isotherm of shale sample A at 75 °C

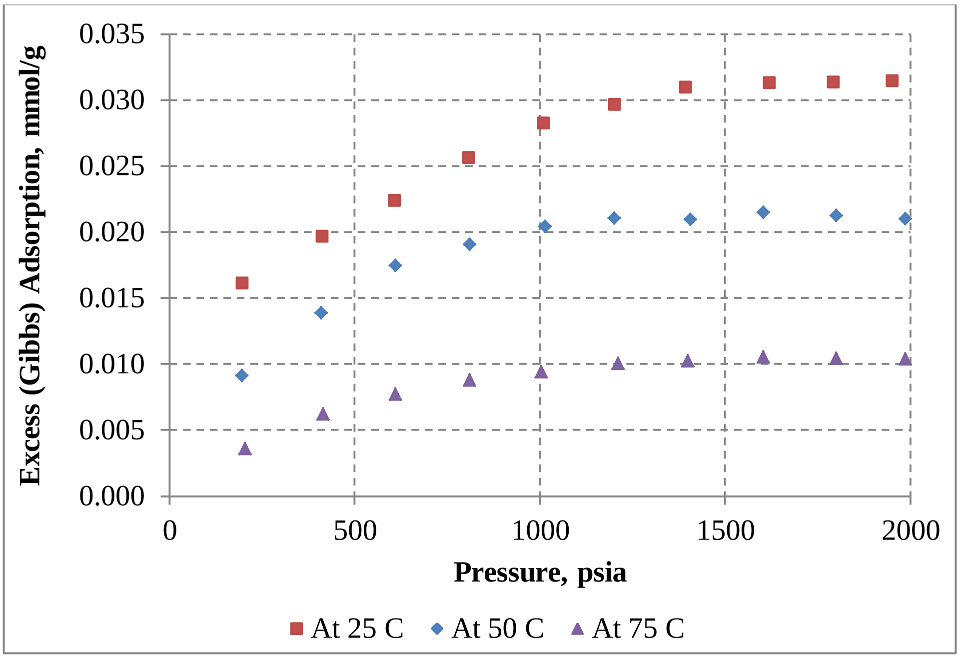

Figure 8.20: Comparison of Run#4, 5, 6- Methane adsorption isotherm of shale sample A

As seen in Figure 8.20, adsorption of methane decreases with increasing temperature. It is known that adsorption is exothermic because in order to form new bonds due to physical attraction, heat is released. Hence, the bonds between adsorbate (methane) and adsorbent (shale A) are weakened with increasing temperature and desorption occurs. This causes decrease in adsorption with increasing temperature.

As seen in Figure 8.20, adsorption capacities increase almost linearly for every pressure intervals but as pressure increases further, the increase of adsorption capacities decrease. Shales have nano-porous structures in shale matrix so they have molecular size diameters of pore dimensions. Therefore, there are potential forces from the neighboring walls of the pores. These forces increase the interaction energy between adsorbent surface and gas molecules, which causes an increase in adsorption and may cause complete filling of pores at low pressures. This is a typical behavior of Type I adsorption isotherm (See Chapter 4.3.1). Hence, after filling of almost all pores at low pressures, adsorption becomes almost constant at high pressures. This indicates that pore sizes and surface area are important for adsorption capacities and behaviors.

8.2.1.1 Adsorption Models for Run#4 & Run#5 & Run#6

- ✓ After conducting Run#4, 5, 6 , results were evaluated by using Langmuir model and Ono-Kondo models. The parameters of Langmuir model's fitting to experimental data are listed in Table 8.28. As seen in Figure 8.24, experimental methane adsorption data on shale sample A at 25, 50, and 75 ^{o}C were fitted fairly by Langmuir model.

Table 8.28: Langmuir isotherm parameters for Run#4, Run#5, Run#6 (Methane adsorption on shale sample A)

Model Parameters	Run#4 (25 ^{o}C)	Run#5 (50 ^{o}C)	Run#6 (75 ^{o}C)
n_L	0.0371 mmol/g	0.0256 mmol/g	0.0134 mmol/g
P_L	327 psia	316 psia	468 psia
R^2	0.981	0.985	0.984

- ✓ The results of Ono-Kondo monolayer model's fitting to experimental data are listed in Table 8.29, Table 8.30 and Table 8.31 for Run#4, 5, 6.

Table 8.29: Ono-Kondo monolayer parameters for Run#4, Run#5, Run#6 (Methane adsorption on shale sample A)

	Run#4 (25 ^{o}C)	Run#5 (50 ^{o}C)	Run#6 (75 ^{o}C)
AAD (%)	3.643	2.582	3.294
ε_{fs}/k, (K)	-855	-980	-885
C, mmol/g	0.0317	0.0206	0.0120
Surface Area, m^2/g	9.350	6.447	3.980

As seen in Figure 8.24, experimental methane adsorption data on shale sample A for Run#4, 5, 6 were fitted fairly by Ono-Kondo monolayer model. Excess adsorption values were corrected by Ono-Kondo monolayer model for absolute adsorption. As seen in Figure 8.21, 8.22, and 8.23, there are significant differences between absolute adsorption and excess adsorption, indicating the high capability of Ono-Kondo models compared to Langmuir model.

As seen in Table 8.29, parameters of Ono-Kondo monolayer model changes with temperature. In Table 8.29, surface area of shale sample A decreases with decreasing adsorption due to increasing temperature. Surface area calculations were made by using experimental adsorption data because there is a direct relation with surface area and adsorption capacity. When surface area increases, adsorption capacity increases. Hence, surface area values were calculated for Run#4, 5, 6 by using Ono-Kondo monolayer matlab program (See Appendix B). For shale sample A , surface area calculated by the experimental data of Run#4 is higher compared to Run#5 and Run#6 because of high adsorption of methane at 25 ^{o}C.

When adsorption capacity increases, the coverage of gas molecules on the surface of adsorbent increases. Hence, for shale sample A at 25 ^{o}C, due to its high adsorption capacities compared to its adsorption capacities at 50 ^{o}C and 75 ^{o}C, more gas molecules covered the surface of shale sample A. Surface area calculations by the help of Ono-Kondo models are done by evaluating the coverage of adsorbate on adsorbent. That is why, most accurate surface area calculations should be done by using experimental adsorption data at low temperatures because adsorption capacities are high at low temperatures, causing almost complete coverage of gas molecules on adsorbent. However, for this study, instead of having accurate surface area values , it is very important to have surface area values approximately to understand porous structure of the samples used in this study.

Table 8.30: Ono-Kondo monolayer model results for Run#4 (Methane adsorption on shale sample A at 25 ^{o}C)

Pressure, psia	Excess (Gibbs) Adsorption, mmol/g	Adsorbed Phase Density, mol/l	Absolute Adsorption, mmol/g
196	0.0162	5.573	0.0179
412	0.0197	8.720	0.0228
607	0.0224	10.720	0.0269
807	0.0256	12.362	0.0320
1010	0.0283	13.753	0.0367
1201	0.0297	14.884	0.0400
1393	0.0310	15.876	0.0433
1619	0.0313	16.899	0.0458
1791	0.0314	17.584	0.0476
1951	0.0315	18.150	0.0493

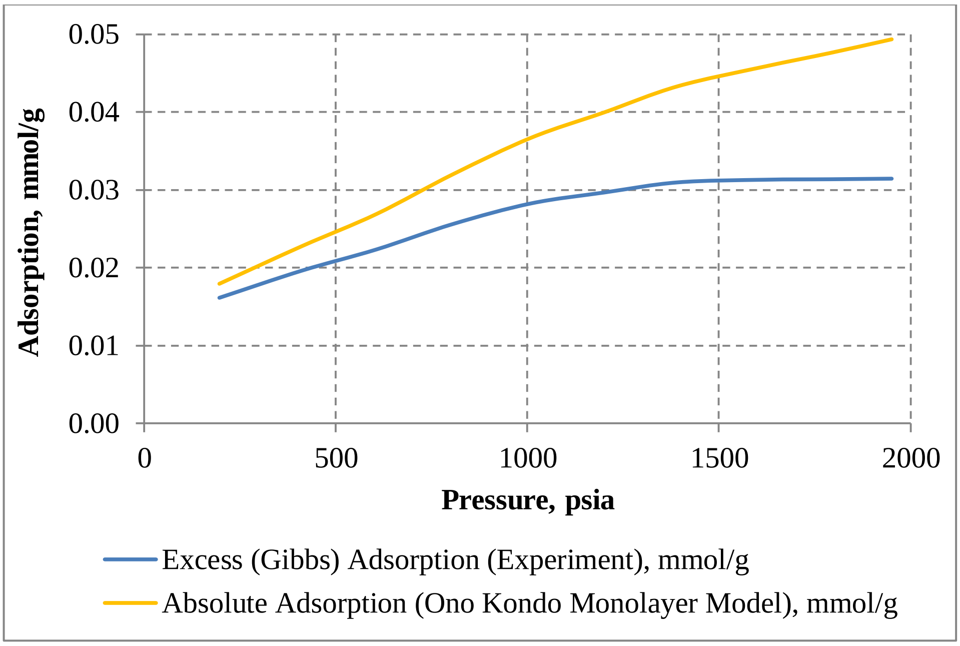

Figure 8.21: Absolute adsorption for Run#4

Table 8.31: Ono-Kondo monolayer model results for Run#5 (Methane adsorption on shale sample A at 50 ^{o}C)

Pressure, psia	**Excess (Gibbs) Adsorption, mmol/g**	**Adsorbed Phase Density, mol/l**	**Absolute Adsorption, mmol/g**
196	0.0091	5.909	0.0100
409	0.0139	9.080	0.0157
609	0.0174	11.120	0.0205
811	0.0191	12.712	0.0231
1014	0.0204	14.025	0.0256
1201	0.0210	15.051	0.0271
1406	0.0209	16.019	0.0279
1603	0.0215	16.830	0.0296
1800	0.0212	17.541	0.0303
1987	0.0210	18.135	0.0309

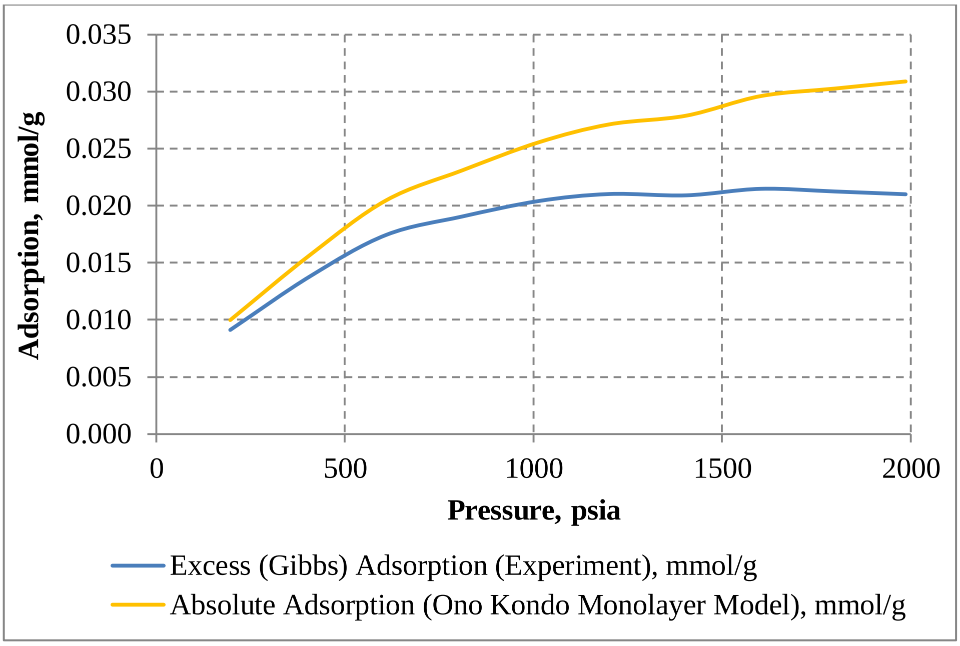

Figure 8.22: Absolute adsorption for Run#5

Table 8.32: Ono-Kondo monolayer model results for Run#6 (Methane adsorption on shale sample A at 75 ^{o}C)

Pressure, psia	Excess (Gibbs) Adsorption, mmol/g	Adsorbed Phase Density, mol/l	Absolute Adsorption, mmol/g
203	0.0036	4.248	0.0040
415	0.0062	6.908	0.0072
609	0.0077	8.714	0.0093
811	0.0088	10.231	0.0109
1004	0.0094	11.456	0.0121
1211	0.0100	12.595	0.0132
1400	0.0102	13.507	0.0139
1603	0.0105	14.382	0.0147
1800	0.0104	15.144	0.0150
1987	0.0104	15.796	0.0154

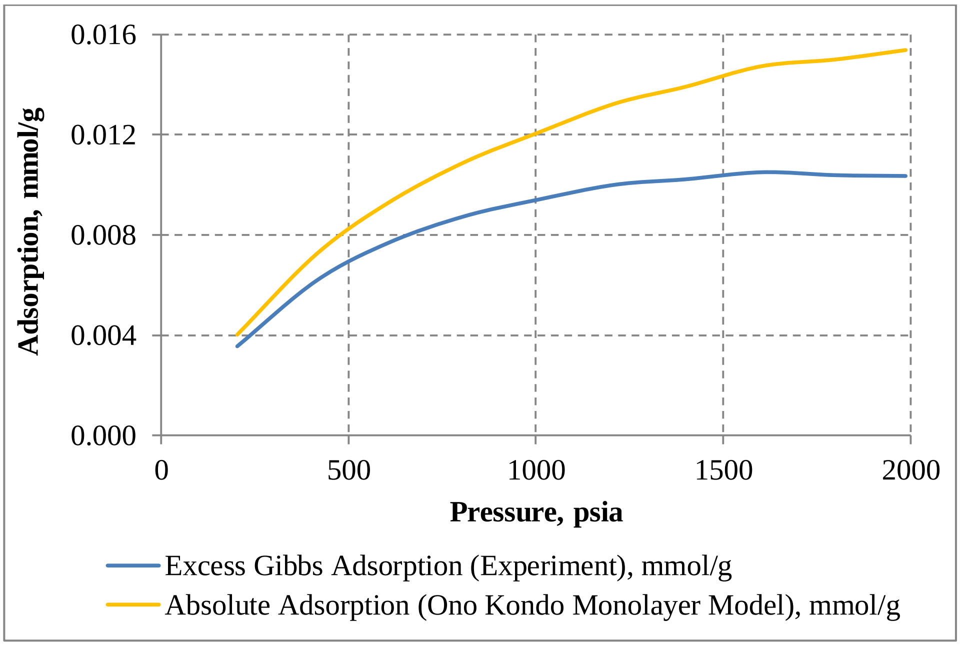

Figure 8.23: Absolute adsorption for Run#6

✓ The results of Ono-Kondo three-layer model's fitting to experimental data are listed in Table 8.33, Table 8.34, Table 8.35, and Table 8.36. As seen in Figure 8.24, experimental methane adsorption data on shale sample A for Run#4, 5, 6 were fitted fairly by Ono-Kondo three-layer model.

Table 8.33: Ono-Kondo three-layer model results for Run#4

Pressure (psia)	**Bulk Phase**	**1st Layer**	**2nd Layer**	**3rd Layer**
	$x_b=\rho_b/\rho_{mc}$	$x_1=\rho_{adsorbed1}/\rho_{mc}$	$x_2=\rho_{adsorbed2}/\rho_{mc}$	$x_3=\rho_{adsorbed3}/\rho_{mc}$
196	0.0239	0.2282	0.0229	0.0239
412	0.0515	0.3646	0.0485	0.0516
607	0.0776	0.4523	0.0725	0.0777
807	0.1056	0.5243	0.0982	0.1057
1010	0.1352	0.5852	0.1256	0.1354
1201	0.1640	0.6346	0.1525	0.1643
1393	0.1936	0.6777	0.1804	0.1940
1619	0.2292	0.7219	0.2143	0.2297
1791	0.2565	0.7513	0.2405	0.2571
1951	0.2817	0.7756	0.2648	0.2822

Table 8.34: Ono-Kondo three-layer model results for Run#5

Pressure (psia)	**Bulk Phase**	**1st Layer**	**2nd Layer**	**3rd Layer**
	$x_b=\rho_b/\rho_{mc}$	$x_1=\rho_{adsorbed1}/\rho_{mc}$	$x_2=\rho_{adsorbed2}/\rho_{mc}$	$x_3=\rho_{adsorbed3}/\rho_{mc}$
196	0.0219	0.2457	0.0210	0.0219
409	0.0465	0.3841	0.0438	0.0466
609	0.0705	0.4736	0.0657	0.0705
811	0.0952	0.5435	0.0885	0.0953
1014	0.1209	0.6009	0.1121	0.1210
1201	0.1450	0.6456	0.1345	0.1452
1406	0.1717	0.6875	0.1596	0.1720
1603	0.1978	0.7224	0.1842	0.1981
1800	0.2239	0.7528	0.2091	0.2243
1987	0.2486	0.7781	0.2328	0.2490

Table 8.35: Ono-Kondo three-layer model results for Run#6

Pressure (psia)	Bulk Phase	1st Layer	2nd Layer	3rd Layer
	$x_b=\rho_b/\rho_{mc}$	$x_1=\rho_{adsorbed1}/\rho_{mc}$	$x_2=\rho_{adsorbed2}/\rho_{mc}$	$x_3=\rho_{adsorbed3}/\rho_{mc}$
203	0.0210	0.1783	0.0204	0.0210
415	0.0434	0.2938	0.0416	0.0434
609	0.0644	0.3729	0.0613	0.0645
811	0.0867	0.4394	0.0820	0.0867
1004	0.1083	0.4929	0.1022	0.1084
1211	0.1318	0.5426	0.1243	0.1320
1400	0.1534	0.5823	0.1446	0.1536
1603	0.1768	0.6202	0.1667	0.1770
1800	0.1995	0.6530	0.1883	0.1998
1987	0.2209	0.6809	0.2088	0.2212

Table 8.36: Ono-Kondo three-layer model regression parameters for Run#4, 5, 6

	Run#4 (25 °C)	Run#5 (50 °C)	Run#6 (75 °C)
AAD (%)	4.00	2.213	2.988
ε_{fs}/k, (K)	-820	-950	-865
C, mmol/g	0.0328	0.0210	0.0121
Surface Area, m^2/g	9.678	6.586	4.029

As seen in Table 8.33, 34, and 35, adsorption occurred as monolayer in Run#4, 5 and 6 because first layer's densities are higher than bulk phase densities. However, second and third layer's densities are close to bulk phase densities. It is also known that Type I adsorption isotherm happens as monolayer because of microporous structure of shales. Hence, this supports Ono-Kondo three-layer model's results. Due to shale samples' molecule sizes of pore size networks, adsorption is expected to occur as monolayer. Moreover, as seen in Table 8.29 and Table 8.36, model parameters of Ono-Kondo three-layer model are close to the parameters of Ono-Kondo monolayer model. Small differences in adsorption parameters for Ono-Kondo models are mostly related to regression model used in the program and differences in initial guesses of fluid-solid energy parameters.

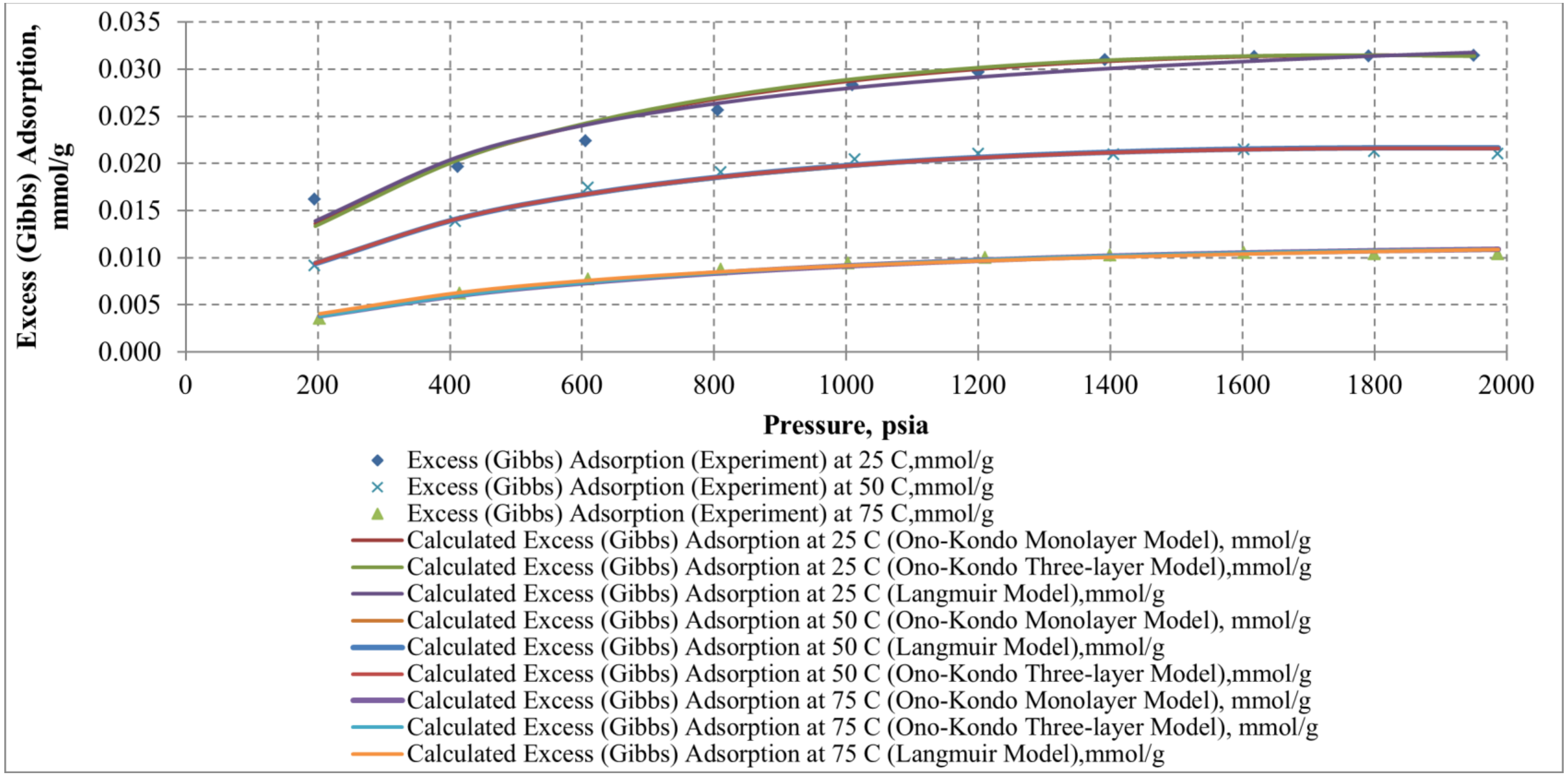

Figure 8.24: Adsorption models for Run#4, 5, 6- Methane adsorption isotherms of shale sample A at different temperatures

8.2.2 Run#7 & Run#8 & Run#9: Carbon dioxide Adsorption on Shale Sample A at 25 ^oC, 50 ^oC, and 75 ^oC

After placing the cells into the constant temperature water bath and void volume calculations (Table 8.24 and Figure 8.16), carbon dioxide adsorption experiments were conducted at 25, 50, and 75 ^oC. The aim of carbon dioxide adsorption experiments of shale sample A is to investigate possible storage of carbon dioxide to shale gas reservoirs after depletion or as a recovery technique.

Experimental adsorption results of Run#7, 8, 9 are listed in Table 8.37, 38, 39 According to the results of Run#7, Run#8 and Run#9, carbon dioxide adsorption capacities are very high compared to methane adsorption capacities of shale sample A. This is because of stronger dispersion effects between carbon dioxide molecules and molecules on the surface of shale sample A compared to methane molecules'.

Table 8.37: Run#7- Carbon dioxide adsorption on shale sample A at 25 ^oC

Pressure , psia	Excess(Gibbs) Adsorption, mmol/g	Absolute Uncertainty in Excess Adsorption, mmol/g
203	0.0661	0.0040
437	0.0924	0.0067
656	0.1040	0.0103
769	0.1080	0.0131
1103	0.1148	0.0606
1443	0.1077	0.0646
1591	0.1008	0.0659
2037	0.0834	0.0686

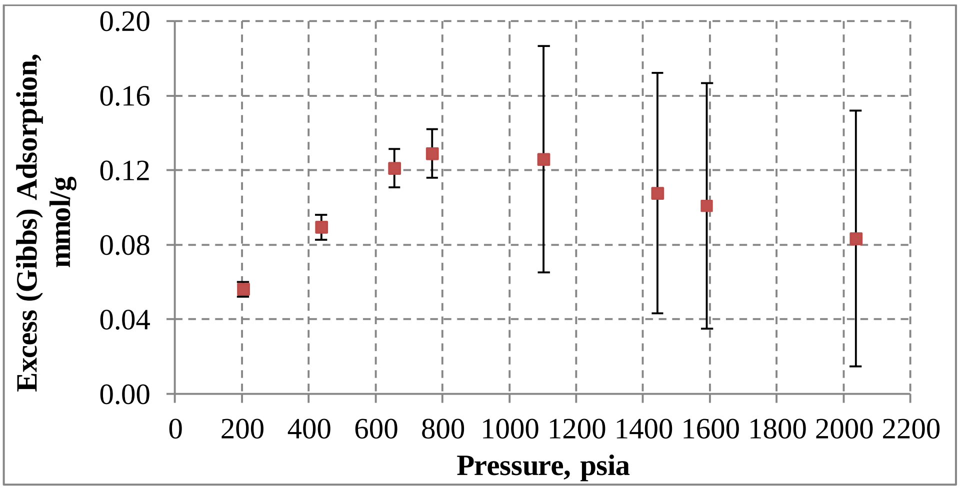

Figure 8.25: Run#7-Carbon dioxide adsorption isotherm of shale sample A at 25 ^oC

For Run#7, carbon dioxide adsorption capacities on shale sample A were measured at 25 °C. As seen in Figure 8.25, carbon dioxide adsorption capacities increase linearly until around 800 psia and then suddenly adsorption decreases sharply because carbon dioxide is in liquid state around 933 psia at 25 °C (See Appendix C).

Table 8.38: Run#8- Carbon dioxide adsorption on shale sample A at 50 °C

Pressure, psia	**Excess(Gibbs) Adsorption, mmol/g**	**Absolute Uncertainty in Excess Adsorption, mmol/g**
203	0.0366	0.0039
432	0.0505	0.0064
637	0.0686	0.0093
865	0.0799	0.0132
1005	0.0865	0.0165
1192	0.0928	0.0222
1402	0.0942	0.0332
1626	0.0860	0.0383
1803	0.0818	0.0433
2016	0.0712	0.0473

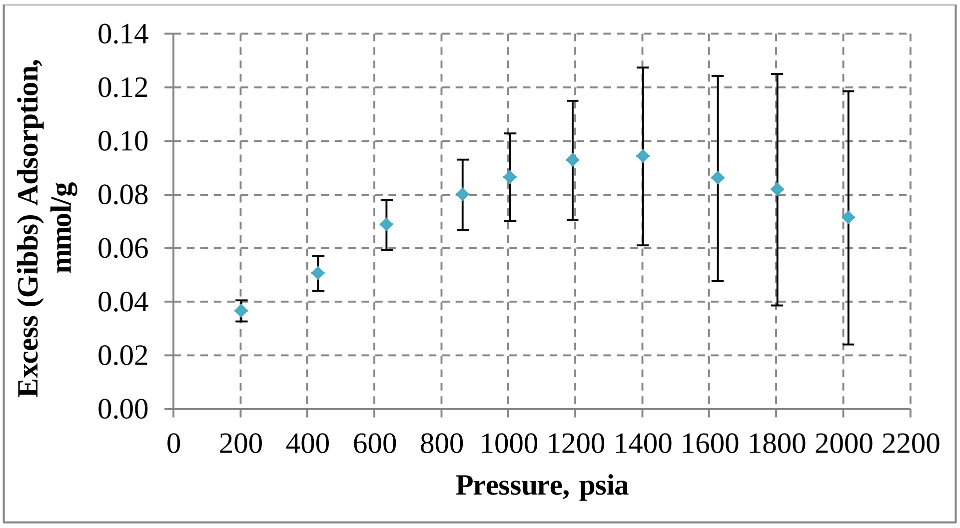

Figure 8.26: Run#8- Carbon dioxide adsorption isotherm of shale sample A At 50 °C

For Run#8 and Run#9, carbon dioxide adsorption capacities on shale sample A were measured at 50 °C and 75 °C. As seen in Figure 8.26 and Figure 8.27, carbon dioxide adsorption capacities increase linearly until around 1200 psia and then suddenly adsorption decreases in significant amounts because carbon dioxide is in supercritical region after 1200 psia at 50 ^{o}C and 75 ^{o}C (See Appendix C).

Table 8.39: Run#8- Carbon dioxide adsorption on shale sample A at 75 ^{o}C

Pressure , psia	Excess(Gibbs) Adsorption, mmol/g	Absolute Uncertainty in Excess Adsorption, mmol/g
199	0.0173	0.0040
417	0.0317	0.0065
627	0.0452	0.0094
821	0.0524	0.0136
1039	0.0591	0.0170
1257	0.0651	0.0242
1422	0.0695	0.0352
1676	0.0692	0.0393
1810	0.0670	0.0443
2060	0.0627	0.0493

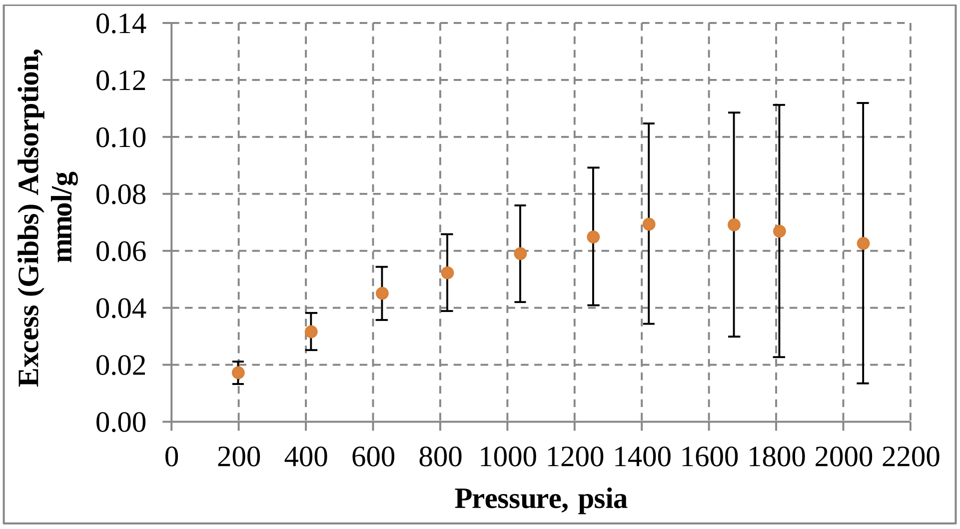

Figure 8.27: Run#8-Carbon dioxide adsorption isotherm of shale sample A at 75 ^{o}C

As seen in Figure 8.25, 8.26, 8.27, adsorption capacity of carbon dioxide is higher than adsorption capacity of methane on shale sample A. However, still uncertainties due to experiments become very important for shale samples' experiments. More attention were taken for shale samples' adsorption experiments in this study to reduce experimental uncertainties (See Chapter 6.2.4).

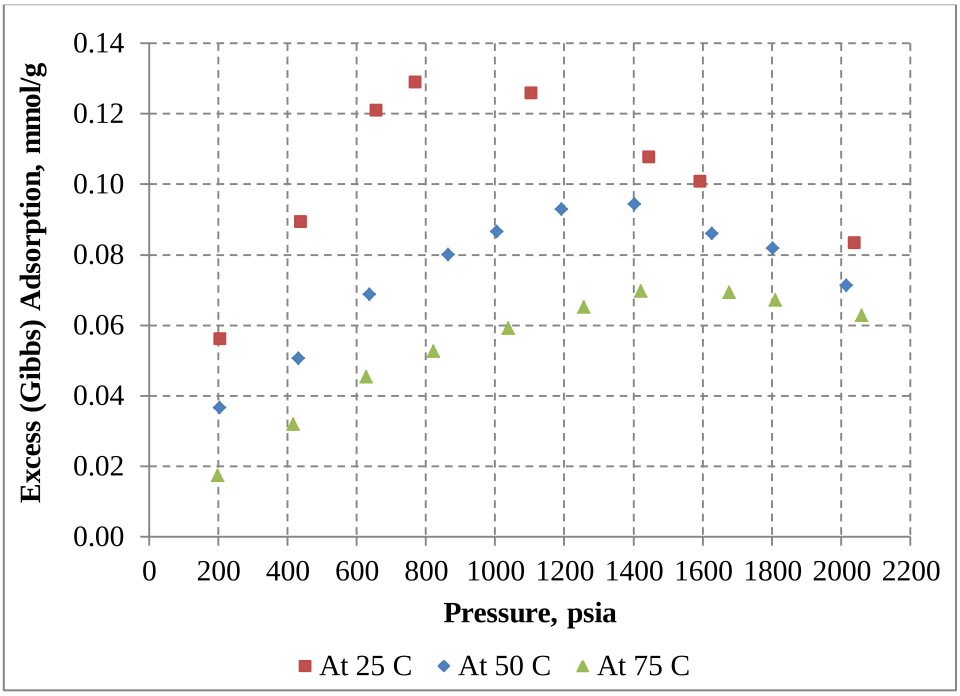

Figure 8.28: Comparison of Run#7, 8, 9- Carbon dioxide adsorption isotherm of shale sample A

As seen in Figure 8.28, adsorption of carbon dioxide decreases with increasing temperature. Due to different phase behaviors of carbon dioxide at different temperatures, isotherms' shapes are quite different, especially at 25 ^{o}C, after 800 psia, carbon dioxide's phase changes from gaseous state to liquid state. Hence, with increasing pressure, excess adsorption reaches peak and then starts decreasing. This indicates that the contribution of adsorption at high pressures is diminished as compared to the compression of the bulk gas.

Moreover, adsorption capacities of methane and carbon dioxide were compared for shale sample A. At 25 ^{o}C, carbon dioxide adsorption is 4.03 times (as an average), at 50 ^{o}C, carbon dioxide adsorption is 4.02 times, at 75 ^{o}C carbon dioxide adsorption is 6.05 times higher than methane adsorption on shale sample A.

8.2.2.1 Adsorption Models for Run#7 & Run#8 & Run#9

- ✓ Langmuir model is not valid for carbon dioxide adsorption at high pressures because of supercritical/liquid region. Hence, for carbon dioxide adsorption experimental data, Ono-Kondo monolayer and Ono-Kondo three layer models were used.

- ✓ The results of Ono-Kondo monolayer model's fitting to experimental data for shale sample A are listed in Table 8.40, Table 8.41, Table 8.42, and Table 8.43. As seen in Table 8.41, 42, 43 and Figure 8.29, experimental carbon dioxide adsorption data on shale sample A at 25 ^{o}C, 50 ^{o}C, 75 ^{o}C were fitted fairly by Ono-Kondo monolayer model.

Table 8.40: Ono-Kondo monolayer parameters for Run#7, Run#8, and Run#9 (Carbon dioxide adsorption on shale sample A)

	Run#7 (25 ^{o}C)	**Run#8 (50 ^{o}C)**	**Run#9 (75 ^{o}C)**
AAD (%)	3.983	3.400	4.998
ε_{fs}/k, (K)	-425	-700	-665
C, mmol/g	0.376	0.1318	0.103
Surface Area, m^2/g	72.815	28.139	24.323

Table 8.41: Ono-Kondo monolayer model results for Run#7 (Carbon dioxide adsorption on shale sample A at 25 ^{o}C)

Pressure, psia	**Excess (Gibbs) Adsorption, mmol/g**	**Adsorbed Phase Density, mol/l**	**Absolute Adsorption, mmol/g**
203	0.0173	2.103	0.0790
437	0.0317	4.260	0.1362
656	0.0452	6.390	0.2006
769	0.0524	7.704	0.2262
1103	0.0591	21.347	0.6777
1443	0.0651	21.902	0.7059
1591	0.0695	22.051	0.7075
2037	0.0692	22.364	0.7030

Table 8.42: Ono-Kondo monolayer model results for Run#8 (Carbon dioxide adsorption on shale sample A at 50 °C)

Pressure, psia	Excess (Gibbs) Adsorption, mmol/g	Adsorbed Phase Density, mol/l	Absolute Adsorption, mmol/g
203	0.0366	3.394	0.0437
432	0.0505	6.034	0.0639
637	0.0686	8.038	0.0916
865	0.0799	10.180	0.1140
1005	0.0865	11.560	0.1296
1192	0.0928	13.617	0.1513
1402	0.0942	16.583	0.1795
1626	0.0860	19.788	0.2155
1803	0.0818	20.896	0.2425
2016	0.0712	21.513	0.2427

Table 8.43: Ono-Kondo monolayer model results for Run#9 (Carbon dioxide adsorption on shale sample A at 75 °C)

Pressure, psia	Excess (Gibbs) Adsorption, mmol/g	Adsorbed Phase Density, mol/l	Absolute Adsorption, mmol/g
199	0.0173	2.610	0.0213
417	0.0317	4.755	0.0411
627	0.0452	6.524	0.0614
821	0.0524	8.034	0.0747
1039	0.0591	9.668	0.0889
1257	0.0651	11.308	0.1043
1422	0.0695	12.581	0.1175
1676	0.0692	14.603	0.1289
1810	0.0670	15.674	0.1325
2060	0.0627	17.495	0.1403

✓ The results of Ono-Kondo three-layer model's fitting to experimental data for shale sample A are listed in Table 8.44, 45, 46, and 47.

Table 8.44: Ono-Kondo three-layer model results for Run#7

Pressure (psia)	**Bulk Phase**	**1st Layer**	**2nd Layer**	**3rd Layer**
	$x_b=\rho_b/\rho_{mc}$	$x_1=\rho_{adsorbed1}/\rho_{mc}$	$x_2=\rho_{adsorbed2}/\rho_{mc}$	$x_3=\rho_{adsorbed3}/\rho_{mc}$
203	0.0261	0.0867	0.0257	0.0261
437	0.0627	0.1787	0.0610	0.0627
656	0.1087	0.2709	0.1049	0.1088
769	0.1418	0.3281	0.1366	0.1420
1103	0.7449	0.9134	0.7379	0.7451
1443	0.7952	0.9371	0.7900	0.7954
1591	0.8102	0.9434	0.8055	0.8103
2037	0.8446	0.9569	0.8411	0.8447

Table 8.45: Ono-Kondo three-layer model results for Run#8

Pressure (psia)	**Bulk Phase**	**1st Layer**	**2nd Layer**	**3rd Layer**
	$x_b=\rho_b/\rho_{mc}$	$x_1=\rho_{adsorbed1}/\rho_{mc}$	$x_2=\rho_{adsorbed2}/\rho_{mc}$	$x_3=\rho_{adsorbed3}/\rho_{mc}$
203	0.0237	0.1361	0.0230	0.0237
432	0.0542	0.2483	0.0518	0.0542
637	0.0863	0.3352	0.0818	0.0863
865	0.1304	0.4287	0.1230	0.1306
1005	0.1647	0.4890	0.1553	0.1650
1192	0.2255	0.5787	0.2131	0.2260
1402	0.3376	0.7071	0.3217	0.3382
1626	0.5094	0.8445	0.4936	0.5101
1803	0.5932	0.8919	0.5795	0.5938
2016	0.6512	0.9184	0.6394	0.6517

Table 8.46: Ono-Kondo three-layer model results for Run#9

Pressure (psia)	**Bulk Phase**	**1st Layer**	**2nd Layer**	**3rd Layer**
	$x_b=\rho_b/\rho_{mc}$	$x_1=\rho_{adsorbed1}/\rho_{mc}$	$x_2=\rho_{adsorbed2}/\rho_{mc}$	$x_3=\rho_{adsorbed3}/\rho_{mc}$
199	0.0212	0.1088	0.0208	0.0212
417	0.0466	0.2012	0.0451	0.0466
627	0.0741	0.2785	0.0710	0.0741
821	0.1026	0.3446	0.0978	0.1026
1039	0.1391	0.4162	0.1323	0.1392
1257	0.1820	0.4878	0.1731	0.1823
1422	0.2200	0.5431	0.2094	0.2204
1676	0.2898	0.6304	0.2768	0.2903
1810	0.3320	0.6762	0.3181	0.3326
2060	0.4145	0.7536	0.3998	0.4151

As seen in Table 8.44, 45, 46 and Figure 8.29, experimental carbon dioxide adsorption data on shale sample A at 25 °C, 50 °C and 75 °C were fitted fairly by Ono-Kondo three-layer model.

In Table 8.44, 45, 46, it is observed that adsorption occurred as monolayer in Run#7, 8, 9 because of density differences in layers. As seen in Table 8.47, model parameters of Ono-Kondo three-layer model are close to the parameters of Ono-Kondo monolayer model, which is the indication of monolayer adsorption.

Table 8.47: Ono-Kondo three-layer model regression parameters for Run#7,8,9

	Run#7 (25 °C)	**Run#8 (50 °C)**	**Run#9 (75 °C)**
AAD (%)	4.415	3.900	4.461
ε_{fs}/k, (K)	-405	-660	-645
C, mmol/g	0.394	0.1396	0.106
Surface Area, m^2/g	76.269	29.792	24.897

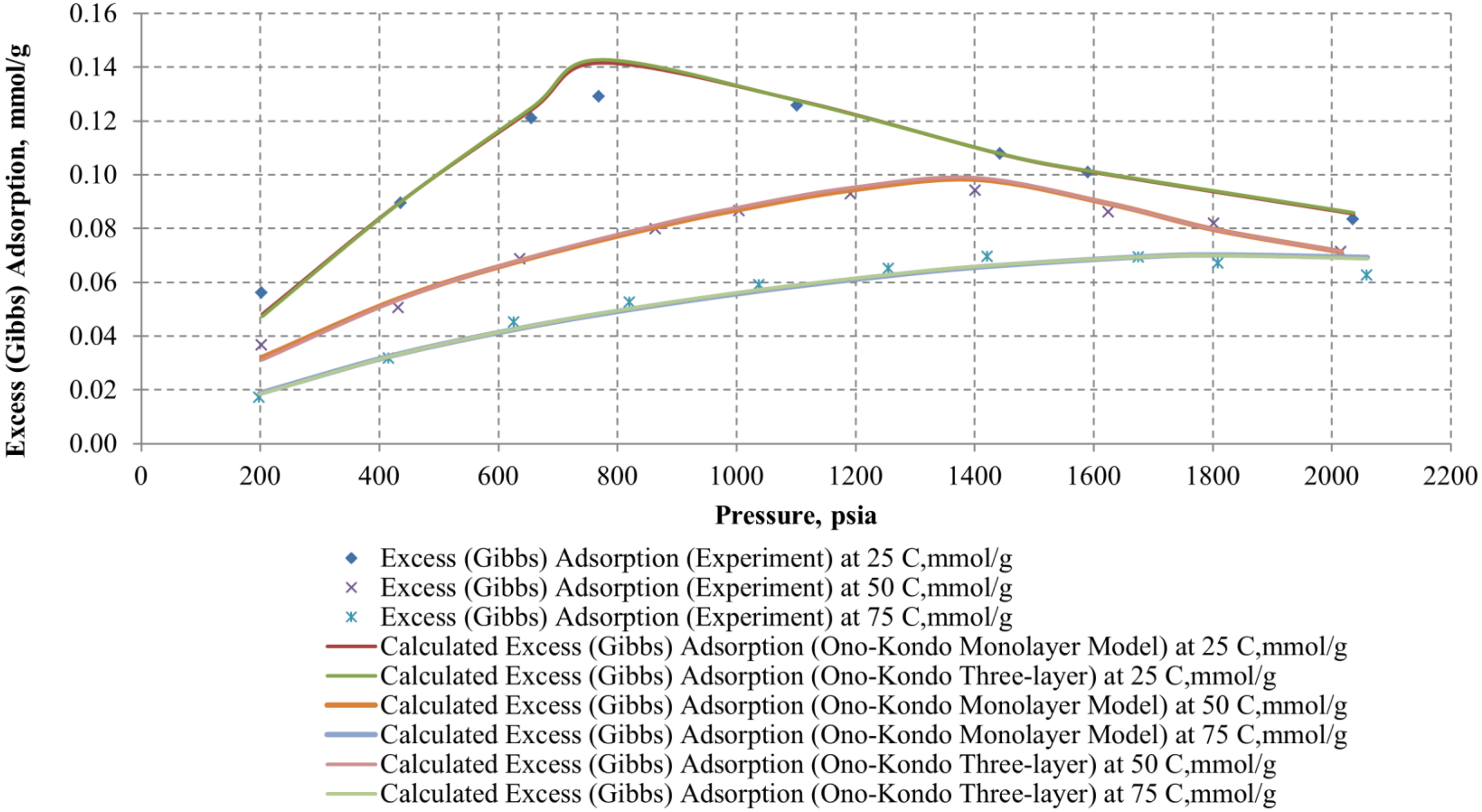

Figure 8.29: Adsorption models for Run#7, 8, 9- Carbon dioxide adsorption isotherms of shale sample A at different temperatures

8.3 Adsorption Experiments Results of Shale Sample B

Shale samples of B field were used for the adsorption experiments at different temperatures for both pure methane and pure carbon dioxide. Before using the samples, they were crushed to 20/35 and 100 mesh sizes. Then, shale samples were heated at 120 °C to avoid any moisture effects. The sample cell (122.4 cm^3) was filled by 121.7 g of sample for Run#10, 11, 12, 13, 14, 15, 16 and 143.1 g of sample for Run#17. Void volumes of the sample cell were measured at different pressure stages by using non-adsorbing gas helium.

Figure 8.30: A picture of shale sample B

After placing the cells into the constant temperature water bath, the following data was obtained:

Table 8.48: Experimental data for adsorption experiments with shale sample B

	Run#10, 11, 12, 13, 14, 15, 16	Run#17
Reference Cell Volume :	44.3cm^3	44.3 cm^3
Sample Weight :	121.7 g	143.1 g
Sample Cell Volume :	122.4 cm^3	122.4 cm^3
Mesh Size :	20/35	100
Average Void Volume :	58.61 cm^3	52.90 cm^3

Figure 8.31 and Figure 8.32 show the void volumes at different pressure values:

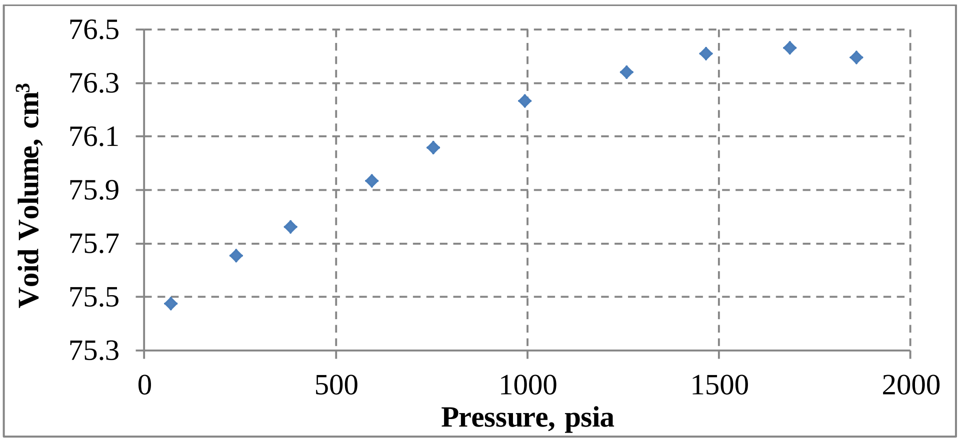

Figure 8.31: Run#10,11,12,13,14,15,16-Helium void volume of the sample cell filled with shale sample B

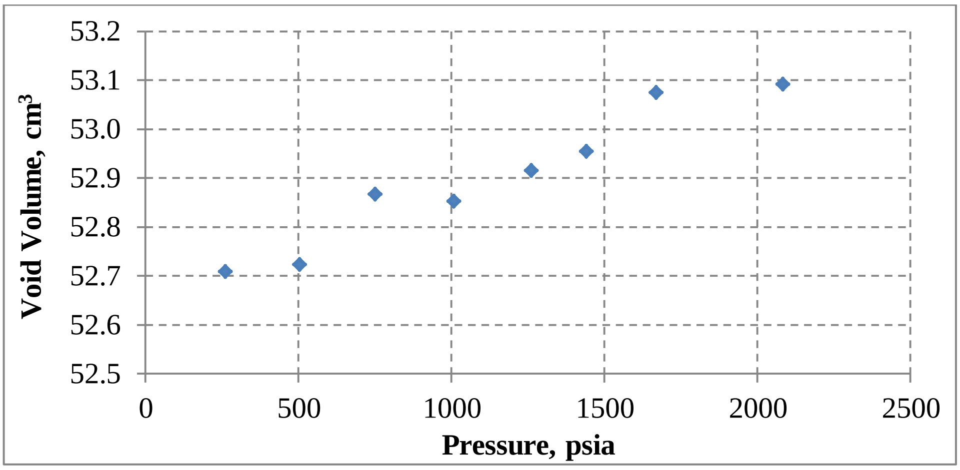

Figure 8.32: Run#17-Helium void volume of the sample cell filled with shale sample B

After determining void volumes, leakage tests were conducted at 2500 psia for 24 hours. Then, adsorption experiments on shale sample B were conducted at 25, 50, and 75 °C for both pure methane and pure carbon dioxide.

8.3.1 Run#10 & Run#11 & Run#12 & Run#13 & Run#17: Methane Adsorption on Shale Sample B at 25 °C, 50 °C, and 75 °C

After placing the cells into the constant temperature water bath and void volume calculations (Table 8.48 and Figure 8.31), methane adsorption experiments were conducted at 25 , 50 and 75 °C. In order to check the repeability of adsorption experiments in this study, methane adsorption experiment at 25 °C (Run#10) was repeated with Run#11 and another methane adsorption experiment with 100 mesh size sample (Run#17) was conducted at 25 °C to see the effect of mesh size on adsorption.

Table 8.49: Run#10- Methane adsorption on shale sample B at 25 °C

Pressure, psia	Excess(Gibbs) Adsorption, mmol/g	Absolute Uncertainty in Excess Adsorption, mmol/g
190	0.0197	0.0024
403	0.0265	0.0037
602	0.0325	0.0050
805	0.0361	0.0063
1002	0.0394	0.0077
1201	0.0412	0.0092
1403	0.0437	0.0107
1598	0.0446	0.0122
1798	0.0447	0.0137
2005	0.0450	0.0153

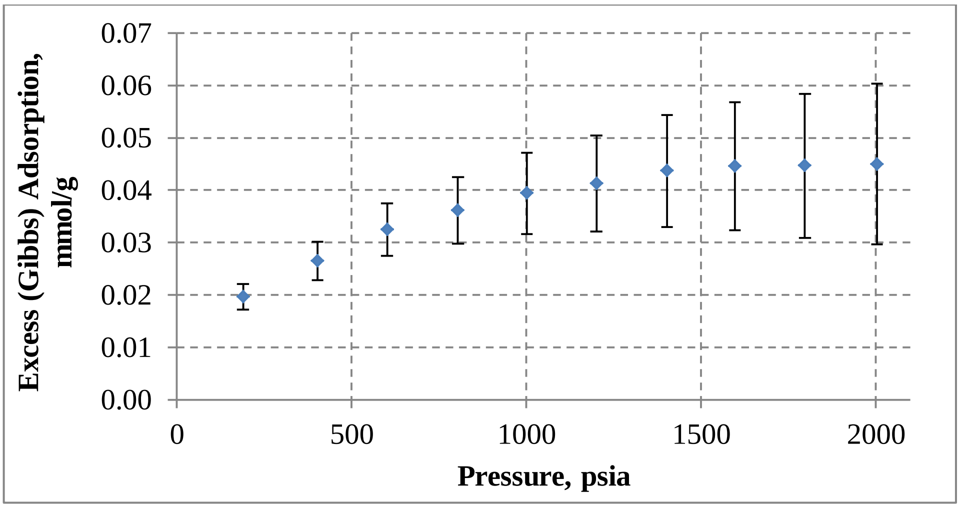

Figure 8.33: Run#10-Methane adsorption isotherm of shale sample B at 25 °C

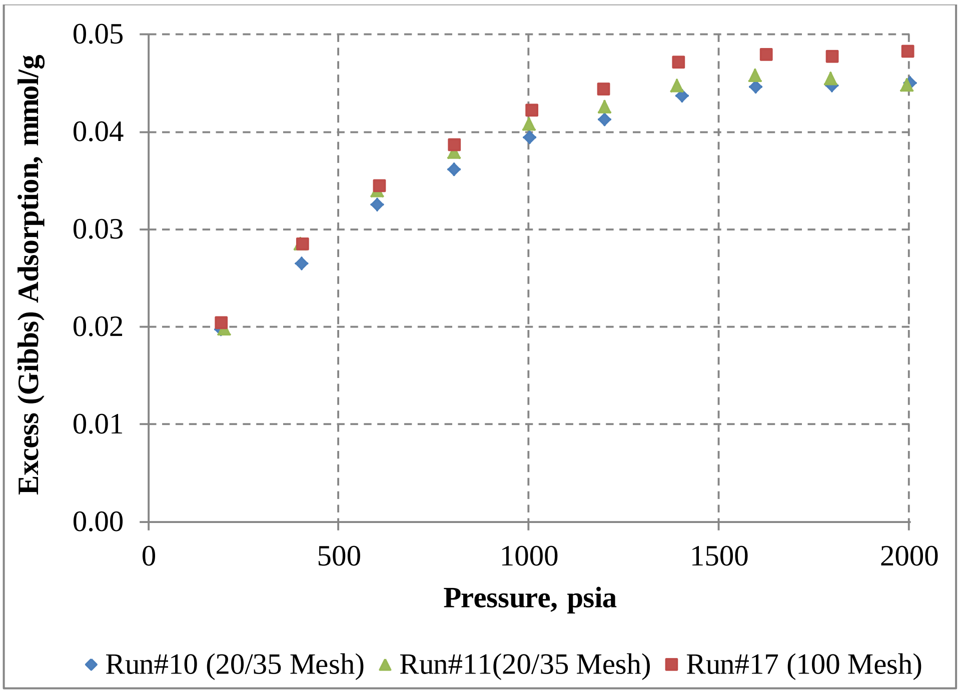

Figure 8.34: Comprasion of methane adsorption experiments of shale sample B at 25 ^{o}C

As seen in Figure 8.34, methane adsorption experiments were conducted at the same conditions for Run#10 and Run#11. In these experiments, 20/35 mesh size sample was used. However, in Run#17, 100 mesh size sample was used. According to the results of these three experiments, it was shown that adsorption experiments in this study was repeatable and also mesh size does not affect adsorption capacity. Moreover, equilibrium times of 20/35 mesh size and 100 mesh size's experiments are almost equal.

Table 8.50: Run#12- Methane adsorption on shale sample B at 50 ^{o}C

Pressure , psia	Excess(Gibbs) Adsorption, mmol/g	Absolute Uncertainty in Excess Adsorption, mmol/g
193	0.0077	0.0022
403	0.0125	0.0033
602	0.0181	0.0044
801	0.0210	0.0056
1001	0.0238	0.0068
1204	0.0262	0.0081
1400	0.0281	0.0093
1606	0.0298	0.0106
1799	0.0297	0.0119
2000	0.0301	0.0131

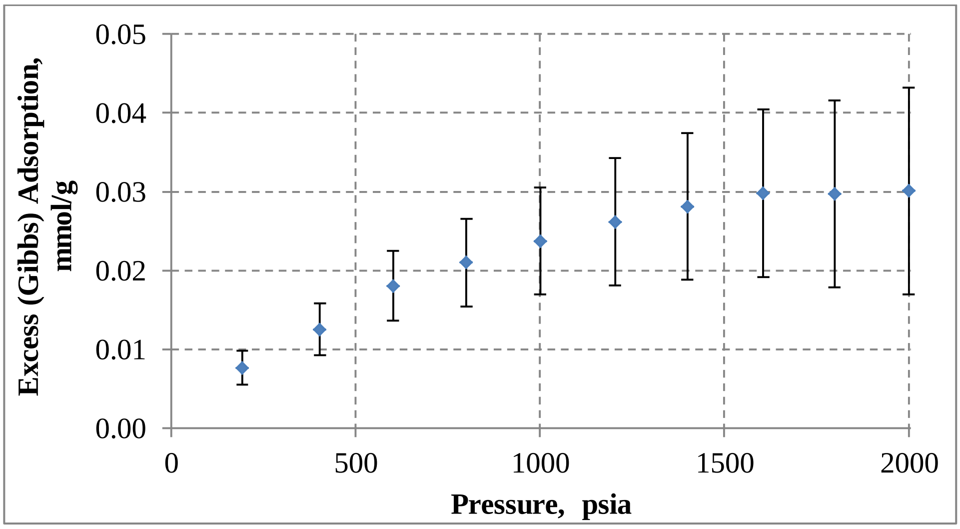

Figure 8.35: Run#12-Methane adsorption isotherm of shale sample B at 50 ^{o}C

Table 8.51: Run#13- Methane adsorption on shale sample B at 75 ^{o}C

Pressure , psia	**Excess(Gibbs) Adsorption, mmol/g**	**Absolute Uncertainty in Excess Adsorption, mmol/g**
195	0.0039	0.0031
402	0.0078	0.0047
601	0.0113	0.0063
801	0.0132	0.0080
1004	0.0152	0.0097
1200	0.0167	0.0116
1399	0.0175	0.0133
1600	0.0184	0.0157
1798	0.0185	0.0178
1993	0.0187	0.0204

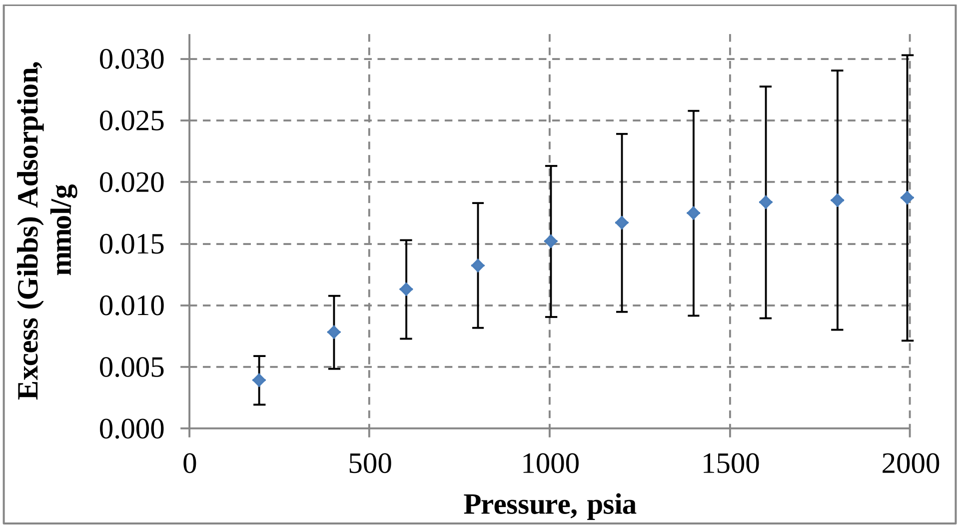

Figure 8.36: Run#13-Methane adsorption isotherm of shale sample B at 75 ^{o}C

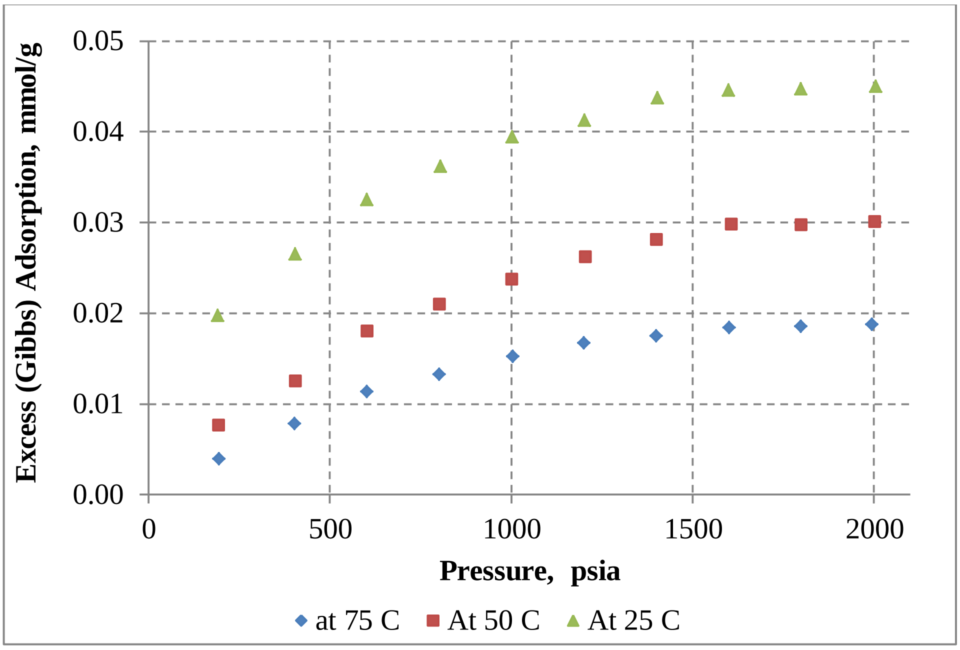

Figure 8.37: Comparison of Run#10, 12, 13-Methane adsorption isotherm of shale sample B

As seen in Figure 8.37, adsorption capacities of methane decrease with increasing temperature. It is known that adsorption is exothermic because in order to form new bonds, heat is released. Hence, the bonds between adsorbate and adsorbent are weakened and desorption occurs.

As seen in Figure 8.37, adsorption isotherms are in the classification of Type I. Adsorption capacities increase almost linearly for every pressure intervals but as pressure increases further, increase in adsorption amounts decrease. This is related to the complete filling of pores. However, for shale sample A, complete filling of pores was observed earlier. Hence, this difference between shale sample A and B indicates that pores of shale sample B is bigger than pores of shale sample A.

Methane adsorption capacities of shale sample B are 1.4, 1.2, 1.6 times higher than methane adsorption capacities of shale sample A at 25, 50, and 75 ^{o}C respectively. By using literature adsorption data, a figure was prepared by Chareonsuppanimit *et al.* (2012), in which there is a relation between adsorption capacity and total organic content (TOC). Hence, when methane and carbon dioxide adsorption capacities of shale sample A and B are considered by using Figure 8.38, both TOC values of shale sample A and B are in the range of 0 and 5 %. It is known that TOC of shale sample B is equal to 3.63 % so figure 8.38 gives a good approximation for TOC values. Adsorption capacities of shale sample B are higher than adsorption capacities of shale sample A. Therefore, it is expected that TOC of shale sample B is higher than TOC of shale sample A and/or clay contents of shale sample B are higher than clay contents of shale sample A.

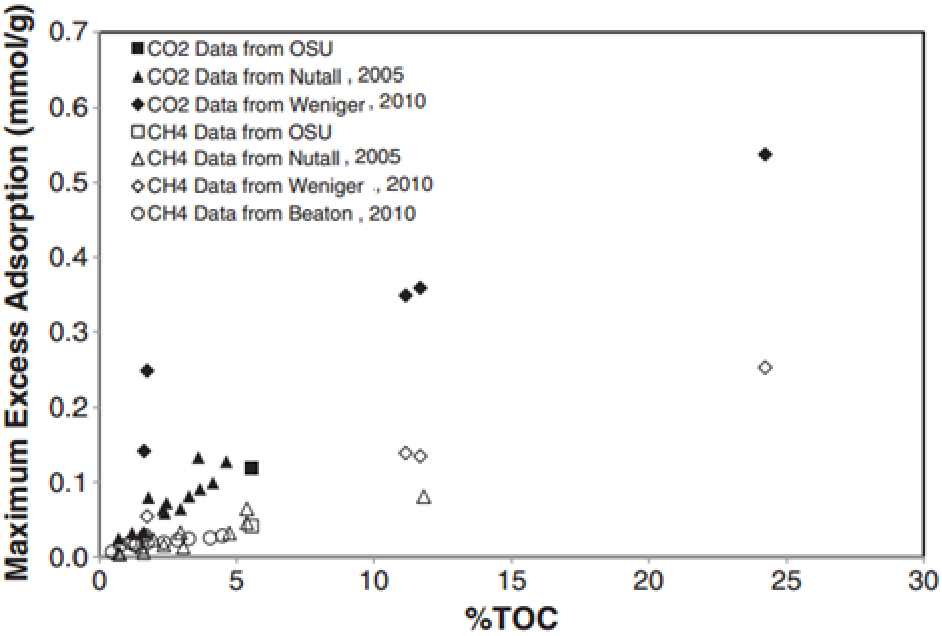

Figure 8.38: Maximum excess adsorption of CH_4 and CO_2 as a function of total organic carbon content: data from the literature (Chareonsuppanimit *et al.*, 2012)

8.3.1.1 Adsorption Models for Run#10 & Run#12 & Run#13

✓ After conducting Run#10, 12, 13, results were evaluated by using Langmuir model and Ono-Kondo models. The parameters of Langmuir model's fitting to experimental data are listed in Table 8.52. As seen in Figure 8.42, experimental methane adsorption data on shale sample B at 25, 50, and 75 °C were fitted fairly by Langmuir Model.

Table 8.52: Langmuir isotherm parameters for Run#10, Run#12, Run#13 (Methane adsorption on shale sample B)

Model Parameters	**Run#10 (25 °C)**	**Run#12 (50 °C)**	**Run#13 (75 °C)**
V_L	0.0545 mmol/g	0.0463 mmol/g	0.0293 mmol/g
P_L	387.9 psia	965 psia	992 psia
R^2	0.995	0.996	0.994

- ✓ The results of Ono-Kondo monolayer model's fitting to experimental data are listed in Table 8.53, Table 8.54 and Table 8.55 for Run#10, 12, 13.

Table 8.53: Ono-Kondo monolayer parameters for Run#10, Run#12, Run#13 (Methane adsorption on shale sample B)

	Run#10 (25 °C)	**Run#12 (50 °C)**	**Run#13 (75 °C)**
AAD (%)	2.406	2.177	4.268
ε_{fs}/k, (K)	-785	-540	-490
C, mmol/g	0.0489	0.0523	0.0408
Surface Area, m^2/g	14.398	16.070	13.550

As seen in Figure 8.42, experimental methane adsorption data on shale sample B for Run#10, 12 and 13 were fitted fairly by Ono-Kondo monolayer model. Excess adsorption values were corrected by Ono-Kondo monolayer model for absolute adsorption. As seen in Figure 8.39, 40, 41, there are significant differences between absolute adsorption and excess adsorption, indicating the high capability of Ono-Kondo models compared to Langmuir model.

As seen in Table 8.53, the parameters of Ono-Kondo monolayer model are listed for Run#10, 12 and 13. By using this model, surface area values were obtained. Surface area values obtained for shale sample B are 1.5, 2.4 and 3.4 times higher than the surface area values of shale sample A at 25, 50 and 75 °C respectively. Hence, this supports late complete filling of pores of shale sample B at higher pressures compared to shale sample A's.

Table 8.54: Ono-Kondo monolayer model results for Run#10 (Methane adsorption on shale sample B at 25 °C)

Pressure, psia	Excess (Gibbs) Adsorption, mmol/g	Adsorbed Phase Density, mol/l	Absolute Adsorption, mmol/g
190	0.0197	4.721	0.0222
403	0.0265	7.689	0.0312
602	0.0325	9.696	0.0399
805	0.0361	11.355	0.0461
1002	0.0394	12.724	0.0523
1201	0.0412	13.928	0.0569
1403	0.0437	15.012	0.0627
1597	0.0446	15.937	0.0667
1798	0.0447	16.785	0.0697
2004	0.0450	17.556	0.0733

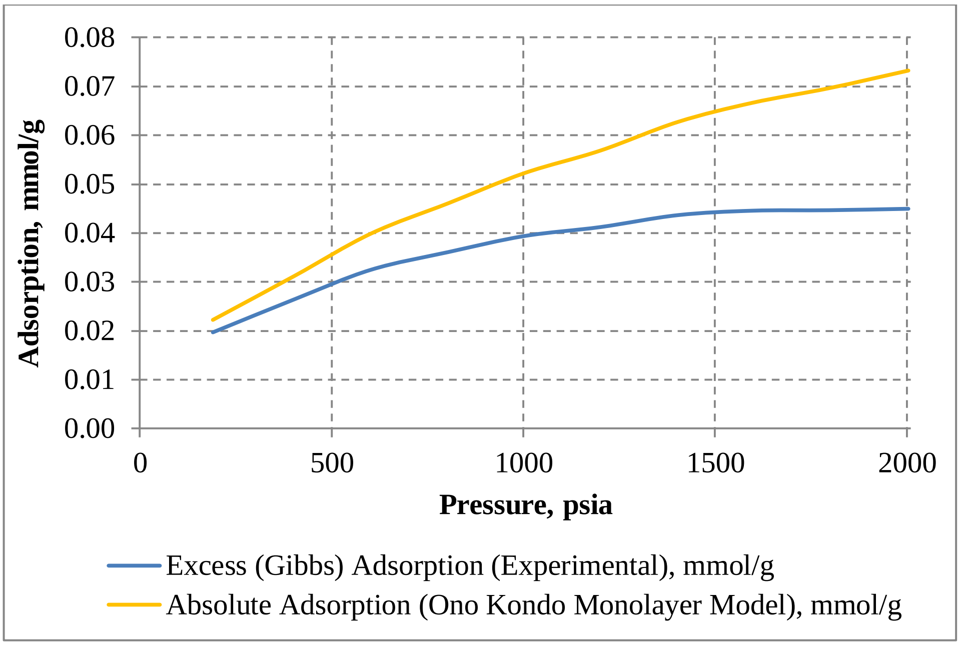

Figure 8.39: Absolute adsorption for Run#10

Table 8.55: Ono-Kondo monolayer model results for Run#12 (Methane adsorption on shale sample B at 50 °C)

Pressure, psia	**Excess (Gibbs) Adsorption, mmol/g**	**Adsorbed Phase Density, mol/l**	**Absolute Adsorption, mmol/g**
193	0.0077	2.242	0.0099
403	0.0125	4.135	0.0169
602	0.0181	5.634	0.0254
801	0.0210	6.953	0.0307
1001	0.0238	8.151	0.0361
1204	0.0262	9.263	0.0414
1400	0.0281	10.254	0.0461
1606	0.0298	11.221	0.0507
1799	0.0297	12.063	0.0524
2000	0.0301	12.880	0.0551

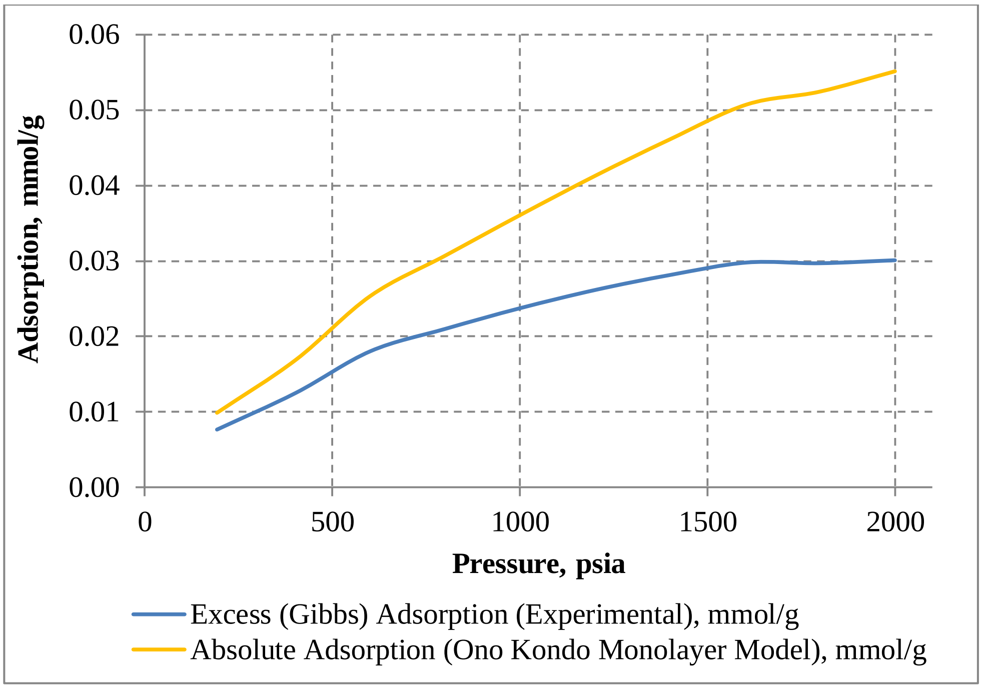

Figure 8.40: Absolute Adsorption for Run#12

Table 8.56: Ono-Kondo monolayer model results for Run#13 (Methane adsorption on shale sample B at 75 ^{o}C)

Pressure, psia	Excess (Gibbs) Adsorption, mmol/g	Adsorbed Phase Density, mol/l	Absolute Adsorption, mmol/g
195	0.0039	1.701	0.0056
402	0.0078	3.216	0.0117
601	0.0113	4.488	0.0175
801	0.0132	5.633	0.0213
1004	0.0152	6.701	0.0253
1200	0.0167	7.658	0.0288
1399	0.0175	8.563	0.0312
1600	0.0184	9.417	0.0339
1798	0.0185	10.211	0.0354
1993	0.0187	10.945	0.0369

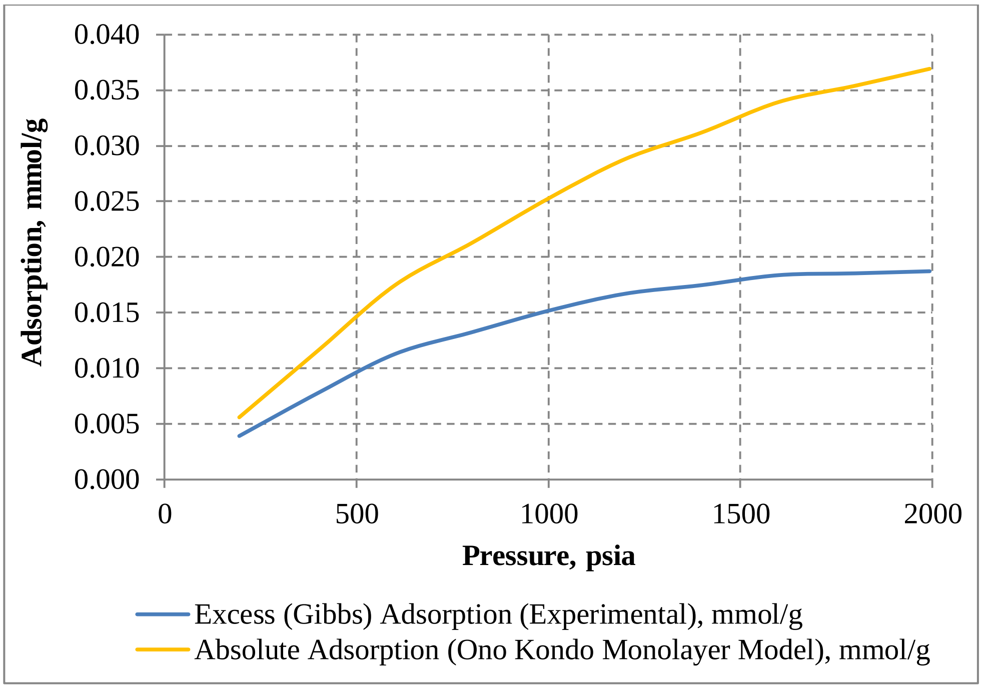

Figure 8.41: Absolute Adsorption for Run#13

✓ As seen in Figure 8.42, experimental methane adsorption data on shale sample B for Run#10,12,13 were fitted fairly by Ono-Kondo three-layer model.

Table 8.57: Ono-Kondo three-layer model results for Run#10

Pressure (psia)	**Bulk Phase**	**1st Layer**	**2nd Layer**	**3rd Layer**
	$x_b=\rho_b/\rho_{mc}$	$x_1=\rho_{adsorbed1}/\rho_{mc}$	$x_2=\rho_{adsorbed2}/\rho_{mc}$	$x_3=\rho_{adsorbed3}/\rho_{mc}$
190	0.0232	0.1983	0.0223	0.0232
403	0.0504	0.3279	0.0478	0.0504
602	0.0770	0.4161	0.0724	0.0771
805	0.1054	0.4890	0.0986	0.1055
1002	0.1341	0.5488	0.1253	0.1343
1201	0.1640	0.6012	0.1533	0.1643
1403	0.1953	0.6480	0.1829	0.1957
1598	0.2259	0.6877	0.2120	0.2263
1798	0.2576	0.7239	0.2424	0.2581
2005	0.2900	0.7565	0.2739	0.2906

Table 8.58: Ono-Kondo three-layer model results for Run#12

Pressure (psia)	**Bulk Phase**	**1st Layer**	**2nd Layer**	**3rd Layer**
	$x_b=\rho_b/\rho_{mc}$	$x_1=\rho_{adsorbed1}/\rho_{mc}$	$x_2=\rho_{adsorbed2}/\rho_{mc}$	$x_3=\rho_{adsorbed3}/\rho_{mc}$
193	0.0216	0.0971	0.0213	0.0216
403	0.0459	0.1802	0.0448	0.0459
602	0.0696	0.2463	0.0675	0.0696
801	0.0940	0.3044	0.0908	0.0940
1001	0.1192	0.3571	0.1149	0.1193
1204	0.1454	0.4059	0.1398	0.1455
1400	0.1710	0.4492	0.1644	0.1711
1606	0.1982	0.4912	0.1905	0.1984
1799	0.2237	0.5277	0.2151	0.2240
2000	0.2503	0.5629	0.2409	0.2506

Table 8.59: Ono-Kondo three-layer model results for Run#13

Pressure (psia)	**Bulk Phase**	**1st Layer**	**2nd Layer**	**3rd Layer**
	$x_b=\rho_b/\rho_{mc}$	$x_1=\rho_{adsorbed1}/\rho_{mc}$	$x_2=\rho_{adsorbed2}/\rho_{mc}$	$x_3=\rho_{adsorbed3}/\rho_{mc}$
195	0.0201	0.0734	0.0199	0.0201
402	0.0420	0.1395	0.0413	0.0420
601	0.0636	0.1952	0.0622	0.0636
801	0.0855	0.2455	0.0834	0.0856
1004	0.1083	0.2923	0.1054	0.1083
1200	0.1306	0.3343	0.1269	0.1307
1399	0.1534	0.3739	0.1488	0.1535
1600	0.1764	0.4111	0.1711	0.1765
1798	0.1993	0.4456	0.1931	0.1994
1993	0.2216	0.4775	0.2148	0.2217

Table 8.60: Ono-Kondo three-layer model regression parameters for Run#10,12,13

	Run#10 (25 °C)	**Run#12 (50 °C)**	**Run#13 (75 °C)**
AAD (%)	2.741	2.025	4.093
ε_{fs}/k, (K)	-765	-540	-490
C, mmol/g	0.0496	0.0506	0.0403
Surface Area, m^2/g	14.627	15.835	13.376

As seen Table 8.57, 58, 59, when density fractions are compared, it can be concluded that adsorption occurs as monolayer for shale sample B. Moreover, the results of Ono-Kondo three-layer model are almost equal to each other compared to the results of Ono-Kondo monolayer model.

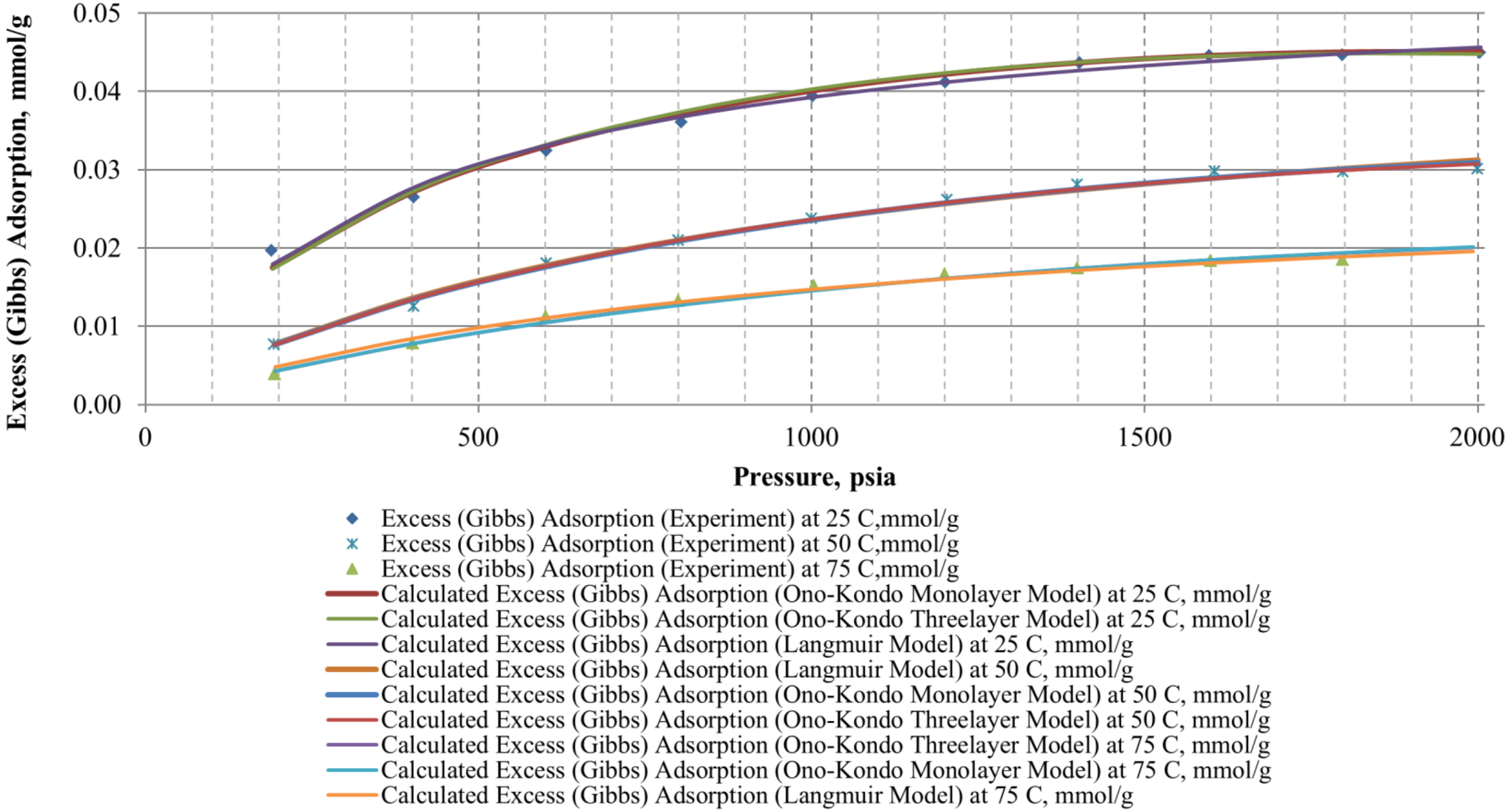

Figure 8.42: Adsorption models for Run#10, 12, 13-Methane adsorption isotherms of shale sample B at different temperatures

8.3.2 Run#14 & Run#15 & Run#16: Carbon dioxide Adsorption on Shale Sample B at 25 °C, 50 °C, and 75 °C

After placing the cells into the constant temperature water bath and void volume calculations (Table 8.48 and Figure 8.31), carbon dioxide adsorption experiments were conducted at 25, 50, and 75 °C. The aim of carbon dioxide adsorption experiments of shale sample B is to investigate possible storage of carbon dioxide to shale gas reservoirs after depletion or as a recovery technique.

Adsorption experimental results of Run#14,15 and 16 are listed in Table 8.61, 62 and 63. According to the results of Run#14, Run#15 and Run#16, carbon dioxide adsorption capacities are higher compared to methane adsorption capacities of shale sample B. This is because of stronger dispersion effects between carbon dioxide molecules and molecules on the surface of shale sample B compared to that of methane molecules'.

Table 8.61: Run#14- Carbon dioxide adsorption on shale sample B at 25 °C

Pressure, psia	Excess(Gibbs) Adsorption, mmol/g	Absolute Uncertainty in Excess Adsorption, mmol/g
174	0.102	0.003
435	0.155	0.004
641	0.182	0.006
917	0.211	0.008
1113	0.150	0.016
1402	0.126	0.019
1665	0.111	0.025
1885	0.103	0.030
2016	0.098	0.038

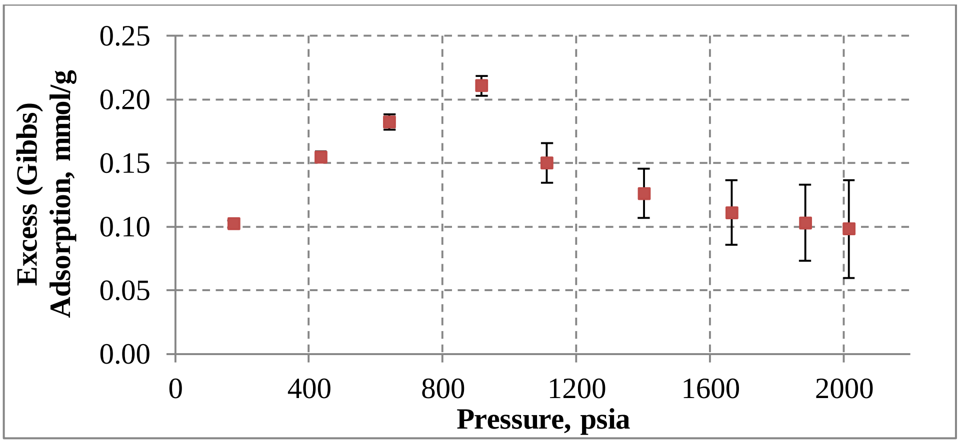

Figure 8.43: Run#14-Carbon dioxide adsorption isotherm of shale sample B at 25 °C

For Run#14, carbon dioxide adsorption capacities on shale sample B were measured at 25 °C. As seen in Figure 8.43, carbon dioxide capacity increases linearly until around 800 psia and then suddenly adsorption decreased in significant amount because carbon dioxide is in liquid state around 933 psia at 25 °C (See Appendix C).

Table 8.62: Run#15- Carbon dioxide adsorption on shale sample B at 50 °C

Pressure , psia	**Excess(Gibbs) Adsorption, mmol/g**	**Absolute Uncertainty in Excess Adsorption, mmol/g**
216	0.051	0.003
415	0.072	0.004
638	0.097	0.006
820	0.112	0.007
1047	0.121	0.0103
1233	0.130	0.0139
1448	0.107	0.0204
1545	0.095	0.0249
1868	0.076	0.0308
1987	0.067	0.0317

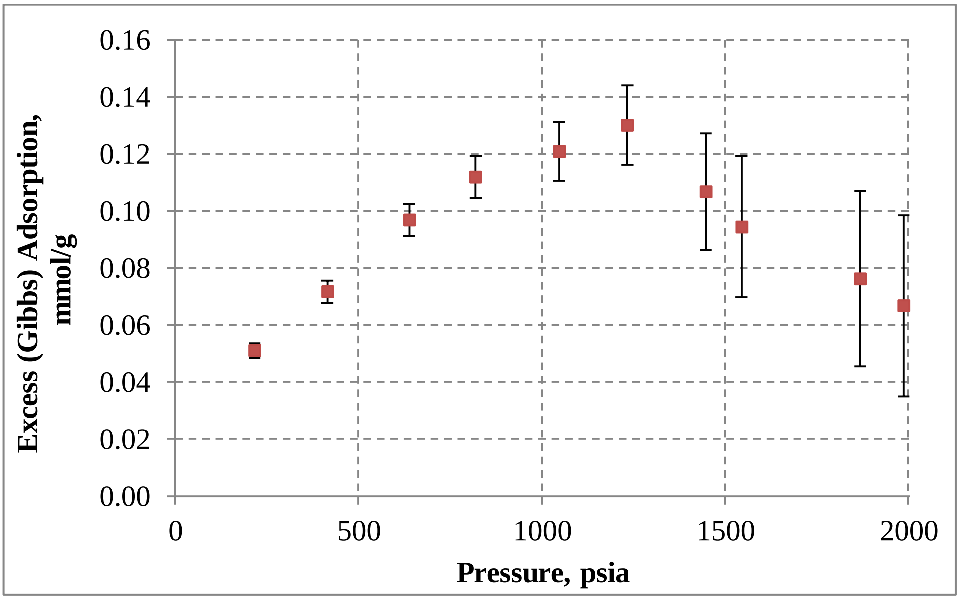

Figure 8.44: Run#15-Carbon dioxide adsorption isotherm of shale sample B at 50 °C

For Run#15 and Run#16, carbon dioxide adsorption capacities on shale sample B were measured at 50 and 75 °C. As seen in Figure 8.44 and Figure 8.45, carbon dioxide capacities increase linearly until around 1200 psia and then suddenly adsorption decreased in significant amount because carbon dioxide is in supercritical region after 1200 psia at 50 and 75 °C (Appendix C).

Table 8.63: Run#16- Carbon dioxide adsorption on shale sample B at 75 °C

Pressure , psia	Excess(Gibbs) Adsorption, mmol/g	Absolute Uncertainty in Excess Adsorption, mmol/g
184	0.039	0.002
411	0.058	0.004
608	0.067	0.005
812	0.078	0.007
1010	0.085	0.008
1146	0.091	0.010
1454	0.088	0.013
1657	0.080	0.016
1813	0.071	0.019
2000	0.068	0.022

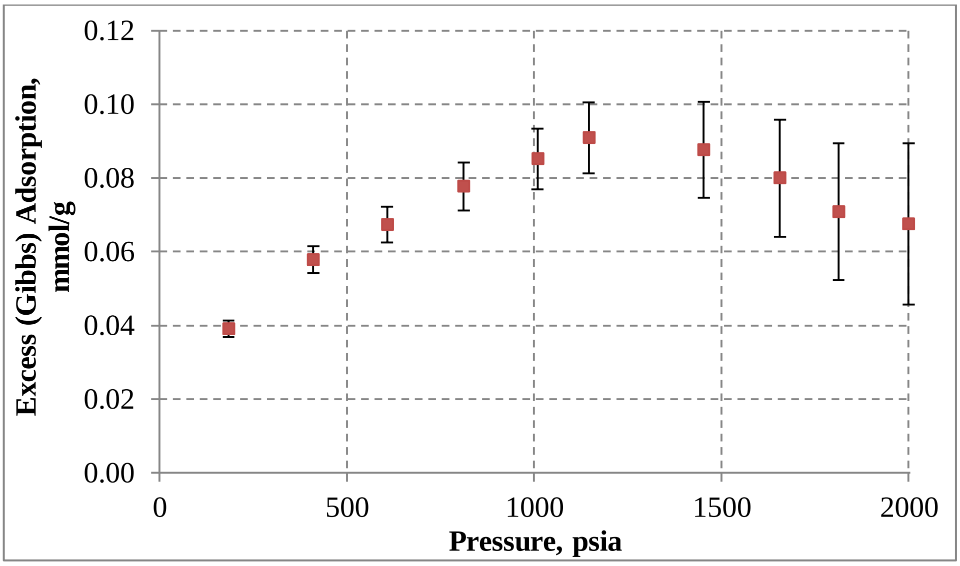

Figure 8.45: Run#16- Carbon dioxide adsorption isotherm of shale sample B at 75 °C

As seen in Figure 8.43, 8.44, and 8.45, adsorption of carbon dioxide is higher than adsorption of methane on shale sample B. However, still uncertainties due to experimental errors are important because of low adsorption capacities. More attention was taken for shale samples' adsorption experiments in this study to reduce experimental uncertainties (Chapter 6.2.4).

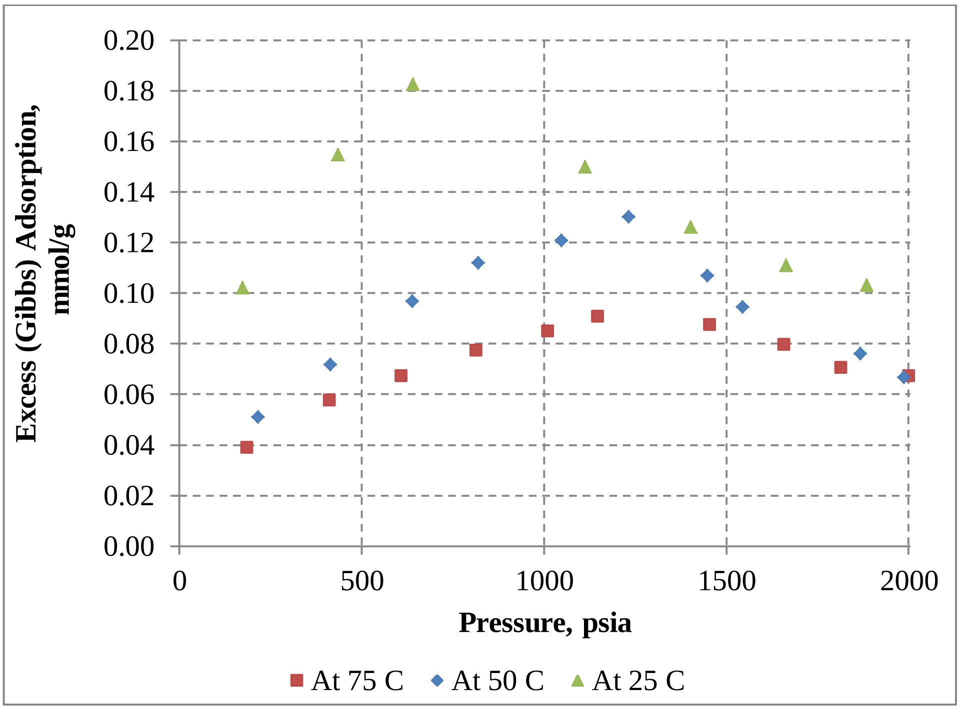

Figure 8.46: Comparisons of Run#14, 15, 16- Carbon dioxide adsorption isotherms of shale sample B

As seen in Figure 8.46, adsorption of carbon dioxide decreases with increasing temperature. With increasing pressure, excess adsorption reaches peak and then starts decreasing. This indicates that the contribution of adsorption at high pressures is diminished as compared to the compression of the bulk gas.

Moreover, the adsorption capacities of methane and carbon dioxide of sample B were compared. At 25 ^{o}C, carbon dioxide adsorption is 4 times (as an average), at 50 ^{o}C, carbon dioxide adsorption is 4.5 times, at 75 ^{o}C carbon dioxide adsorption is 5.7 times higher than methane adsorption on shale sample B.

8.3.2.1 Adsorption Models for Run#14 & Run#15 & Run#16

- ✓ Langmuir model does not have capability to fit on carbon dioxide adsorption experimental data at high pressures.

- ✓ The results of Ono-Kondo monolayer model's fitting to experimental data are listed in Table 8.64, Table 8.65, Table 8.66, and Table 8.67. As seen in Table 8.65, 66, 67 and Figure 8.47, experimental carbon dioxide adsorption data on shale sample B at 25, 50 , and 75 °C were fitted fairly by Ono-Kondo monolayer model.

Table 8.64: Ono-Kondo monolayer parameters for Run#14, Run#15, Run#16 (Carbon dioxide adsorption on shale sample B)

	Run#14 (25 °C)	**Run#15 (50 °C)**	**Run#16 (75 °C)**
AAD (%)	5.689	6.791	5.642
ε_{fs}/k, (K)	-635	-995	-1200
C, mmol/g	0.365	0.114	0.0741
Surface Area, m^2/g	70.661	24.274	17.444

Table 8.65: Ono-Kondo monolayer model results for Run#14 (Carbon dioxide adsorption on shale sample B at 25 °C)

Pressure, psia	**Excess (Gibbs) Adsorption, mmol/g**	**Adsorbed Phase Density, mol/l**	**Absolute Adsorption, mmol/g**
174	0.102	6.234	0.123
435	0.155	9.145	0.201
641	0.182	11.623	0.254
917	0.211	13.389	0.346
1113	0.150	15.544	0.693
1402	0.126	17.426	0.696
1665	0.111	19.944	0.695
1885	0.103	20.978	0.709
2016	0.0981	22.314	0.713

Table 8.66: Ono-Kondo monolayer model results for Run#15 (Carbon dioxide adsorption on shale sample B at 50 °C)

Pressure, psia	Excess (Gibbs) Adsorption, mmol/g	Adsorbed Phase Density, mol/l	Absolute Adsorption, mmol/g
216	0.051	6.234	0.056
415	0.072	9.145	0.083
638	0.097	11.623	0.117
820	0.112	13.389	0.142
1047	0.121	15.544	0.165
1233	0.130	17.426	0.193
1448	0.107	19.944	0.189
1545	0.095	20.978	0.190
1868	0.076	22.314	0.213
1987	0.067	22.479	0.202

Table 8.67: Ono-Kondo monolayer model results for Run#16 (Carbon dioxide adsorption on shale sample B at 75 °C)

Pressure, psia	Excess (Gibbs) Adsorption, mmol/g	Adsorbed Phase Density, mol/l	Absolute Adsorption, mmol/g
184	0.039	6.674	0.042
411	0.058	10.253	0.065
608	0.067	12.374	0.078
812	0.078	14.143	0.093
1010	0.085	15.613	0.107
1146	0.091	16.541	0.117
1454	0.088	18.449	0.123
1657	0.080	19.578	0.121
1813	0.071	20.352	0.115
2000	0.068	21.117	0.120

✓ As seen in Table 8.68, 69, 70 and Figure 8.47, experimental carbon dioxide adsorption data on shale sample B at 25, 50 and 75 °C were fitted fairly by Ono-Kondo three-layer model.

Table 8.68: Ono-Kondo three-layer model results for Run#14

Pressure (psia)	**Bulk Phase**	**1st Layer**	**2nd Layer**	**3rd Layer**
	$x_b=\rho_b/\rho_{mc}$	$x_1=\rho_{adsorbed1}/\rho_{mc}$	$x_2=\rho_{adsorbed2}/\rho_{mc}$	$x_3=\rho_{adsorbed3}/\rho_{mc}$
174	0.0221	0.0867	0.0257	0.0261
435	0.0624	0.1787	0.0610	0.0627
641	0.1051	0.2709	0.1049	0.1088
917	0.2185	0.3281	0.1366	0.1412
1113	0.7470	0.9134	0.7379	0.7451
1402	0.7905	0.9371	0.7900	0.7954
1665	0.8168	0.9434	0.8055	0.8103
1885	0.8342	0.9569	0.8411	0.8447
2016	0.8432	0.9695	0.8452	0.8456

Table 8.69: Ono-Kondo three-layer model results for Run#15

Pressure (psia)	**Bulk Phase**	**1st Layer**	**2nd Layer**	**3rd Layer**
	$x_b=\rho_b/\rho_{mc}$	$x_1=\rho_{adsorbed1}/\rho_{mc}$	$x_2=\rho_{adsorbed2}/\rho_{mc}$	$x_3=\rho_{adsorbed3}/\rho_{mc}$
216	0.0253	0.2627	0.0238	0.0253
415	0.0517	0.3913	0.0478	0.0517
638	0.0865	0.5010	0.0792	0.0866
820	0.1208	0.5786	0.11021	0.1210
1047	0.1766	0.6724	0.1617	0.1770
1233	0.2424	0.7530	0.2238	0.2431
1448	0.3720	0.8585	0.3505	0.3730
1545	0.4515	0.9011	0.4305	0.4524
1868	0.6143	0.9561	0.5988	0.6150
1987	0.6449	0.9629	0.6308	0.6455

Table 8.70: Ono-Kondo three-layer model results for Run#16

Pressure (psia)	Bulk Phase	1st Layer	2nd Layer	3rd Layer
	$x_b=\rho_b/\rho_{mc}$	$x_1=\rho_{adsorbed1}/\rho_{mc}$	$x_2=\rho_{adsorbed2}/\rho_{mc}$	$x_3=\rho_{adsorbed3}/\rho_{mc}$
184	0.0196	0.2759	0.0184	0.0196
411	0.0459	0.4333	0.0422	0.0460
608	0.0715	0.5272	0.0650	0.0716
812	0.1012	0.6052	0.0918	0.1014
1010	0.1339	0.6695	0.1214	0.1342
1146	0.1593	0.7099	0.1448	0.1597
1454	0.2280	0.7920	0.2093	0.2287
1657	0.2841	0.8400	0.2633	0.2848
1813	0.3331	0.8726	0.3114	0.3340
2000	0.3951	0.9047	0.3733	0.3960

Table 8.71: Ono-Kondo three-layer model regression parameters for Run#14,15, 16

	Run#14 (25 °C)	Run#15 (50 °C)	Run#16 (75 °C)
AAD (%)	4.452	5.928	5.181
ε_{fs}/k, (K)	-475	-965	-1155
C, mmol/g	0.394	0.117	0.0764
Surface Area, m^2/g	75.152	24.911	17.966

In Table 8.68, 69, 70, As seen Table 8.68, 69, 70, when density fractions are compared, it can be concluded that adsorption occurs as monolayer for shale sample B. Moreover, the results of Ono-Kondo three-layer model are almost equal to each other compared to the results of Ono-Kondo monolayer model.

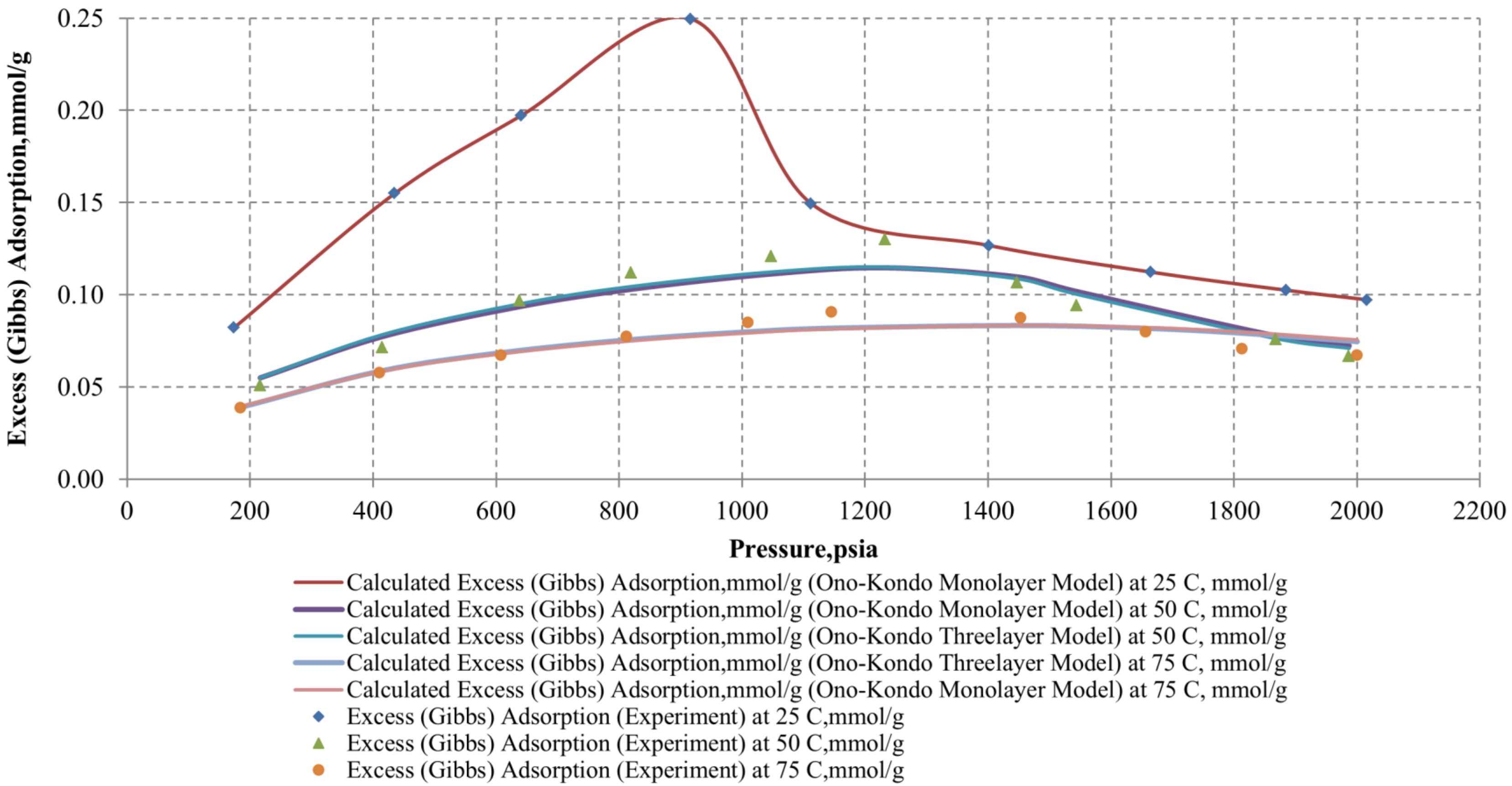

Figure 8.47: Adsorption models for Run#14, 15, 16-Carbon dioxide adsorption isotherms of shale sample B at different temperatures

8.4 Mixed Gas Adsorption Approximation

Adsorption of mixtures of gases is complicated compared to adsorption of pure gases. A matlab program written in this study for Ono-Kondo model for binary mixtures was used to make predictions about binary mixtures of methane and carbon dioxide. As an equation of states in the model, Peng and Robinson equations of states (EOS) were prefered. However, for the evaluation of experimental data, EOS of Angus for methane and EOS of Span and Wagner for carbon dioxide are advised because of their high accuracy. In the model, pure adsorption capacities and Ono-Kondo monolayer parameters of methane and carbon dioxide at 75 ^{o}C was used in order to make adsorption estimations for binary mixtures of methane and carbon dioxide.

To conduct experiments related to adsorption of mixtures of gases, more detailed experimental setup is needed, which is too expensive. Hence, by using this Ono-Kondo model for mixtures, some predictions can be done. In shale gas reservoirs, after depletion or as a recovery technique, carbon dioxide might be injected. Hence, it is important to have information about adsorption of methane and carbon dioxide mixtures.

According to the results of experiments in this study, carbon dioxide adsorption is higher than methane adsorption. Hence, in mixtures, much carbon dioxide is adsorbed than methane. A matlab program was written in this study for Ono-Kondo model for binary mixtures for shale samples A and B (See Appendix B).

In Figure 8.48 and 49, at different feed compositions, methane and carbon dioxide adsorption values and total adsorption values obtained from the matlab program of Ono-Kondo model for binary mixtures were shown for shale sample A at 75 ^{o}C :

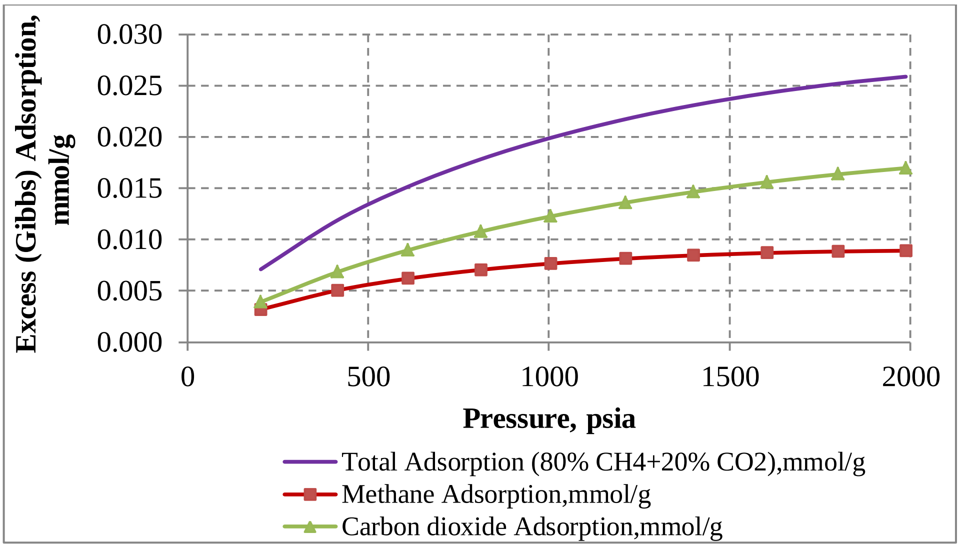

Figure 8.48: Adsorption of binary mixtures of 80% methane+ 20 % carbon dioxide by using Ono-Kondo model for mixtures for shale sample A at 75 ^{o}C

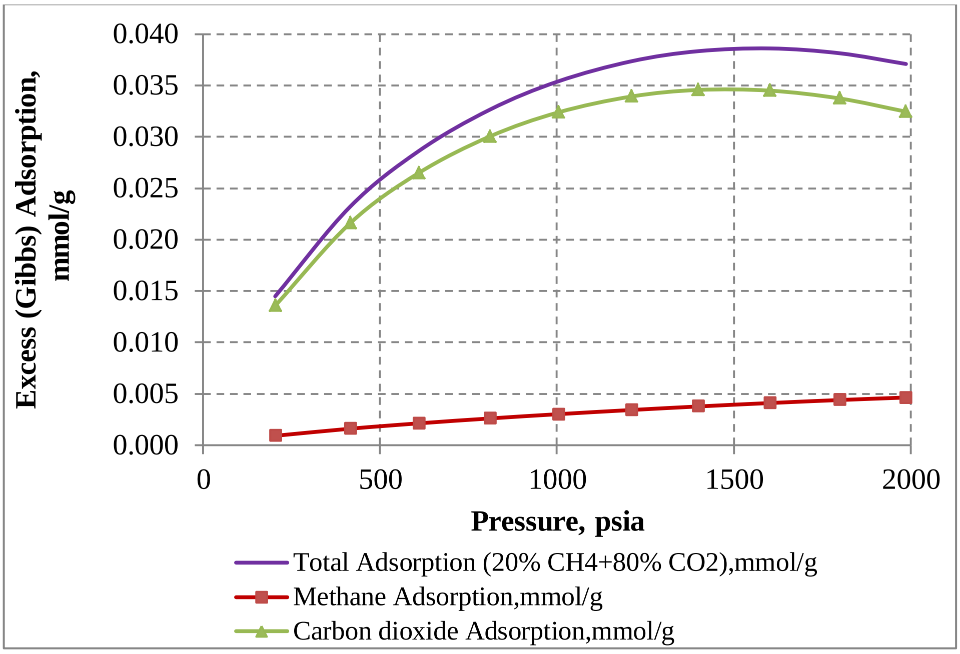

Figure 8.49: Adsorption of binary mixtures of 20% methane+ 80 % carbon dioxide by using Ono-Kondo model for mixtures for shale sample A at 75 ^{o}C

In Figure 8.50 and 8.51, at different feed compositions, methane and carbon dioxide adsorption values and total adsorption values obtained from the matlab program were shown for shale sample B at 75 ^{o}C :

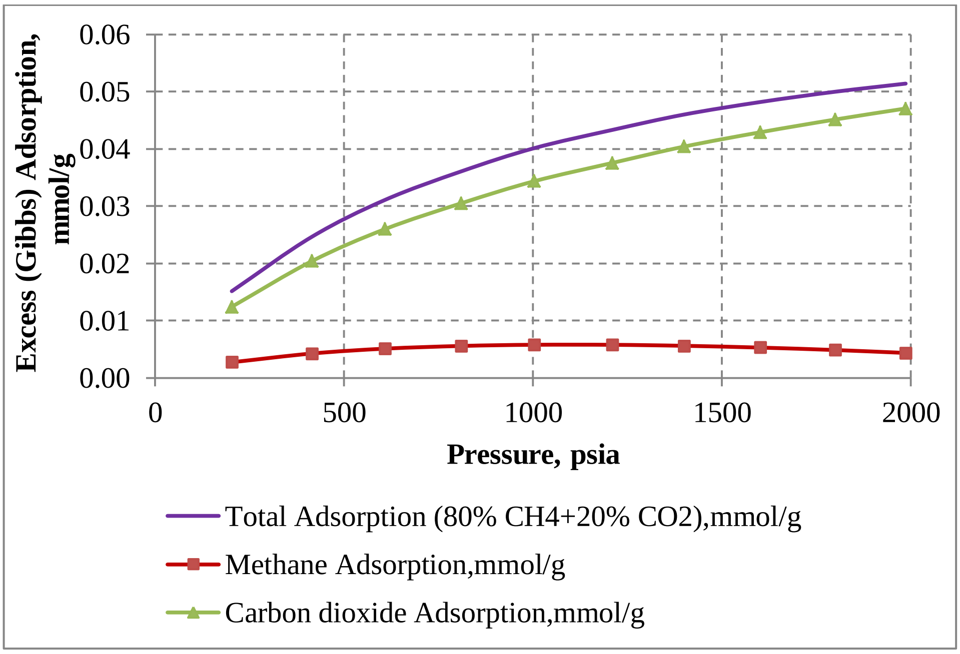

Figure 8.50: Adsorption of binary mixtures of 80% methane+ 20 % carbon dioxide by using Ono-Kondo model for mixtures for shale sample B at 75 ^{o}C

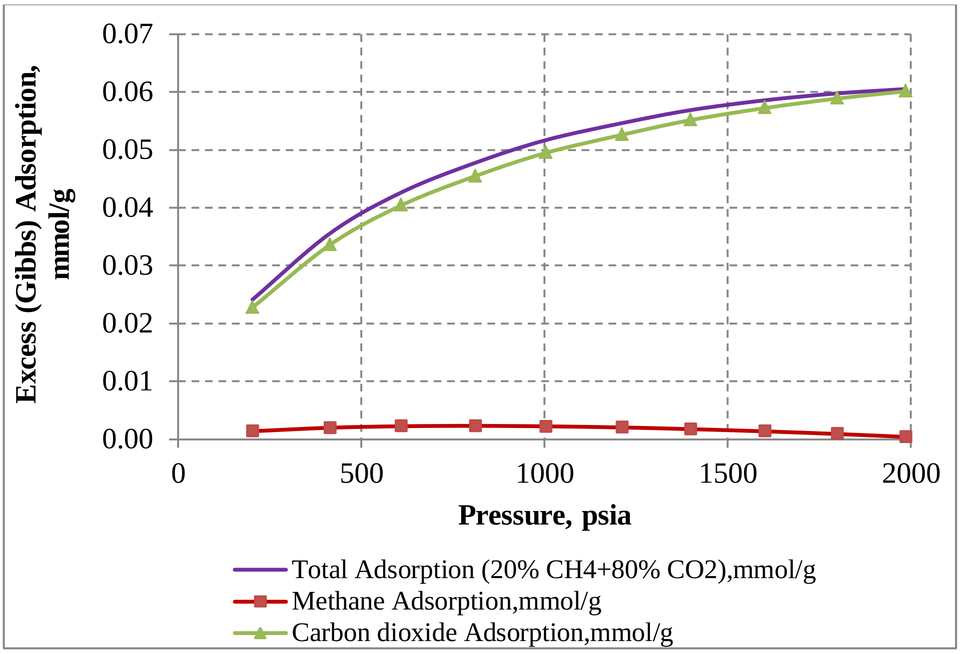

Figure 8.51: Adsorption of binary mixtures of 20% methane+ 80 % carbon dioxide by using Ono-Kondo model for mixtures for shale sample B at 75 ^{o}C

As seen in figures above, the contribution of carbon dioxide to adsorption is very high for binary mixtues of methane and carbon dioxide on both shale sample A and B. As seen in Figure 8.48 and 8.50, although carbon dioxide's feed compositions (20 %) are very low compared to methane feed compositions (80 %), its adsorption capacities are very high compared to methane adsorption capacities in mixture**.**

For shale sample B, both methane adsorption and carbon dioxide adsorption capacities are higher than the adsorption capacities of shale sample A. However, the gap between methane and carbon dioxide adsorption capacities of shale sample B is bigger than shale sample A's as seen figures above. Hence, for mixtures, as seen in Figure 8.50 and 8.51, much carbon dioxide is adsorbed compared to methane because of high intermolecular attractions between carbon dioxide molecules and molecules on the surface of shale sample B.

According to adsorption data of binary mixtures, injection of carbon dioxide for storage or as a recovery technique, shale B reservoir is much appropriate than shale A reservoir.

8.5 Initial Gas-in Place Calculations in Shale Gas Reservoirs

Shale gas reservoirs are classified as unconventional reserves. Hence, initial gas-in place calculations for conventional reserves cannot be used for shale gas reserves. Ambrose *et al.* (2010) proposed a new technique for shale gas-in place calculations. However, in Ambrose *et al.* (2010)'s equations for shale gas in-place calculations, only Langmuir model parameters are used and also volume occupied by adsorbed molecules is ignored. In this study, in addition to Langmuir model, Ono-Kondo models were used to evaluate experimental adsorption data. Hence, simple modifications were done in Ambrose *et al.* (2010)'s shale gas-in place calculations in this study.

Instead of adsorbed gas amount calculated by Langmuir model in Ambrose *et al.* (2010)'s calculations, adsorption parameters calculated by Ono-Kondo monolayer model was preferred because in this study, it was indicated that adsorption occurs as monolayer in shale gas reservoirs.

$$G_a = G_{sL}\frac{P}{P+P_L} \qquad \rightarrow \qquad G_a = 1518C\left(\frac{\rho_{ads}}{\rho_{mc}} - \frac{\rho_{gas}}{\rho_{mc}}\right) \qquad (8.1)$$

Where, G_a: gas adsorbed on the surface, scf/ton, G_L: Langmuir volume, scf/ton, P_L:Langmuir pressure,psia, C: maximum adsorption capacity (Ono-Kondo model parameter), mmol/g, ρ_{ads} : adsorbed gas density, g/cm^3, ρ_{mc} : adsorbed-phase density corresponding to the maximum adsorption capacity, g/cm^3

Initial shale gas-in place equation of Ambrose *et al.* (2010) was converted to the form in which Ono-Kondo monolayer model was used. Then, equation 8.1 was inserted into equation 8.2 and then, equation 8.3 was obtained.

$$G_{st} = \frac{32.0368}{B_g}\left[\frac{\phi(1-S_w)}{\rho_b} - \frac{1.318\times10^{-6}\hat{M}}{\rho_s}G_a\right] + G_a$$

, Ambrose *et al.* (2010)

(8.2) →

$$G_{st} = \frac{32.0368}{B_g}\left[\frac{\phi(1-S_w)}{\rho_b} - \frac{2.001\times10^{-3}\hat{M}}{\rho_{ads}}\left(C\left(\frac{\rho_{ads}}{\rho_{mc}} - \frac{\rho_{gas}}{\rho_{mc}}\right)\right)\right] + \left(1518C\left(\frac{\rho_{ads}}{\rho_{mc}} - \frac{\rho_{gas}}{\rho_{mc}}\right)\right)$$

(8.3)

where G_{st}: total gas in place, scf/ton, M: apparent natural-gas molecular weight, g/g-mole, ϕ: porosity, fraction, S_w: water saturation, dimensionless, ρ_b: bulk-rock density, g/cm^3, ρ_{gas} : free-gas-phase density, g/cm^3, ρ_{ads}: adsorbed-phase density, g/cm^3, ρ_{mc} or ρ_s: adsorbed-phase density corresponding to the maximum adsorption capacity, g/cm^3

In Ambrose *et al.* (2010)'s equations and equation 8.3 formed in this study, volume occupied by adsorbed gas is ignored. Especially at high pressures, volume occupied by adsorbed gas becomes important. Hence, in the following equation, a correction was done for volume occupied by adsorbed gas by using adsorbed phase density.

By using equation 7.15, excess (Gibbs) adsorption was converted to absolute adsorption:

$$G_{a\_absolute} = 1518C\left(\frac{\rho_{ads}}{\rho_{mc}} - \frac{\rho_{gas}}{\rho_{mc}}\right)\left(\frac{\rho_{ads}}{\rho_{ads} - \rho_{gas}}\right) \rightarrow G_{a\_absolute} = 1518C\left(\frac{\rho_{ads}}{\rho_{mc}}\right)$$

(8.4)

Then, equation 8.4 was inserted into equation 8.2 and the following equation for shale gas-in place was obtained:

$$G_{st} = \frac{32.0368}{B_g}\left[\frac{\phi(1-S_w)}{\rho_b} - \frac{2.001\times10^{-3}\hat{M}C}{\rho_{mc}}\right] + \left(1518C\left(\frac{\rho_{ads}}{\rho_{mc}} - \frac{\rho_{gas}}{\rho_{mc}}\right)\right)$$

(8.5)

- ✓ For both shale gas reservoir A and shale gas reservoir B, porosity and water saturation values were assumed and pure methane adsorption parameters of Ono-Kondo monolayer model at 75 °C were used (Table 8.72):

Table 8.72: Shale properties of shale sample A and B

	Shale Sample A	**Shale Sample B**
ϕ, fraction :	0.06	0.06
S_w, fraction :	0.35	0.35
ρ_b, g/cm^3 :	1.97	2.06
C, mmol/g :	0.0120	0.0408
P_L, psia :	468	992
G_{sL} (n_L) :	10.20 scf/ton (0.0134 mmol/g)	22.24 scf/ton (0.0293 mmol/g)

The aim of assumed shale gas reservoirs A and B was to show the methodology for shale gas-in place calculations. Therefore, shale gas-in place results by using equation 8.2 and the equations obtained in this study were compared.

Table 8.73: Shale gas-in place calculations by equations for shale sample A at 75 ^{o}C

	With Langmuir Model (Equation 8.2)				With Ono-Kondo Monolayer Model (Equation 8.3)				With Absolute Adsorption with Ono-Kondo Monolayer Model (Equation 8.5)			
P, psia	**G_a, scf/ton**	**G_f, scf/ton**	**G_t, scf/ton**	**% Adsorbed Gas**	**G_a, scf/ton**	**G_f, scf/ton**	**G_t, scf/ton**	**% Adsorbed Gas**	**G_a, scf/ton**	**G_f, scf/ton**	**G_t, scf/ton**	**% Adsorbed Gas**
500	5.3	18.2	23.4	22.4	5.1	17.6	22.7	22.4	6.0	17.5	23.5	25.7
1000	6.9	37.1	44.0	15.7	6.9	36.3	43.3	16.0	8.9	35.9	44.8	19.8
1500	7.8	56.6	64.4	12.0	7.9	55.7	63.6	12.4	10.9	54.9	65.8	16.6
2000	8.2	76.2	84.5	9.8	8.3	75.3	83.6	9.9	12.3	74.0	86.3	14.3
2500	8.6	95.3	103.9	8.2	8.4	94.6	103.0	8.2	13.5	92.6	106.1	12.7
3000	8.8	113.4	122.2	7.2	8.4	112.8	121.2	6.9	14.4	110.3	124.7	11.6
3500	9.0	130.1	139.1	6.4	8.3	129.8	138.1	6.0	15.3	126.6	141.9	10.8
4000	9.1	145.4	154.5	5.9	8.5	145.2	153.7	5.5	16.2	141.5	157.7	10.3
4500	9.2	159.1	168.3	5.5	8.7	159.1	167.8	5.2	17.2	154.9	172.1	10.0
5000	9.3	171.4	180.7	5.1	9.5	171.4	180.9	5.2	18.6	167.0	185.6	10.0

Where G_a: adsorbed gas amount, G_f: free gas amount, G_t: total gas-in place

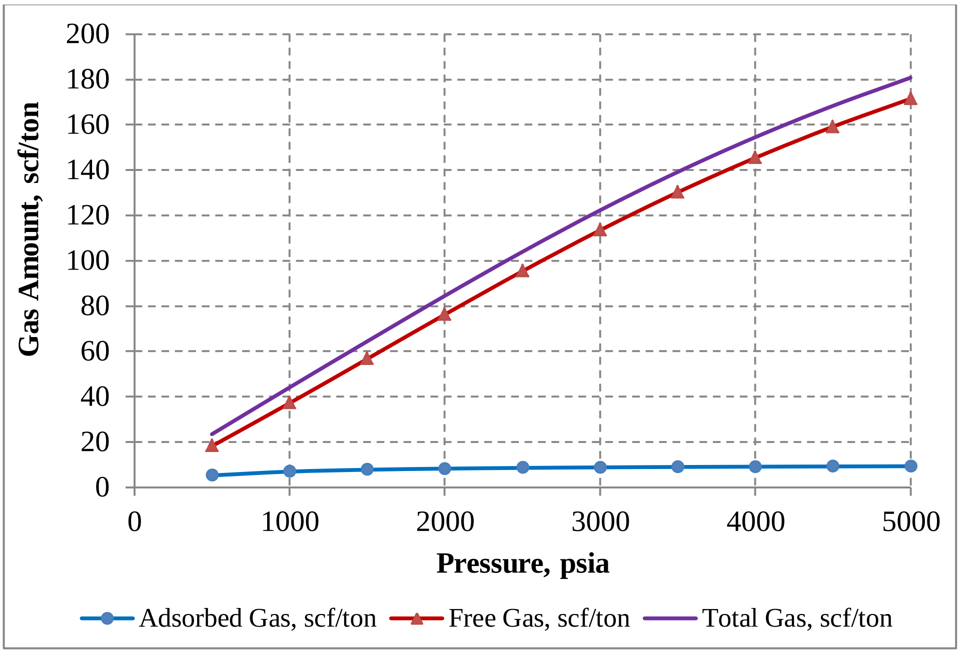

Figure 8.52: Shale gas-in place calculations by using equation 8.2 for shale sample A at 75 °C

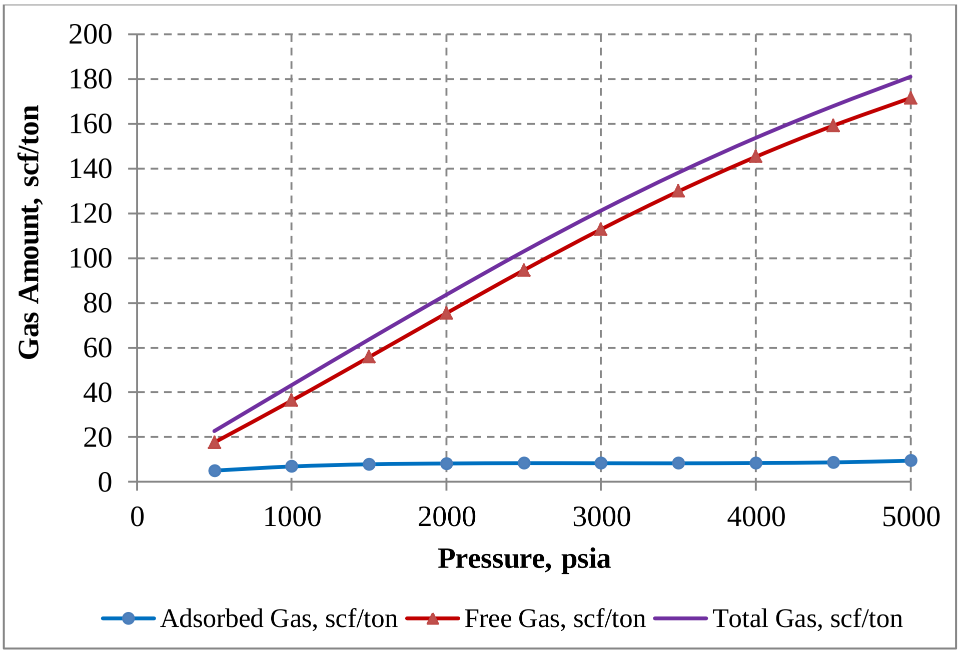

Figure 8.53: Shale gas-in place calculations by using equation 8.3 for shale sample A at 75 °C

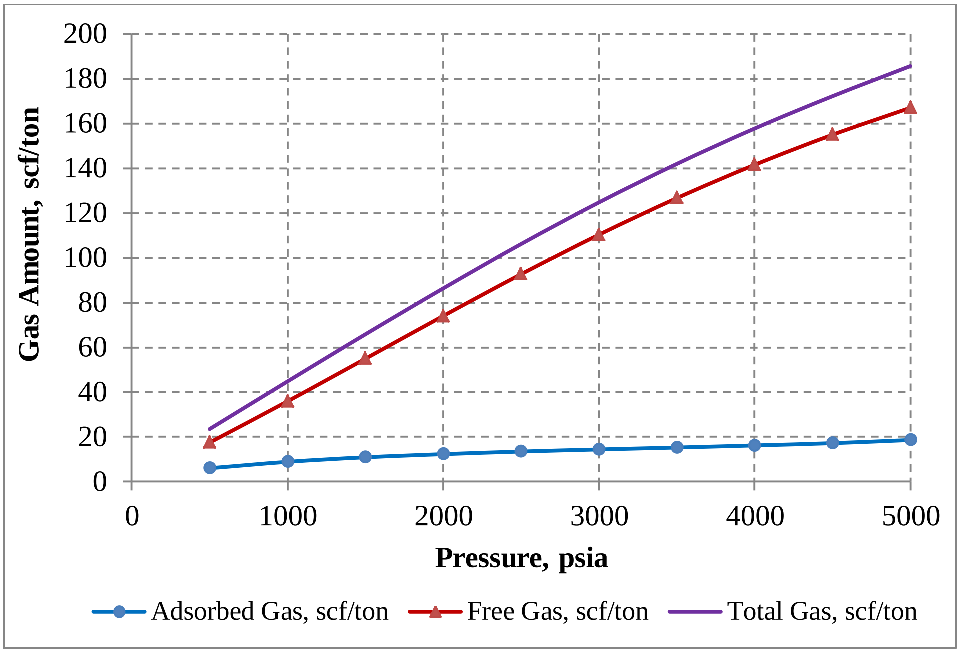

Figure 8.54: Shale gas-in place calculations by using equation 8.5 for shale sample A at 75 ^{o}C

Shale gas-in place calculations for shale sample A were made by using equation 8.2 and the modified equations in this study. As seen in Table 8.73, the results of equation 8.2 and equation 8.3 (with Ono-Kondo monolayer model) are close to each other because both models have good fittings results of experimental adsorption data. Moreover, in both equations, volumes of adsorbed phases were ignored.

However, in order to correct the volume of gas adsorbed in the experiments, equation8.5 (Absolute adsorption by Ono-Kondo monolayer model) was used for initial gas-in place calculations. As seen in Table 8.73, there are significant differences in the amounts of adsorbed gas and free gas compared to equation 8.2 and equation 8.3’s results. Between 5000 and 500 psia, absolute adsorbed gas percentage changes between 10 to 25.7 % for shale sample A.

Table 8.74: Shale gas-in place calculations by equations for shale sample B at 75 ^{o}C

	With Langmuir Model (Equation 8.2)				**With Ono-Kondo Monolayer Model (Equation 8.3)**				**With Absolute Adsorption with Ono-Kondo Monolayer Model (Equation 8.5)**			
P, psia	**G_a, scf/ton**	**G_f, scf/ton**	**G_t, scf/ton**	**% Adsorbed Gas**	**G_a, scf/ton**	**G_f, scf/ton**	**G_t, scf/ton**	**% Adsorbed Gas**	**G_a, scf/ton**	**G_f, scf/ton**	**G_t, scf/ton**	**% Adsorbed Gas**
500	7.5	17.2	24.7	30.2	7.0	15.4	22.4	31.1	10.2	14.4	24.6	41.6
1000	11.2	34.9	46.0	24.2	11.0	32.1	43.1	25.6	17.7	29.5	47.2	37.5
1500	13.4	52.9	66.3	20.2	13.6	49.5	63.2	21.6	23.9	45.2	69.0	34.6
2000	14.9	71.0	85.9	17.3	15.4	67.4	82.8	18.6	29.2	60.9	90.0	32.4
2500	15.9	88.6	104.5	15.2	16.4	85.0	101.5	16.2	33.7	76.2	109.9	30.6
3000	16.7	105.1	121.9	13.7	16.8	102.0	118.8	14.2	37.4	90.7	128.1	29.2
3500	17.3	120.5	137.8	12.6	17.5	117.7	135.2	13.0	41.1	104.2	145.2	28.3
4000	17.8	134.4	152.2	11.7	17.9	132.0	150.0	12.0	44.3	116.4	160.6	27.6
4500	18.2	146.9	165.1	11.0	18.6	144.9	163.6	11.4	47.4	127.4	174.9	27.1
5000	18.6	158.1	176.7	10.5	19.6	156.4	176.0	11.1	50.6	137.3	188.0	26.9

Where G_a: adsorbed gas amount, G_f: free gas amount, G_t: total gas-in place

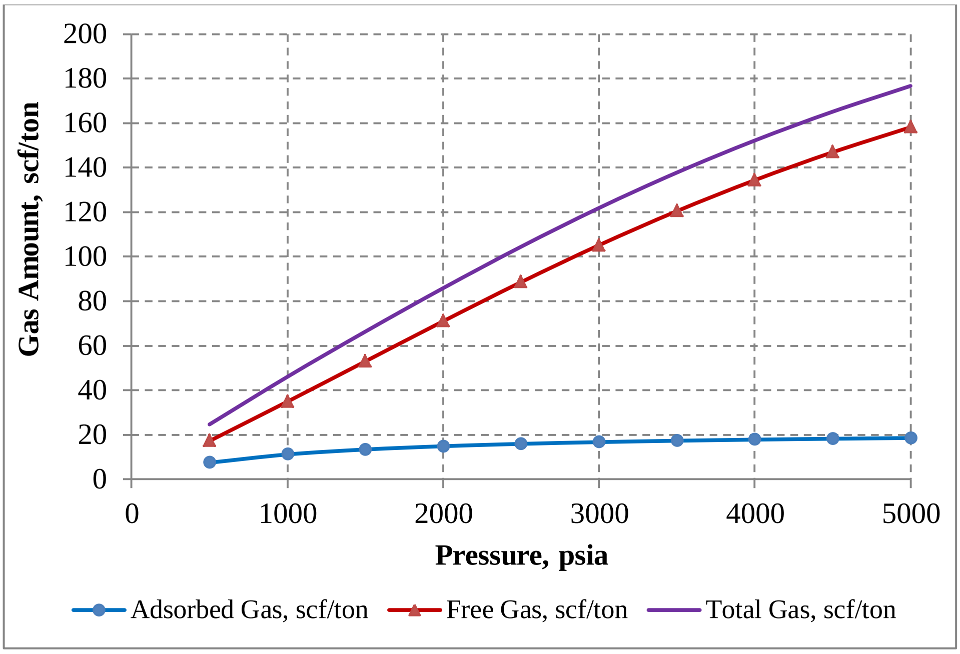

Figure 8.55: Shale gas-in place calculations by using equation 8.2 for Shale Sample B at 75 °C

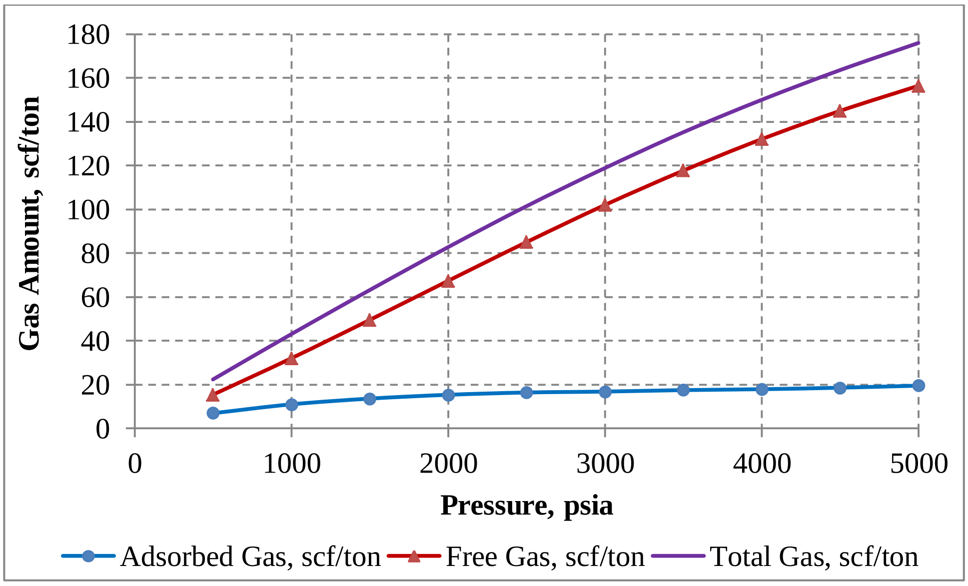

Figure 8.56: Shale gas-in place calculations by using equation 8.3 for shale sample B at 75 °C

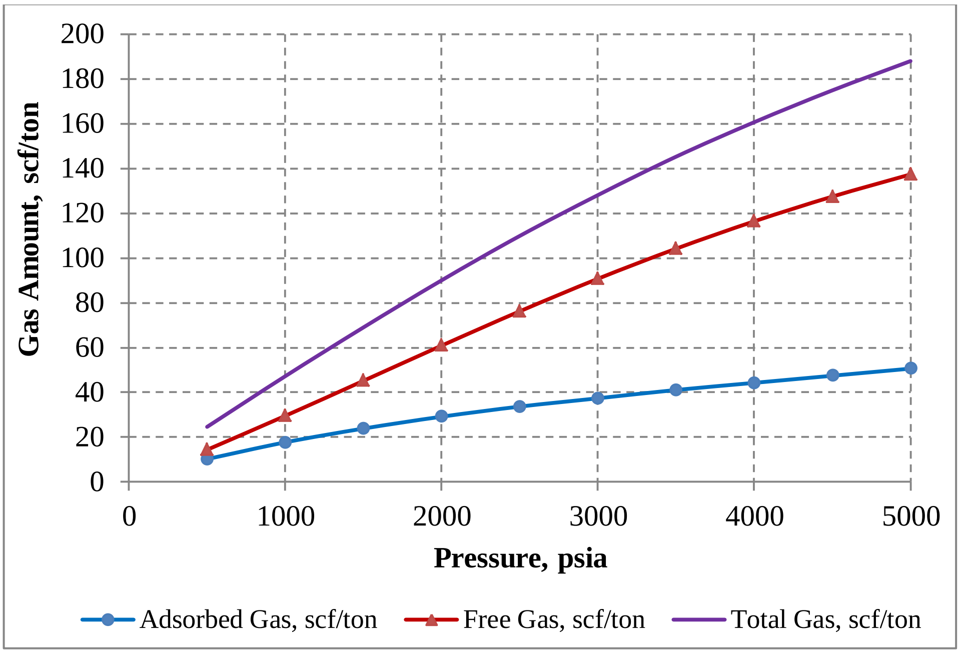

Figure 8.57: Shale gas-in place calculations by using equation 8.5 for shale sample B at 75 ^{o}C

Shale gas-in place calculations for shale sample B were made by using equation 8.2 and the modified equations in this study. As seen in Table 8.74, the results of equation 8.2 and equation 8.3 (with Ono-Kondo Monolayer Model) are close to each other. Hence, according to the results, between 5000 psia and 500 psia, adsorbed gas percentage changes from 11.1 to 31.1 % for shale reservoir B.

However, in order to correct the volume of gas adsorbed in the experiments, equation 8.5 (Absolute Adsorption by Ono-Kondo Monolayer Model) was used for initial gas-in place calculations. As seen in Table 8.74, between 5000 and 500 psia, absolute adsorbed gas percentage changes between 26.9 to 41.6 % for shale reservoir B. These values are 1.3 to 2.4 times higher than adsorbed gas percentage calculated by equation 8.2 and equation 8.3. Therefore, this shows that equation 8.5 in which a correction made for absolute adsorption can be preferred for shale gas-in place calculations.

According to the results of initial gas in place calculations, adsorbed gas capacities of methane in shale reservoir B are 1.6 to 2.7 times higher than the adsorbed gas capacities of methane in shale reservoir A.

CHAPTER 9

CONCLUSION

In this study, an experimental work and Matlab programs developed were performed to investigate adsorption capacities and behaviors of shale gas reservoirs. The following concluding remarks were obtained:

- ✓ By using BPL activated carbon, the capability of the experiments conducted in this study and adsorption calculation procedures were proved. Moreover, it was shown that BPL activated carbon adsorption capacities are very high compared to shale sample both for methane and carbon dioxide. Hence, BPL might be a good candidate for adsorbed gas storage of methane.

- ✓ Adsorption experiments of pure methane and pure carbon dioxide were conducted at different temperatures. It was observed that increasing temperature decreases adsorption capacity. Hence, the effect of temperature is important for adsorption.

- ✓ As seen in adsorption isotherms, as pressure increases, adsorption capacity increases until the complete filling of pores and/or supercritical region of adsorbate. For desorption, it was observed that when pressure decreases, most of desorption happens immediately because of high interconnectivity of samples in the sample cell. However, for shale gas reservoir, fractures are generally closed and there are interconnectivity problems between shale matrix and fractures. After successful hydraulic fracturing operations, gas production through fractures causes desorption of gas from shale matrix though fractures. Therefore, it can be concluded that pressure and temperature are determining factors for adsorption capacities and behaviors.

- ✓ Adsorption isotherms of pure methane and pure carbon dioxide were constructed for shale sample A and shale sample B at different temperatures. Both for shale sample A and shale sample B, carbon dioxide adsorption capacities are higher than methane adsorption capacities. Hence, shale gas reservoirs might be good options for carbon dioxide storage. Moreover, carbon dioxide injection might be used as a recovery technique for methane production from shale gas reservoirs. For the possible injection of carbon dioxide into shale gas reservoirs, by using Ono-Kondo model for mixtures, some predictions of adsorption of methane and carbon dioxide mixtures were done. The model is a good approach to understand the behaviors of carbon dioxide and methane mixtures in shale gas reservoirs. According to the model results, carbon dioxide injection as a recovery technique or storage is better option for shale reservoir B compared to shale reservoir A.

- ✓ Langmuir model was used to evaluate experimental adsorption data in this study. It has good fittings at low pressure, but at high pressures, especially for carbon dioxide, it is not valid. Although it is practical, Langmuir model is not enough to explain adsorption behaviors compared to Ono-Kondo models.

- ✓ Ono-Kondo models are highly capable to adsorption data both at high and low pressures compared to Langmuir model. Ono-Kondo models can be evaluated for different layers of adsorption. In this study, Ono-Kondo monolayer and Ono-Kondo three-layer models were used and compared. According to the models' data, adsorption for both shale sample A and shale sample B occurred as monolayer. Both shale samples A and B's adsorption curve types are in the classification of Type I, which occurs generally in monolayer of adsorption. Due to nanoporous structures of shale gas reservoirs, adsorption occurs as monolayer. Hence, for shale gas reservoirs, Ono-Kondo monolayer model is enough to have good fittings of adsorption data.

- ✓ By using Ono-Kondo models, surface area predictions were done for shale sample A and B. Standard surface area calculations by BET model and equipment are expensive. However, with Ono-Kondo models, surface area values are calculated approximately, which is very important to understand the porous structure of adsorbent used.

- ✓ In Langmuir model, the volume of adsorbed phase is ignored. However, as pressure increases, the volume of adsorbed phase becomes important for adsorbed gas and free gas calculations. Hence, Ono-Kondo models have capability to make predictions about adsorbed phase densities because adsorbed phase densities are used to calculate absolute adsorption by correcting excess (Gibbs) adsorption values.

- ✓ Shale gas-in place equations proposed by Ambrose *et al.*(2010) were modified simply for Ono-Kondo monolayer model. Modified shale gas-in place equations in this study were used for shale-in place calculations for shale gas reservoir A and B at 75 ^{o}C. When the results with original and modified equations were compared, it was understood that adsorbed gas amounts for both shale gas reservoir A and B with modified equation are higher than the values with original equations. Hence, modified equation in which the volume of adsorbed gas considered in this study is suggested for shale gas-in place calculations.

CHAPTER 10

RECOMMENDATION

Based on the experience gained in the present study, the following suggestions are recommended for future research in this area:

After conducting the experiments with BPL activated carbon, shale sample A and B, many observations were done according the results of the experiments. Although BPL was used to show the reliability of the experiments in this study, more experiments related to BPL can be performed for methane storage as adsorbed gas. Moreover, shale gas reservoirs are heterogeneous. Hence, adsorption experiments should be conducted with many samples taken from different places and depths of shale gas reservoirs. Total organic carbon (TOC), clay contents, pore sizes, ash contents, etc., of these samples should be known. This will be helpful to understand the effects of TOC, temperature, clay contents, or water on adsorption in shale gas reservoirs reservoirs. Moreover, this is very important for the most accurate initial gas-in place calculations in shale gas reservoirs. The accuracy of experimental set-up should be increased for most accurate adsorption isotherms by increasing sensitivity of pressure transducers, thermocouples, constant water temperature bath and pump.

REFERENCES

Air Pollution Training Institute (APTI), 2008. Adsorption. Retrieved from: http://www.epa.gov/eogapti1/Materials/APTI%20415%20student/415%20Student%20Manual/415_Chapter_4_12-15-2008.pdf (Accessed on August 25, 2012).

Angus, S., Armstrong, B., de Reuck, K. M., 1978. *International Thermodynamic Tables of the Fluid State-5: Methane*. Pergamon Press: New York.

Ambrose, R.J., Hartman, R.C., Campos, M.D., Akkutlu, Y.I., Sondergeld, C.H., 2010. Shale Gas-in-Place Calculations Part I: New Pore-Scale Considerations, in: *SPE Unconventional Gas Conference, SPE Paper 131772*, Pittsburgh, Pennsylvania, USA.

Arri, L.E., Yee, D., Morgan, W.D., Jeansonne, M.W., 1992. Modeling Coal bed Methane Production With Binary Gas Sorption, in: *SPE Rocky Mountain Regional Meeting, SPE 24363*, Casper, Wyoming, USA.

Bantraj, K., 2011. Studies on Adsorption Isotherms and Heats of Adsorption of CH4 on Microporous and Mesoporous Adsorbents. Bachelor of Technology, National Institute of Technology, Rourkela, India.

Boyer, C., Clark, B., Jochen,V., Lewis, R., Miller, C.K., 2011. Shale Gas: A Global Resource. *Oilfield Review Autumn: 23, no. 3*. Schlumberger.

Busch, A., Gensterblum, Y., Kroos, B.M., 2003. Methane and CO_2 sorption and desorption measurements on dry Argonne premium coals: pure components and mixtures. *International Journal of Coal Geology 55* 205– 224.

Calgon Carbon. BPL 4x6 Activated Carbon Properties. Retrieved from: http://www.calgoncarbon.com/carbon_products/BPL4x6.pdf.pdf (Accessed on September 27, 2012).

Chareonsuppanimit, P., Mohammad, S.A., Robinson, R.L., Gasem, K.A.M., 2012. High-pressure adsorption of gases on shales: Measurements and modeling. *International Journal of Coal Geology 95* 34–46

Cipolla, C.L., Lolon, E.P., Erdle, J.C., Rubin, B., 2010. Reservoir Modelling in Shale Gas Reservoirs, in: *SPE Eastern Regional Meeting, SPE Paper 125530*, Charleston, West Virginia, USA.

Condon, J.B., 2006. *Surface Area and Porosity Determinations by Physisorption-Measurements and Theory*. Elsevier Science Publishers B.V., Amsterdam.

Crain, E.R., 2011. Unicorns in the Garden of Good and Evil: Part 4- Shale Gas. Retrieved from: http://www.spec2000.net/00-publications.htm (Accessed on October 7, 2012).

Czepirski, L., Balys, M.R., Czerpirska, E.K., 2000. Some Generalization of Langmuir Adsorption Isotherm. *Internet Journal of Chemistry, 3, 14 [ISSN: 1099-8292]* Article 14.

Dabrowski, A., 2001. Adsorption-from theory to practice. *Advances in Colloid and Interface Science. 93.* 135-224.

Do, D.D., 1998. *Adsorption Analysis: Equilibra and Kinetics*. Imperial College Press, London, UK

Dubinin, M.M., 1960. The Potential Theory of Adsorption of Gases and Vapors for Adsorbents with Energetically Nonuniform Surfaces. *Chemical Review 60 (2):* 235-241.

EIA, 2011. Annual Energy Outlook. U.S.Energy Information Administration. Retrieved from: http://www.eia.gov/forecasts/archive/aeo11 (Accessed on November 2, 2012).

EIA, 2011. World Shale Gas Resources: An Initial Assessment of 14 Regions Outside the United States. U.S. Energy Information Administration. Retrieved from:http://www.eia.gov/analysis/studies/worldshalegas (Accessed on October 22, 2012).

Gregg, S.J., Sing, K.S.W., 1982. *Adsorption, Surface Area and Porosity*. Academic Press Inc.London, UK

Gutierrez, C., Felipe, T., Osorio, Nelson, Restrepo, R., Patricia, D., 2009. Unconventional Natural Gas Reserves. *Energética, Núm. 41*, pp. 61-72.

Hall, F.E., Zhou, C., Gasem, K.A.M., Robinson, R.L., Yee, D., 1994. Adsorption of Pure Methane, Nitrogen, and Carbon Dioxide and Their Binary Mixtures on Wet Fruitland Coal, in: *Eastern Regional Conference, SPE Paper 29194*, Charleston, WW, U.S.A.

Haydel, J.J. and Kobayashi, R. 1967. Adsorption Equilibria in the Methane-Propane-Silica Gel System at High Pressures. *Ind. Eng. Chem. Funda-men. 6 (4)*: 564–554.

Heller, R.J., Zoback, M.D., 2011. Adsorption, Swelling and Viscous Creep of Synthetic Clay Samples, in: *45th US Rock Mechanics / Geomechanics Symposium*, San Francisco, CA, USA.

Humayun, R., Tomasko, D.L., 2000. High-resolution adsorption isotherms of supercritical carbon dioxide on activated carbon. *AICHE Journal 10*, 2065–2075.

Kang, S.M., 2011. Carbon dioxide Storage Capacity of Barnett Shale. A Thesis for Master of Science, University of Oklahoma, USA.

Kuila, U., Prasad, M., 2011. Surface Area and Pore-size Distribution in Clays and Shales, in: *the SPE Annual Technical Conference and Exhibition, SPE Paper 146869*, Denver, USA

Kumar, A., 2011. Adsorption of Methane on Activated Carbon By Volumetric Method. Master of Technology (Chemical Engineering). National Institute of Technology, Rourkela, India.

Kumar, H., Elsworth, D., Marone, C.J., Mathews, J., 2010. Permeability Evolution of Shale and Coal Under Differential Sorption of He, CH_4 And CO_2. *Presented at the 2010 Fall Meeting of the American Geophysical Union*.

Lancaster, D.E., Holditch, S.A., Hill, D.G., 1993. A Multi-Laboratory Comparison of Isotherm Measurements on Antrim Shale Samples. *SCA Conference Paper Number 9303*, Otsego County, MI, USA.

Leahy-Dios A., Das M., Agarwal A., Kaminsky R.D., 2011. Modeling of Transport Phenomena and Multicomponent Sorption for Shale Gas and Coalbed Methane in an Unstructured Grid Simulator, in: *the SPE Annual Technical Conference and Exhibition, SPE Paper 147352* , Denver, Colorado, USA.

Lewis,R.,Ingraham, D., Pearcy, M.,Williamson, J., Sawyer, W., Frantz, F., 2004. New Evalaution Techniques for Gas Shale Reservoirs. *Reservoir Symposium*, Schlumberger.

Lu, X.C., Li, F.C., Watson, A.T., 1993. Adsorption Studies of Natural Gas Storage in Devonian Shales, in: *SPE Annual Technical Conference and Exhibition, SPE Paper 26632*, Houston, U.S.A.

Luo J., Liu, Y., Jiang, C., Chu, W., Jie, W., Xie, H., 2011. Experimental and Modelling Study of Methane Adsorption on Activated Carbon Derived from Anthracite. *Journal of Chemical& Engineering Data 56*, 4919-4926.

Matott, L.S., 2007. *IsoFit Documentation and User's Guide Version 1.2*. State University of New York at Buffalo, USA.

Mavor, M.J., Owen, L.B., Pratt, T.J., 1990. Measurement and evaluation of coal sorption isotherm data. *SPE 20728*, pp. 157–170.

McCarthy, R.D., Arp, V.D., 1990. A new wide range equation of state for helium. *Adv Cryogenic Eng 35*:1465–75.

Menon, P.G., 1968. Adsorption at high pressures. *Chem. Rev. 68 (3)*: 277–294.

Micromeritics. Gas Adsorption Theory Poster. Retrieved from: http://www.micromeritics.com/repository/files/gas_adsorption_theory_poster.pdf (Accessed on December 8, 2012).

Ming .H.J., 2009. Adsorption evaporative emission control system for vehicles. National university of Singapore, PhD Thesis.

Mohammad, S.A., Fitzgerald, J., Robinson, R.L., Gasem, K.A.M, 2009. Experimental Uncertainties in Volumetric Methods for Measuring Equilibrium Adsorption. *Energy & Fuels, 23*, 2810–2820.

Mohammad, S.A., Chen, J.S., Fitzgerald, J.E., Robinson, R.L., Gasem, K.A.M., 2009a. Adsorption of pure carbon dioxide on wet argonne coals at 328.2 K and pressures up to 13.8 MPa. *Energy & Fuel, 23,* 1107–1117.

Mohammad, S.A., Chen, J.S., Robinson, R.L.J., Gasem, K.A.M., 2009b. Generalized Simplified Local-Density/Peng-Robinson Model for Adsorption of Pure and Mixed Gases on Coals. *Energy & Fuels, 23*, 6259-6271.

National Energy Board, 2009. A Primer for Understanding Canadian Shale Gas - Energy Briefing Note. Retrieved from: http://www.neb-one.gc.ca/clf nsi/rnrgynfmtn/nrgyrprt/ntrlgs/prmrndrstndngshlgs2009/prmrndrstndngshlgs2009-eng.html (Accessed on November 10, 2012).

NIST Chemistry WebBook, "Thermophysical Properties of Fluid Systems". Retrieved from: http://webbook.nist.gov/chemistry/fluid/ (Accessed on between October, 2012 and May, 2013).

Pashin, J.C., Grace, R.L.B., Kopaska-Merkel, D.C., 2010. Devonian Shale Plays in the Black Warrior Basin and Appalachian Thrust Belt of Alabama. *International Coalbed & Shale Gas Symposium*, Tuscaloosa Alabama, USA.

Reich, R., Ziegler, W.T., Rogers, K.A., 1980. Adsorption of Methane, Ethane, and Ethylene Gases and Their Binary and Ternary Mixtures and Carbon Dioxide on Activated Carbon at 212-301 K and Pressures to 35 Atmospheres. *Ind. Eng. Chem. Process Des. Dev.*, 19, 336-344.

Reid, R.C., Prausnitz, J.M., Poling B.E., 1987. *The Properties of Gases and Liquids*. McGraw-Hill, New York, USA.

Ross, D. and Bustin, M., 2008. The importance of shale composition and pore structure upon gas storage potential of shale gas reservoirs: *Marine and Petroleum Geology, 44*, 233-244.

Ruthven, D.M., 1984. *Principles of Adsorption and Adsorption Processes*. John Wiley&Sons, Inc.New York USA

Saghafia, A., Faizb, M., Robertsa, D., 2007. CO_2 storage and gas diffusivity properties of coals from Sydney Basin, Australia. *International Journal of Coal Geology Volume 70, Issues 1–3*, 240–254.

Salman, A.M., Wattenbarger, R.A., 2011. Accounting For Adsorbed Gas in Shale Gas Reservoirs, in: *SPE Middle East Oil and Gas Show and Conference, SPE Paper 141085*, Manama, Bahrain.

Sherwin, J.A., 2011. *Langmuir Monolayers in Thin Film Technology*. Nova Science Publishers, Inc. New York, USA.

Siemons, N., Busch, A., 2007. Measurement and interpretation of supercritical CO2 sorption on various coals. *International Journal of Coal Geology 69*, 229–242.

Song, B., Economides, M.J., Economides, C.E, 2011. Design of Multiple Fracture Horizontal Wells in Shale Gas Reservoirs, in: *SPE Hydraulic Fracturing Technology Conference and Exhibition, SPE Paper 140555*, The Woodlands, Texas, USA.

Span, R., Wagner, W., 1996. A New Equation of State for Carbon Dioxide Covering the Fluid Region from the Triple Point Temperature to 1100 K at Pressures up to 800 MPa. *J. Phys. Chem. Ref. Data , 25*, 1509-1590.

Sudibandriyo, M., Pan, Z., Fitzgerald, J.E., Robinson, R.L., Gasem, K.A.M., 2003. Adsorption of Methane, Nitrogen, Carbon Dioxide, and Their Binary Mixtures on Dry Activated Carbon at 318.2 K and Pressures up to 13.6 MPa. *Langmuir, 19*, 5323-5331

Sudibandriyo, M., Mohammad, S.A., Robinson, R.L.J., Gasem K.A.M., 2010. Ono–Kondo lattice model for high-pressure adsorption: Pure gases. *Fluid Phase Equilibria 299*, 238–251.

Sudibandriyo, M., 2010, A Simple Technique for Surface Area Determination Through Supercritical CO2 Adsorption. *Makara, Teknologi, Vol.14 No.1:* 1-6.

Sudibandriyo M., Mohammad S.A., Robinson, R.L.J., Gasem K.A.M, 2011. OnoKondo Model for High-Pressure Mixed-Gas Adsorption on Activated Carbons and Coals. *Energy & Fuels, 25*, 3355–3367.

Sunjay, B., Kothari, N., 2011. Unconventional Energy Sources: Shale Gas. *10th Offshore Mediterranean Conference and Exhibition*, Ravenna, Italy
Suzuki, M., 1990. *Adsorption Engineering.* Kodansha Ltd, Tokyo and Elsevier Science Publishers B.V., Amsterdam.

Thomas, W.J., Crittenden, B. , 1998. *Adsorption Technology&Design*. Elsevier Science & Technology Books.

TPAO, 2011. 2011 Yılı Ham Petrol ve Doğal Gaz Sektör Raporu. Turkiye Petrolleri Anonim Ortakligi. Retrieved from:
http://www.enerji.gov.tr/yayinlar_raporlar/Sektor_Raporu_TPAO_2011.pdf.
(Accessed on October 1, 2012).

Velanki, S.B., 1995. Adsorption of Binary Gas Mixtures on Wet Fruitland Coal and Compressibility Factor Predictions. Master of Science. Oklohoma State University, USA.

Wang, Y., Ercan, C., Khawajah, A., Othman, R., 2011. Experimental and Theoretical Study of Methane Adsorption on Granular Activated Carbon. *Wiley Online Library* (doi 10.1002/aic.12611).

Yardimci, O., 2011. Türkiye’deki Doğal Gaz Piyasası: Geçmiş 25 Yıl, Gelecek 25 Yıl. *Ekonomi Bilimleri Dergisi. Cilt 3, No 2, I SSN: 1309-8020.*

APPENDIX A

ERROR ANALYSIS IN ADSORPTION EXPERIMENTS

A.1-Experimental Errors in the Fixed-Volume Adsorption Experiments

The expected uncertainties in the reported adsorption data is based on the theory of multi-variate error propagation. The following error formula is used for this method (Mohammad *et al.*, 2009):

$$\sigma_y^2 = \sum_{i=1}^{NV}\left[\left(\frac{\partial y}{\partial x_i}\right)^2 \sigma_{x_i}^2\right] \tag{A.1}$$

where NV is the number of measured variables, i is the variable index, and σ_{xi} is the standard deviation of the measurement x_i. The uncertainty expression above assumes that the input variables are uncorrelated and that first-order approximations are sufficient:

$$\frac{\partial y}{\partial x}\Delta x >> \frac{\partial^2 y}{\partial x^2}(\Delta x)^2 \tag{A.2}$$

Where Δx is the deviation in the measurement x for a given point.

A.1.1 Error in the Amount Injected

The amount of gas adsorbed is calculated by the following formula:

$$n_{ads} = n_{inj} - n_{unads} - n_{sol} \tag{A.3}$$

By using the theory of multi-variate error propagation, the following formula is obtained:

$$\sigma_{n_{ads}}^2 = \left(\frac{\partial n_{ads}}{\partial n_{inj}}\right)^2 \sigma_{n_{inj}}^2 + \left(\frac{\partial n_{ads}}{\partial n_{unads}}\right)^2 \sigma_{n_{unads}}^2 + \left(\frac{\partial n_{ads}}{\partial n_{unads}}\right)^2 \sigma_{n_{sol}}^2 \tag{A.4}$$

By inserting equation A.1 into equation A.4, the error in the amount adsorbed is obtained as:

$$\sigma^2_{n_{ads}} = \sigma^2_{n_{inj}} + \sigma^2_{n_{unads}} + \sigma^2_{n_{sol}} \tag{A.5}$$

Where σ_{nads}, σ_{ninj}, σ_{nunads}, and σ_{nsol}, are the uncertainties in the amount of gas adsorbed, injected, unadsorbed in the cell, and dissolved in water, respectively.

A.1.2 Error in the Amount Injected

In fixed-volume adsorption experiment method, a series of injections are done from a reference cell to sample cell. The amount injected into the sample cell from the jth state (which is the higher-pressure initial state before the injection) to kth state of the reference cell is:

$$n^{inj}_{j,k} = n^{\mathrm{Re}\,f}_{j} - n^{\mathrm{Re}\,f}_{k} = V^{\mathrm{Re}\,f}\left(\rho_j - \rho_k\right) = \frac{V^{\mathrm{Re}\,f}}{R}\left(\frac{P_j}{T_j Z_j} - \frac{P_k}{T_k Z_k}\right) \tag{A.6}$$

The total amount injected from the reference cell to the sample cell and from the first through the Nth injection is:

$$n^{inj}_{N} = \sum_{j=1,k=j+1}^{N} n^{inj}_{j,k} \tag{A.7}$$

After N injections have been made from the reference cell to the sample cell, there are 2N independent measurements each of the temperature and pressure and one volume measurement (of the reference cell). The expected squared error in the amount injected at the Nth injection is the resultant sum of the expected squared errors for each injection from the jth to the kth state:

$$\sigma^2_{n^{inj}_{N}} = \sum_{j=1,\,j=k+1}^{N} \sigma^2_{n^{inj}_{j,k}} \tag{A.8}$$

The expected error of an injection from the jth to the kth state is:

$$\sigma^2_{n^{inj}_{j,k}} = \left(\frac{\partial n^{inj}_{j,k}}{\partial V^{\mathrm{Re}\,f}}\right)^2 \sigma^2_{V^{\mathrm{Re}\,f}} + \left(\frac{\partial n^{inj}_{j,k}}{\partial \rho_j}\right)^2 \sigma^2_{\rho_j} + \left(\frac{\partial n^{inj}_{j,k}}{\partial \rho_k}\right)^2 \sigma^2_{\rho_k} \tag{A.9}$$

Which yields the following:

$$\sigma^2_{n^{inj}_{j,k}} = \left(\rho_j - \rho_k\right)^2 \sigma^2_{V^{\mathrm{Re}\,f}} + \left(V^{\mathrm{Re}\,f}\right)^2 \left(\sigma^2_{\rho_j} + \sigma^2_{\rho_k}\right) \tag{A.10}$$

The error in the amount injected from the j$^{\mathrm{th}}$ to the k$^{\mathrm{th}}$ state can be related to the amount injected:

$$\sigma^2_{n^{inj}_{j,k}} = \left(n^{inj}_{j,k}\right)^2 \left(\frac{\sigma_{V^{\mathrm{Re}\,f}}}{V^{\mathrm{Re}\,f}}\right) + \left(V^{\mathrm{Re}\,f}\right)^2 \left(\sigma^2_{\rho_j} + \sigma^2_{\rho_k}\right) \tag{A.11}$$

Thus, the error in the amount injected at the N$^{\mathrm{th}}$ injection is:

$$\sigma^2_{n^{inj}_N} = \left(\frac{\sigma^{\mathrm{Re}\,f}_V}{V^{\mathrm{Re}\,f}}\right)^2 \left(n^{inj}_N\right)^2 + \left(V^{\mathrm{Re}\,f}\right)^2 \sum_{j,k=1}^{N} \left(\sigma^2_{\rho_j} + \sigma^2_{\rho_k}\right) \tag{A.12}$$

A.1.3 Error in Density

The error in the amount injected is dependent on the error in the density of gas, σ_ρ. The density may be expressed in terms of gas compressibility factor as:

$$\rho = \frac{P}{ZRT} \tag{A.13}$$

Thus, the error in the density is given as:

$$\begin{aligned} \sigma^2_\rho &= \left(\frac{\partial\rho}{\partial P}\right)^2 \sigma^2_P + \left(\frac{\partial\rho}{\partial T}\right)^2 \sigma^2_T + \left(\frac{\partial\rho}{\partial Z}\right)^2 \sigma^2_Z \\ &= \rho^2 \left(\frac{1}{P} - \frac{1}{Z}\frac{\partial Z}{\partial P}\right)^2 \sigma^2_P + \rho^2 \left(\frac{1}{T} + \frac{1}{Z}\frac{\partial Z}{\partial T}\right)^2 \sigma^2_T + \rho^2 \left(\frac{1}{Z}\right)^2 \sigma^2_Z \end{aligned} \tag{A.14}$$

The derivatives of the compressibility factor can be evaluated at the nominal pressure and temperature using an accurate equation of state.

A.1.4 Error in the Gibbsian Amount Unadsorbed

$$n^{Gibbs}_{unads} = V^{He}_{void}\rho^{Cell}_{gas} \tag{A.15}$$

$$\sigma^2_{n^{Gibbs}_{unads}} = \left(V^{He}_{void}\right)^2 \sigma^2_{\rho^{Cell}_{gas}} + \left(\rho^{Cell}_{gas}\right)^2 \sigma^2_{V^{He}_{void}}$$

(A.16)

Equation A.16 can be written by using Equation A.14. Therefore, a proportional relationship between the expected error in the Gibbsian amount and the amount itself:

$$\sigma^2_{n^{Gibbs}_{unads}} = \left(n^{Gibbs}_{unads}\right)^2 \left[\left(\frac{1}{P} - \frac{1}{Z}\frac{\partial Z}{\partial P}\right)^2 \sigma_P^2 + \left(\frac{1}{T} + \frac{1}{Z}\frac{\partial Z}{\partial T}\right)^2 \sigma_T^2 + \rho^2 \left(\frac{1}{Z}\right)^2 \sigma_Z^2 + \left(\frac{\sigma_{V^{He}_{void}}}{V^{He}_{void}}\right)^2 \right]$$

(A.17)

To calculate the excess adsorption for a specific component i, the equilibrium composition of that component, y_i, is needed in addition to the Gibbsian amount unadsorbed. The expected error is:

$$\sigma^2_{y_i n^{Gibbs}_{unads}} = \left(n^{Gibbs}_{unads}\right)^2 \sigma^2_{y_i} + y_i \sigma^2_{n^{Gibbs}_{unads}} \qquad \text{(A.18)}$$

A.1.5 Error Due to Correction for Adsorption on Wet Adsorbents

Wet adsorbents have a correction that accounts for the fact that the void volume determined by helium is affected by the presence of adsorbed water. A reasonable compromise assumption is that the error in the amount of gas soluble in the adsorbed water is proportional to the amount dissolved gas:

$$\sigma^{Sol,Water}_{gas} = k_{sol} n^{Sol,water}_{gas} \qquad \text{(A.19)}$$

Where a value of 0.05 for k_{sol} might be a reasonable estimate. Errors in this correction can be expected to be greatest in magnitude for gases that are highly soluble in water such as CO_2.

A.1.6 Error in the Gibbsian (Excess) Amount Adsorbed

The excess adsorption is typically presented in units of mmol/gm dry adsorbent. Therefore,

$$n^{Ex} = \frac{1000 n_{ads}}{\left(1 - \lambda_{water}\right) L} \qquad \text{(A.20)}$$

The error in the excess amount of gas adsorbed then becomes:

$$\sigma^2_{n^{Gibbs}} = \left(\frac{\partial n^{Gibbs}}{\partial n_{ads}}\right)^2 \sigma^2_{n_{ads}} + \left(\frac{\partial n^{Gibbs}}{\partial L}\right)^2 \sigma_L^2 + \left(\frac{\partial n^{Gibbs}}{\partial \lambda_{water}}\right)^2 \sigma^2_{\lambda_{water}} \qquad \text{(A.21)}$$

$$\sigma^2_{n^{Gibbs}} = \left(\frac{1000}{(1-\lambda_{water})L}\right)^2 \sigma^2_{n_{ads}} + \left(\frac{1000 n_{ads}}{(1-\lambda_{water})L^2}\right)^2 \sigma^2_L + \left(\frac{1000 n_{ads}}{\lambda^2_{water} L}\right)^2 \sigma^2_{\lambda_{water}}$$

(A.22)

A.2-Gas Injection into an Empty Sample Cell in the Fixed-Volume Adsorption Experiments

The initial pressure in the reference cell necessary for each injection for a given V^{cell}/V^{Ref} is calculated using the following expression:

$$\frac{P_j}{Z_j} = \frac{P_k}{Z_k}\left(1+\frac{V^{Cell}}{V^{\mathrm{Ref}}}\right) - \frac{P_{k-1}}{Z_{k-1}}\left(\frac{V^{Cell}}{V^{\mathrm{Ref}}}\right) \text{ at constant temperature} \qquad \text{(A.19)}$$

Where subscripts j and k refer to the initial and final state, respectively.
The squared error in the amount injected can be obtained as:

$$\left(\frac{\sigma_{n_N^{inj}}}{n_N^{inj}}\right)^2 = \left(\frac{\sigma_V^{\mathrm{Ref}}}{V^{\mathrm{Ref}}}\right)^2 + \left(\frac{V^{\mathrm{Ref}}}{V^{Cell}\rho_N}\right)^2 \sum_{k=1}^{N} \rho_k^2 \left[\left(\frac{1}{P_k} - \frac{1}{Z_k}\frac{\partial Z_k}{\partial P_k}\right)^2 \sigma^2_{P_k} + \left(\frac{1}{T_k} + \frac{1}{Z_k}\frac{\partial Z_k}{\partial T_k}\right)^2 \sigma^2_{T_k}\right]$$

$$+\left(\frac{V^{\mathrm{Ref}}}{V^{Cell}\rho_N}\right)^2 \sum_{k=1}^{N} \rho_j^2 \left[\left(\frac{1}{P_j} - \frac{1}{Z_j}\frac{\partial Z_j}{\partial P_j}\right)^2 \sigma^2_{P_j} + \left(\frac{1}{T_j} + \frac{1}{Z_j}\frac{\partial Z_j}{\partial T_j}\right)^2 \sigma^2_{T_j}\right]$$

(A.20)

Where T: Temperature, Z: gas compressibility factor, V^{ref}: reference cell volume, V^{cell}: sample cell volume, V^{He}_{Void}: helium void volume, n_{inj}: amount injected, n_{unads}: amount unadsorbed, n_{sol}: amount of gas dissolved in water, n^{Ex}: excess adsorption, L: mass of sample, λ_{water}: mass fraction of water in sample, n^{abs}_{ads}:absolute adsorption, ρ: bulk gas pressure, z_i: feed mole fraction, y_i: gas phase mole fraction, σ_L^2: uncertainty in the mass of sample, σ_{ninj}^2: uncertainty in amount injected, σ_ρ^2: uncertainty in density, σ_{nunads}^2: uncertainty in amount unadsorbed, σ_{nsol}^2: uncertainty in amount dissolved in water, σ_{nunads}^2: uncertainty in amount unadsorbed

In the error propagation in this study, the experimental uncertainties of 0.1 K in temperature, 1 psia in pressure, and 0.3 % in void volume, 0.02 cm^3 in the reference cell volume, and 0.01 g in the amount shale.

With careful design, lower errors can be obtained for the fixed-volume injection method. Specifically, using the a ratio of sample cell to the reference cell of around 2.0 (2.76 in this study) and reducing the void volume in the sample cell can result in significant reduction in expected uncertainties in the amount of gas adsorbed.

APPENDIX B

MATLAB CODES WRITTEN IN THIS STUDY

B.1 Matlab Code for Adsorption and Error Calculations (Adsorption.m)

- ✓ Adsorption.m file is a matlab code written in this study to analyze experimental data to calculate excess adsorption and adsorption uncertainty.

```
%           Adsorption Experiments by Volumetric Method
% Adsorption Calculations by Using Experimental Data & Error Analysis
%                       for Pure Gases
% --------------------------------------------------------------
% Author: Sukru MEREY
% --------------------------------------------------------------
%                         INPUTS
% --------------------------------------------------------------
% n: Number of Pressure Increment Stages
% T: Temperature, Celcius
% w: Weight of Sample in the Sample Cell
% Pr: Reference Cell Pressure Before Expansion, psia
% rhor: Gas Density in Reference Cell Before Expansion at Pr,mol/l***
% Pk: Equilibrium Pressure in Reference Cell and Sample Cell, psia
% rhok: Gas Density at Pk, mol/l***
% Vc: Void Volume in Sample Cell,cm^3
% Vr: Reference Cell Volume, cm^3
% ev: Error in Reference Cell Volume Calculations,fraction (~0.003)
% et: Error in Temperature Recording,Rankine
% ep: Error in Pressure Recording, psia
% ez: Error in Equation of States, fraction**
% ----------------------------------------------------------------
%  OTHER PARAMETERS USED IN ADSORPTION CALCULATIONS
% ----------------------------------------------------------------
% zr: Compressibility Factor at Pr
% zk: Compressibility Factor at Pk
% nrbe: Moles of Gas in Reference Cell Before Expansion, mole
% nrae: Moles of Gas in Reference Cell After Expansion, mole
% ninj: Moles of Gas Injected into Sample Cell After Expansion, mole
% nunads: Moles of Free Gas (Unadsorbed) in Sample Cell,mole
% nex: Gibbs(Excess) Adsorption, mg-mol/g (mmol/g)
% einj2: Squared Error in Amount Injected
% einj2: Squared Error in Amount Unadsorbed
```

```
% eads: Error in Amount Adsorbed,mmol/g


 function []= Adsorption()

  n = input('n:');
  T = input('T,C:');
  w=  input('w,g:');
  Pr = input('Pr,psia:');
  rhor = input('rhor,mol/l:');
  Pk = input('Pk,psia:');
  rhok = input('rhok,mol/l:');
  Vc= input('Vc,cc:');
  Vr= input('Vr,cc:');
  ev= input('ev,fraction:');
  et= input('et,R:');
  ep= input('ep,psia:');
  ez= input('ez,fraction:');

  R=669.9542893;  % gas constant,psia cc/mol R
  Vcr= Vc/Vr;

% Adsorption Calculations by Using Experimental Data[1]
% ----------------------------------------------------
for i=1:n
   zr(i)=0.06894757*Pr(i)/(0.08314462175*rhor(i)*(T+273.15));
   nrbe(i)=(Pr(i)*Vr*0.00003531467/(zr(i)*10.73159*(T+273.15)*1.8))...
       *453.59237;
   zk(i)=Pk(i)/((rhok(i)/1000)*R*(T+273.15)*1.8);

   nrae(i)=(Pk(i)*Vr*0.00003531467/(zk(i)*10.73159*(T+273.15)*1.8))...
       *453.59237;

       if i==1
          ninj(i)=nrbe(i)-nrae(i);

       else
          ninj(i)=nrbe(i)-nrae(i)+ninj(i-1);
       end

    nunads(i)=(Pk(i)*Vc*0.00003531467/(zk(i)*10.73159*(T+273.15)*1.8))...
       *453.59237;
    nex(i)=(ninj(i)-nunads(i))*1000/w;

end
```

```
 % Error Analysis in Volumetric Methods for Measuring Adsorption[2]
% ------------------------------------------------------------

 for i=1:n

    if  i==1
        Pz(i)=(Pk(i)/zk(i))*(1+Vcr);
    else
        Pz(i)=(Pk(i)/zk(i))*(1+Vcr)-(Pk(i-1)/zk(i-1))*Vcr;
    end
    Pzk(i)=Pk(i)/zk(i);
 end


 for i=1:n
    Pj(i)= spline(Pzk,Pk,Pz(i));
    zj(i)=Pj(i)/Pz(i);
    rhoj(i)=Pj(i)/(zj(i)*R*(T+273.15)*1.8);
 end

     a=polyfit(Pj,zj,1);

     zpj=a(1);
     zpk=a(1);


    Ai=0;
    Bi=0;

 for i=1:n

    A(i)=Ai+(rhok(i)/1000)^2*((1/Pk(i)-zpk/zk(i))^2*ep^2+(1/(...
        (T+273.15)*1.8)+zpk/zk(i))^2*et^2);

    B(i)=Bi+rhoj(i)^2*((1/Pj(i)-zpj/zj(i))^2*ep^2+(1/((T+273.15)*1.8)...
        +zpj/zj(i))^2*et^2);
    Ai=A(i);
    Bi=B(i);

    einj2(i)=ev^2+(1/(Vcr*(rhok(i)/1000)))^2*A(i)+(1/(Vcr*...
         (rhok(i)/1000)))^2*B(i);
    eunads2(i)=((1/Pk(i)-zpk/zk(i))^2*ep^2+(1/((T+273.15)*1.8))^2*et^2+...
       (rhok(i)/1000)^2*ez^2/(zk(i)^2)+ev^2);

    eads(i)=(sqrt(ninj(i)^2*einj2(i)+nunads(i)^2*eunads2(i)))*1000/w;
```

```
 end
  fprintf('nads mmol/g    error mmol/g\n');
 fprintf('-----------    -------------\n');
for i=1:n
 fprintf('%d    %d\n',nex(i),eads(i));
end

  end

 %------------------------------------------------------------------
 %                              REFERENCES
 %------------------------------------------------------------------
 %[1]Chareonsuppanimit,P.,Mohammad,S.A.,Robinson,R.L.,Gasem,K.A.M.,
 %2012.High-pressure adsorption of gases on shales: Measurements and
 % modeling. International Journal of Coal Geology 95 (2012) 34–46

 %[2]Mohammad,S.A.,Fitzgerald,J.,Robinson,R.L.,Gasem,K.A.M,2009.
 % Experimental Uncertainties in Volumetric Methods for Measuring
 % Equilibrium Adsorption. Energy & Fuels, 23, 2810–2820.

 %***By using the following website, gas densities for different gases
 % can be calculated: http://webbook.nist.gov/chemistry/fluid/
 % Where:For Methane, Angus's Equations of States and for
 % Carbon dioxide Span&Wagner Equations of States are used.
```

B.2 Matlab Code for Ono-Kondo Monolayer Model (OK.m)

- OK.m file is a matlab code to calculate adsorbed density, absolute adsorption, and surface area by using adsorption experimental data for Ono-Kondo Monolayer Model.

```
% Ono-Kondo Lattice Model for Pure Gas Adsorption-Monolayer [1]
% ---------------------------------------------------------
% Author: Sukru MEREY
% ---------------------------------------------------------
%                       INPUTS
% ---------------------------------------------------------
% n: Number of Pressure Increment Stages
% T: Temperature, Kelvin
% rhob: Gas Density at Equilibrium Pressure,mol/l ***
% nex: Gibbs(Excess) Adsorption,mmol/g
% rhomc:Adsorbed Phase Density Corresponding to the Maximum Adsorption...
% Capacity, mol/l (For Methane:23.37 mol/l; for CO2:23.34 mol/l)
% dff: Fluid-Fluid Interaction Energy Parameter (eff/k), Kelvin
% (For Methane,dff=64.1952 K: For Carbon dioxide,dff=84.4560 K)
% gf1: Initial Guess for dfs (efs/k),Kelvin
% gf2: Final Guess for dfs (efs/k), Kelvin
% -----------------------------------------------------------
%             OTHER PARAMETERS IN CALCULATIONS
% -----------------------------------------------------------
% dfs: Fluid-Solid Interaction Energy Parameter (efs/k),Kelvin
% xb: rhob/rhomc
% xads: rhoads/rhomc
% rhoa: Adsorbed Gas Density, mol/l
% C: A Parameter Related to Maximum Adsorption Capacity, mmol/g
% ncal: Calculated Excess Adsorption, mmol/g
% ADD: Error Between Calculated and Experimental Adsorption, fraction


 function[] = OK()

 Comp = input('If Methane,press 1,if Carbon dioxide,press 2:');
 n = input('n:');
 T = input('T,K:');
 rhob = input('rhob,mol/l:');
 nex = input('nex,mmol/g:');

 rhomc = input('rhomc,mol/l:');
 dff = input('dff:');
 gf1 = input('gf1,K:');
```

```
gf2 = input('gf2,K:');
B=10^8;
b=0.01;

  for dfs=gf1:5:gf2
     syms x
     for i=1:n
          xb(i)=rhob(i)/rhomc;

          f=log(x*(1-xb(i))/(xb(i)*(1-x)))+(7*x-8*xb(i))*dff/T+dfs/T;

          xa(i)=newton(f,b,1e-5);

          c(i)=nex(i)/(2*(xa(i)-xb(i)));
          b=xa(i);
          rhoa(i)=xa(i)*rhomc;

     end
        C=mean(c);

        for i=1:n
            nabs(i)=rhoa(i)*nex(i)/(rhoa(i)-rhob(i));
            ncal(i)=2*C*(xa(i)-xb(i));
            ADD(i)=abs(nex(i)-ncal(i))/nex(i);
        end

        A=mean(ADD)*100;


      if A>B,break,end
         B=A;

  end


% --------------------------------------------------------------------
%                          Surface Area Calculations
% --------------------------------------------------------------------
  if Comp==1
     dmethane=3.758;
     Tbmethane=111.55;
     Caomethane= 0.102/(dmethane*dmethane)+0.0034;
     Texpm=0.0024;
     Area=exp(T*Texpm-log(1/C)-log(Caomethane)-Texpm*Tbmethane)*2;
```

```
 end

 if Comp==2

    Tbco2=216.55;
    Caoco2= 0.0142;
    Texpc=0.0039;
    Area=exp(T*Texpc-log(1/C)-log(Caoco2)-Texpc*Tbco2)*2  ;

 end

fprintf('----------------------------------------------------------\n');
fprintf('                    OUTPUT                          \n');
fprintf('----------------------------------------------------------\n');

fprintf('Error=%d\n',A);
fprintf('dfs,K=%d\n',dfs);
fprintf('C=%d\n',C);
fprintf('Area=%d\n',Area);

fprintf('xb:rhob/rhomc   xa:rhoa/rhomc    rhoa,mol/l    ncal,mmol/g\n');
fprintf('-------------   -------------    -----------   ------------\n');
for i=1:n
fprintf('%d    %d    %d    %d\n',xb(i),xa(i),rhoa(i),ncal(i));
end

fprintf('nabs,mmol/g\n');
fprintf('--------------\n');
for i=1:n
fprintf('%d\n',nabs(i));
end

end

% -------------------------------------------------------------------
%                              REFERENCES
% -------------------------------------------------------------------
% [1]Sudibandriyo,M.,Mohammad, S.A.,Robinson, R.L.J.,Gasem K.A.M.,2010.
% Ono–Kondo lattice model for high-pressure adsorption:
% Pure gases. Fluid Phase Equilibria 299 (2010) 238–251

% ***  By using the following website, gas densities for different gases
% can be calculated: http://webbook.nist.gov/chemistry/fluid/
% Where:For Methane, Angus's Equations of States and for
% Carbon dioxide Span&Wagner Equations of States are used.
```

✓ OK.m uses netwon.m file for Newton Method approximation.

newton.m

```
% Newton Method for Finding Roots, f(x)=0
% --------------------------------------------------
% Author: Sukru MEREY
% --------------------------------------------------
%                    INPUT
% --------------------------------------------------
% f:Function depends on x
% x1: Initial Guess for f(x)=0
% tol: Accuracy of Result
% newton(f,x1,tol)

   function [x]=newton(f,x1,tol)
  global x
      x=x1;
   fx=eval(f);
      for i=1:100
         if abs(fx)<tol, break,end
        x=x+.0051;
        ff=eval(f);
        fdx=(ff-fx)/.001;
        x1=x1-fx/fdx;
        x=x1;
        fx=eval(f);


      end

   end

% -------------------------------------------------------
%                        REFERENCE
% -------------------------------------------------------
% www.saylor.org/site/wp-content/uploads/2011/11/3-8NewtonsMethod1.pdf
```

B.3 Matlab Code for Ono-Kondo Three-layer Model (TOK.m)

- ✓ TOK.m file is a matlab code to calculate adsorbed density, absolute adsorption, and surface area by using adsorption experimental data for Ono-Kondo Threelayer Model.

```
% Ono-Kondo Lattice Model for Pure Gas Adsorption-Three-layer [1]
% ----------------------------------------------------------
% Author: Sukru MEREY
% ----------------------------------------------------------
%                    INPUTS
% ----------------------------------------------------------
% n: Number of Pressure Increment Stages
% T: Temperature, Kelvin
% rhob: Gas Density at Equilibrium Pressure,mol/l ***
% nex: Gibbs(Excess) Adsorption,mmol/g
% rhomc:Adsorbed Phase Density Corresponding to the Maximum Adsorption...
% Capacity, mol/l (For Methane:23.37 mol/l; for CO2:23.34 mol/l)
% dff: Fluid-Fluid Interaction Energy Parameter (eff/k), Kelvin
%(For Methane,dff=64.1952 K: For Carbon dioxide,dff=84.4560 K)
% gf1: Initial Guess for dfs (efs/k),Kelvin
% gf2: Final Guess for dfs (efs/k), Kelvin
% ------------------------------------------------------------
%            OTHER PARAMETERS IN CALCULATIONS
% ------------------------------------------------------------
% dfs: Fluid-Solid Interaction Energy Parameter (efs/k),Kelvin
% xb: rhob/rhomc
% xads: rhoads/rhomc
% rhoa: Adsorbed Gas Density, mol/l
% C: A Parameter Related to Maximum Adsorption Capacity, mmol/g
% ncal: Calculated Excess Adsorption, mmol/g
% ADD: Error Between Calculated and Experimental Adsorption, fraction

function []=TOK()
 Comp = input('If Methane,press 1,if Carbon dioxide,press 2:');
 T = input('T,K:');
 n = input('n:');
 nex = input('nex,mmol/g:');
 rhob = input('rhob,mol/l:');
 rhomc = input('rhomc,mol/l:');
 dff = input('dff,K:');
 gf1 = input('gf1,K:');
 gf2 = input('gf2,K:');

 B=10^8;
```

```
 %main function which call the Newton solver
%call the solver

for dfs=gf1:5:gf2
  Guess=[0.0001;0.0001;0.0001];

    for i=1:n
     xb(i)=rhob(i)/rhomc;
     x=NewtonRap(@Func,@Jac,Guess,1e-5);
     x1(i)=x(1);
     x2(i)=x(2);
     x3(i)=x(3);
     c(i)=nex(i)/(2*(x1(i)+x2(i)+x3(i)-3*xb(i)));

      Guess=[x1(i);x2(i);x3(i)];

   end

     C=mean(c);

         for i=1:n
             ncal(i)=2*C*(x1(i)+x2(i)+x3(i)-3*xb(i));
             ADD(i)=abs(nex(i)-ncal(i))/nex(i);
         end

         A=mean(ADD)*100;

      if A>B,break,end
       B=A;
end


function y = Func(x)

%the function which returns the values of F(x)
y(1)=log((x(1).*(xb(i)-1))/(xb(i)*(x(1)-1)))+dfs/T+(dff*(6*x(1)+x(2)...
     -8*xb(i)))/T;
y(2)=log((x(2).*(xb(i)-1))/(xb(i)*(x(2)-1)))+ (dff*(8*x(2)-8*xb(i)))/T...
    + (dff*(x(1) - 2*x(2) + x(3)))/T;
y(3)=log((x(3).*(xb(i)-1))/(xb(i)*(x(3)-1)))+(dff*(x(2)-x(3)))/T +...
     (dff*(8*x(3) - 8*xb(i)))/T;
y= y';
   end

function J = Jac(x)
```

```
 %The function that returns the Jacobian matrix
J(1,1)=(6*dff)/T+(xb(i)*((xb(i)-1)/(xb(i)*(x(1)-1))-(x(1)*(xb(i)-1))/...
    (xb(i)*(x(1)-1)^2))*(x(1)-1))/(x(1)*(xb(i)-1));
J(1,2) = dff/T;
J(1,3) = 0;
J(2,1)= dff/T;
J(2,2)=(6*dff)/T+(xb(i)*((xb(i)-1)/(xb(i)*(x(2)-1))-(x(2)*(xb(i)-1))...
   /(xb(i)*(x(2)-1)^2))*(x(2)- 1))/(x(2)*(xb(i)-1));
J(2,3)=dff/T;
J(3,1)=0;
J(3,2)=dff/T;
J(3,3)= (7*dff)/T+(xb(i)*((xb(i)-1)/(xb(i)*(x(3)-1))-(x(3)*(xb(i)-1))/...
      (xb(i)*(x(3)-1)^2))*(x(3)-1))/(x(3)*(xb(i)-1));

end


% ---------------------------------------------------------------------
%                       Surface Area Calculations
% ---------------------------------------------------------------------
  if Comp==1
     dmethane=3.758;
     Tbmethane=111.55;
     Caomethane= 0.102/(dmethane*dmethane)+0.0034;
     Texpm=0.0024;
     Area=exp(T*Texpm-log(1/C)-log(Caomethane)-Texpm*Tbmethane)*2;
  end

  if Comp==2

     Tbco2=216.55;
     Caoco2= 0.0142;
     Texpc=0.0039;
     Area=exp(T*Texpc-log(1/C)-log(Caoco2)-Texpc*Tbco2)*2  ;

  end

fprintf('-----------------------------------------------------------\n');
fprintf('                    OUTPUT                           \n');
fprintf('-----------------------------------------------------------\n');

fprintf('xb:rhob/rhomc x1:rhoa1/rhomc x2:rhoa2/rhomc x3:rhoa3/rhomc\n');
fprintf('------------- -------------- -------------- ---------------\n');
for i=1:n
fprintf('%d  %d  %d  %d\n',xb(i),x1(i),x2(i),x3(i));
```

```
end
 fprintf('ncal,mmol/g\n');
 fprintf('--------------\n');
 fprintf('%d\n',ncal);

 fprintf('Error=%d\n',A);
 fprintf('dfs,K=%d\n',dfs);
 fprintf('C=%d\n',C);
 fprintf('Area=%d\n',Area);

end

% -------------------------------------------------------------------
%                           REFERENCES
% -------------------------------------------------------------------
% [1]Sudibandriyo,M.,Mohammad, S.A.,Robinson, R.L.J.,Gasem K.A.M.,2010.
% Ono–Kondo lattice model for high-pressure adsorption:
% Pure gases. Fluid Phase Equilibria 299 (2010) 238–251

% ***  By using the following website, gas densities for different gases
% can be calculated: http://webbook.nist.gov/chemistry/fluid/
% Where:For Methane, Angus's Equations of States and for
% Carbon dioxide Span&Wagner Equations of States are used.
```

✓ TOK.m uses NewtonRap.m file for Newton-Raphson Method approximation.

```
%                   Newton-Raphson Method
% -----------------------------------------------------
% Author: Sukru MEREY
% -----------------------------------------------------
%                        INPUT
% -----------------------------------------------------
% Func:Functions to be solved
% Jacobian: Jacobian Matric for the solution
% Guess: Initial Guess to satify the equations
% tol: Accuracy of Result
% newton(f,x1,tol)
function [solution] = NewtonRap(MyFunc,Jacobian,Guess,tol)


x =Guess;

error = 2*tol;
while error > tol

F = feval(MyFunc,x);

J = feval(Jacobian,x);

dx = J\(-F);

x = x+dx;

F = feval(MyFunc,x);
error = max(abs(F));
end
solution = x;
end

% -------------------------------------------------------------------
%                           REFERENCES
% -------------------------------------------------------------------
% http://www.macalester.edu/aratra/edition2/chapter3/chapt3a.pdf
```

B.4 Matlab Code for Ono-Kondo Model for Binary Mixtures (MOK.m)

- ✓ MOK.m file is a matlab code to calculate theoretical adsorption of binary mixtures by using their pure adsorption data.

```
% Ono-Kondo Lattice Model for Binary Mixtures
% ----------------------------------------------------------
% Author: Sukru MEREY
% ----------------------------------------------------------
%                      INPUTS
% ----------------------------------------------------------
% T: Temperature, Kelvin
% Vvoid: void volume in sample cell, lt
% n: Number of Pressure Increment Stages
% W:weight of sample,g
% za: feed mole fraction of Gas A
% zb: fee mole fraction of Gas B
% nexa: excess adsorption of pure gas A, mmol/g
% rhomca:Adsorbed Phase Density Corresponding to the Max. Adsorption of
% A,mol/l
%dffa: Fluid-Fluid Interaction Energy Parameter  of A (eff/k), Kelvin
%dfsa: Fluid-Solid Interaction Energy Parameter of A (efs/k),Kelvin
%Ca:A Parameter Related to Maximum Adsorption Capacity of A, mmol/g
% ya: mole fraction of A in gas phase
% pca: critical pressure of A, psia
% Tca: critical temperature of A, Kelvin
% wa:accentric factor of A
% nexb: excess adsorption of pure gas B, mmol/g
% rhomcb:Adsorbed Phase Density Corresponding to the Max. Adsorption of
% B,mol/l
%dffb: Fluid-Fluid Interaction Energy Parameter  of B (eff/k), Kelvin
%dfsb: Fluid-Solid Interaction Energy Parameter of B (efs/k),Kelvin
%Cb:A Parameter Related to Maximum Adsorption Capacity of B, mmol/g
% yb: mole fraction of B in gas phase
% pcb: critical pressure of B, psia
% Tcb: critical temperature of B, Kelvin
% wb:accentric factor of B
% ------------------------------------------------------------
%             OTHER PARAMETERS IN CALCULATIONS
% ------------------------------------------------------------
% xb: rhob/rhomc
% rhob: density of bulk phase of pure gas (from NIST), mol/l
% xads: rhoads/rhomc
% rhoa: Adsorbed Gas Density, mol/l
% ncal: Calculated Excess Adsorption, mmol/g
```

```
% ADD: Error Between Calculated and Experimental Adsorption, fraction
 function [] = MOK()

 T = input('T,K:');
Vvoid = input('Vvoid, lt:');
 n = input('n:');
 P = input('P,psia:');
 W= input('W, g:');

 za = input('za, frac:');
  zb = input('zb, frac:');
 nexa = input('nexa, mmol/g:');
 rhomca = input('rhomca, mol/lt:');
 dffa = input('dffa, K:');
 dfsa = input('dfsa, K:');
 Ca = input('Ca, mmol/g:');
 ya=input('ya, frac:');
 pca=input('pca, psia:');
 Tca=input('Tca, K:');
 wa= input('wa:');

 nexb = input('nexb, mmol/g:');
 rhomcb = input('rhomcb, mol/l:');
 dffb = input('dffb, K:');
 dfsb = input('dfsb, K:');
 Cb = input('Cb, mmol/g:');
 yb=input('yb, frac:');
 pcb=input('pcb, psia:');
 Tcb=input('Tcb, K:');
 wb= input('wb:');



 dab=sqrt(dffa*dffb);
 for i=1:n
      x = sym('x');

      E=10^8;

      b=0.001;

      rhomcaa(i)=rhomca;
      rhomcbb(i)=rhomcb;
    while E>0.0000000001
```

```
   rhob(i)=pr([ya(i);yb(i)],P(i),T,[pca;pcb],[Tca;Tcb],[wa;wb],'V');

   xab(i)=ya(i)*rhob(i)/rhomcaa(i);
   xbb(i)=yb(i)*rhob(i)/rhomcbb(i);

   k=NewtonRap(@Func,@Jac,[0.001;0.001],1e-5);
   xa(i)=k(1);
   xb(i)=k(2);

   xabsa(i)=xa(i)/(xa(i)+xb(i));
   xabsb(i)=1.0-xabsa(i);
   rhomcaa(i)=1/(xabsa(i)/rhomca+xabsb(i)/rhomcb);
   rhomcbb(i)=rhomcaa(i);
   %corra(i)=xabsa(i)*xabsb(i)+xabsb(i)*xabsb(i);
   %corrb(i)=xabsb(i)*xabsa(i)+xabsa(i)*xabsa(i);

   nexacal(i)=2*Ca*(xa(i)-xab(i));
   nexbcal(i)=2*Cb*(xb(i)-xbb(i));
   nexmix(i)=nexacal(i)+nexbcal(i);

   f=za-(nexacal(i)+Vvoid*rhob(i)*453.5924*x*1000/W)/(nexmix(i)...
      +Vvoid*rhob(i)*453.5924*1000/W);

   yfa(i)=newton(f,b,1e-8);

   b=yfa(i);

   E=abs(yfa(i)-ya(i));

   ya(i)=yfa(i);
   yb(i)=1-yfa(i);


  end


   ADDa(i)=abs(nexacal(i)-nexa(i))/nexa(i);
  ADDb(i)=abs(nexbcal(i)-nexb(i))/nexb(i);
  ADD(i)=ADDa(i)+ADDb(i);


end
```

```
fprintf('-----------------------------------------------------------\n');
fprintf('                    OUTPUT                        \n');
fprintf('-----------------------------------------------------------\n');
fprintf('     xabsa        xabsb    \n');
fprintf('------------- --------------\n');
for i=1:n
fprintf('%d %d\n',xabsa(i),xabsb(i));
end

fprintf('  nexacal       nexbcal          nexmix   \n');
fprintf('------------- --------------    --------------\n');
for i=1:n
fprintf('%d  %d  %d\n',nexacal(i),nexbcal(i),nexmix(i));
end

fprintf('     ya           yb      \n');
fprintf('------------- --------------\n');
for i=1:n
fprintf('%d %d\n',ya(i),yb(i));
end

fprintf('ADDa=%d\n',mean(ADDa));
fprintf('ADDb=%d\n',mean(ADDb));
fprintf('ADD=%d\n',mean(ADD));

 function y = Func(x)
%the function which returns the values of F(x)
y(1)=log(x(1)*(1-xab(i)-xbb(i))/(xab(i)*(1-x(1)-x(2))))+(7*x(1)-...
    8*xab(i))*dffa/T+(7*x(2)-8*xbb(i))*dab/T+dfsa/T;
y(2)=log(x(2)*(1-xab(i)-xbb(i))/(xbb(i)*(1-x(1)-x(2))))+(7*x(2)-8*...
    xbb(i))*dffb/T+(7*x(2)-8*xab(i))*dab/T+dfsb/T;
y= y';

   end

function J = Jac(x)
 %The function that returns the Jacobian matrix
J(1,1)=(7*dffa)/T+(xab(i)*((xab(i)+xbb(i)-1)/(xab(i)*(x(1)+x(2)-1))...
    -(x(1).*(xab(i)+ xbb(i)-1))/(xab(i)*(x(1)+x(2)-1)^2))*(x(1)+x(2)-1))...
    /(x(1).*(xab(i)+xbb(i)-1));

J(1,2) = (7*dab)/T-1/(x(1)+x(2)-1);

J(2,1)= -1/(x(1)+x(2)-1);
```

```
J(2,2)=(7*dab)/T+(7*dffb)/T+(xbb(i)*((xab(i)+xbb(i)-1)/(xbb(i)*(x(1)+...
    x(2)-1))-(x(2)*(xab(i)+xbb(i)-1))/(xbb(i)*(x(1)+x(2)-1)^2))*(x(1)+...
    x(2)-1))/(x(2).*(xab(i)+xbb(i)-1));
 end

 end
% ------------------------------------------------------------
%                              REFERENCE
% ------------------------------------------------------------
%  Sudibandriyo M., Mohammad S.A., Robinson, R.L.J., Gasem K.A.M, 2011.
% OnoKondo Model for  High-Pressure Mixed-Gas Adsorption on Activated
%Carbons  and Coals.  dx.doi.org/10.1021/ef2005749|Energy Fuels2011, 25,
%3355–3367
```

✓ MOK.m uses pr.m for equations of states and also NetwonRap.m (previously written above) for Newton Rapson Method.

pr.m

```
% Peng-Robinson Equation of State
% --------------------------------------------
% Author: Sukru MEREY
% ......................................................
%                        INPUTS
% --------------------------------------------
% z   = mole fractions of components
% p   = pressure, psia
% T   = temperature, K
% pc  = critical pressure of all components,psia
% Tc  = critical temperature of all components, [K]
% w   = acentric factor of all components
% ph  = phase (L or V)
% ......................................................
%                        OUTPUTS
% --------------------------------------------
% rho  =density, mol/l

function [rho] = pr(z,p,T,pc,Tc,w,ph)

R  = 8.314462175 ; % m3 Pa/(mol K) = J/mol-K
p=p*6894.757;
pc=6894.757*pc;

m    =  0.37464 + 1.54226*w - 0.26992*w.^2;
alfa =  (1 + m.*(1 - (T./Tc).^0.5)).^2;
ai   =  0.45724*(R^2)*(Tc.^2)./pc.*alfa;
bi   =  0.07780*R*Tc./pc;
Q    =  ((ai*ai').^0.5);
a    =  z'*Q*z;
b    =  z'*bi;


% Coefficients of the EoS model equation
c(1) =  1;
c(2) =  b - R*T/p;
c(3) =  -3*b^2 - 2*R*T/p*b + a/p;
c(4) =  b^3 + R*T/p*b^2 - a*b/p;
```

```
% Compressibility factor
% Roots
r    = roots(c);
VR=[];
for i=1:3
if isreal(r(i))
    VR = [VR r(i)];
end
end
 if ph=='L'
     V=min(VR);
 else
     V=max(VR);
 end

 rho=1/(V*1000);% converting from mol/m3 to mol/lt

end


% Ahmed, T., 2007.  Equations of state and PVT analysis Book
```

APPENDIX C

PHASE BEHAVIORS OF METHANE AND CARBON DIOXIDE AT 25, 50 AND 75 ^oC:

C.1 Phase Behaviors of Methane at 25 , 50 and 75 ^oC:

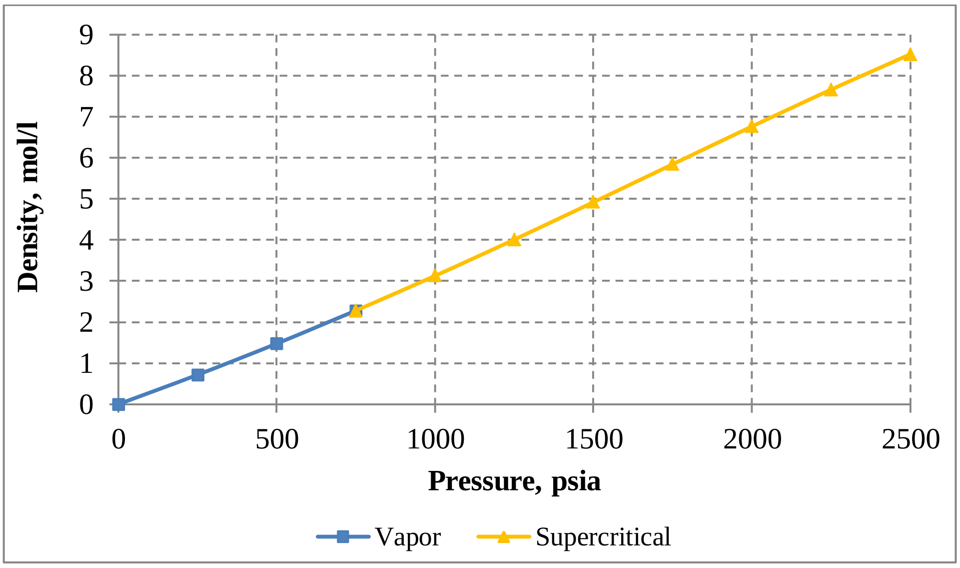

Figure C.1: Density versus pressure graph of methane at 25 ^oC (NIST)

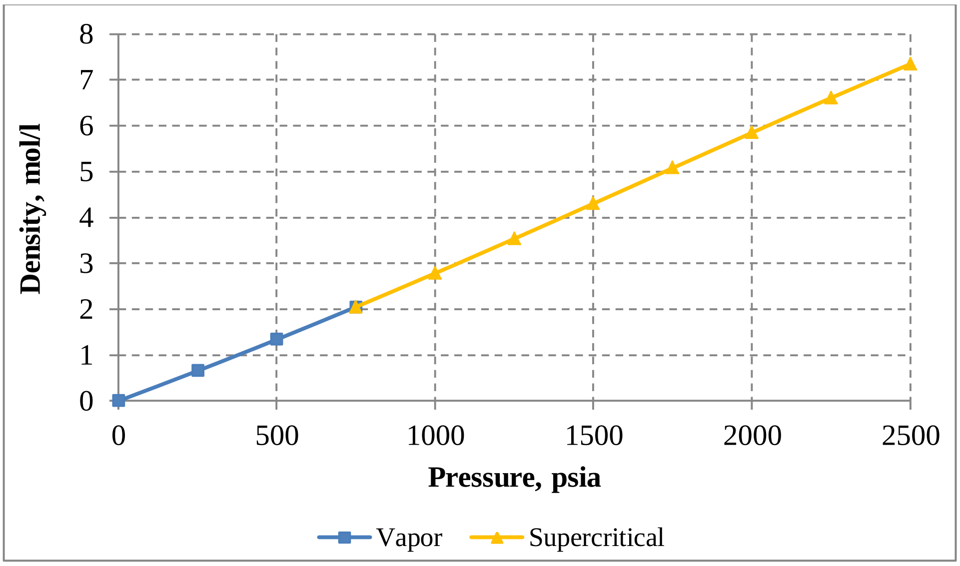

Figure C.2: Density versus pressure graph of methane at 50 ^oC (NIST)

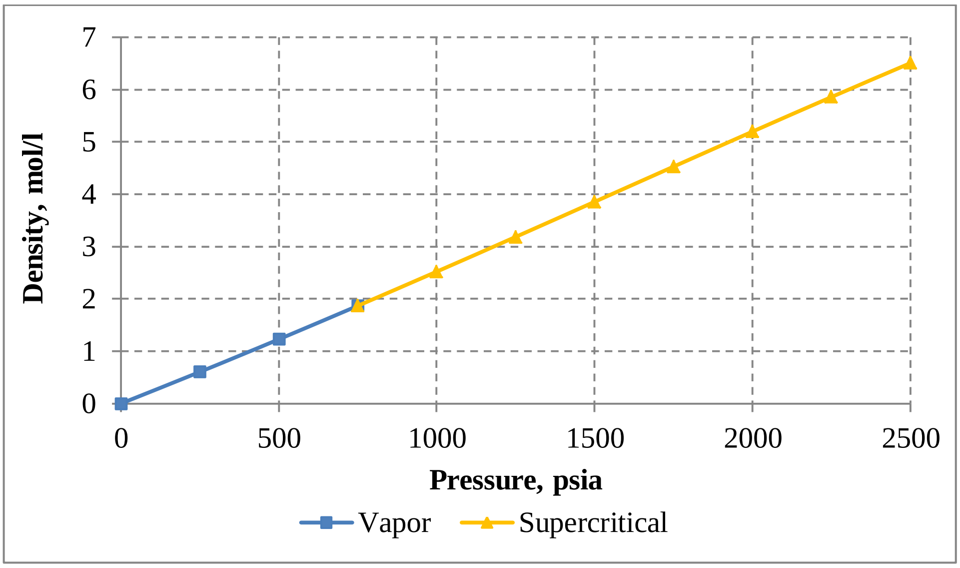

Figure C.3: Density versus pressure graph of methane at 75 ^{o}C (NIST)

C.2 Phase Behaviors of Carbondioxide at 25 , 50 and 75 ^{o}C:

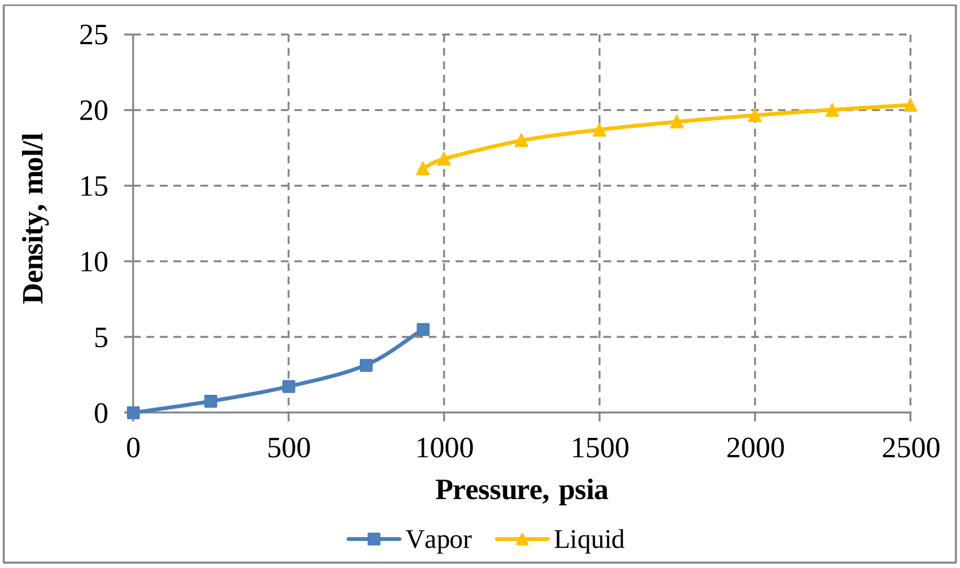

Figure C.4: Density versus pressure graph of carbon dioxide at 25 ^{o}C (NIST)

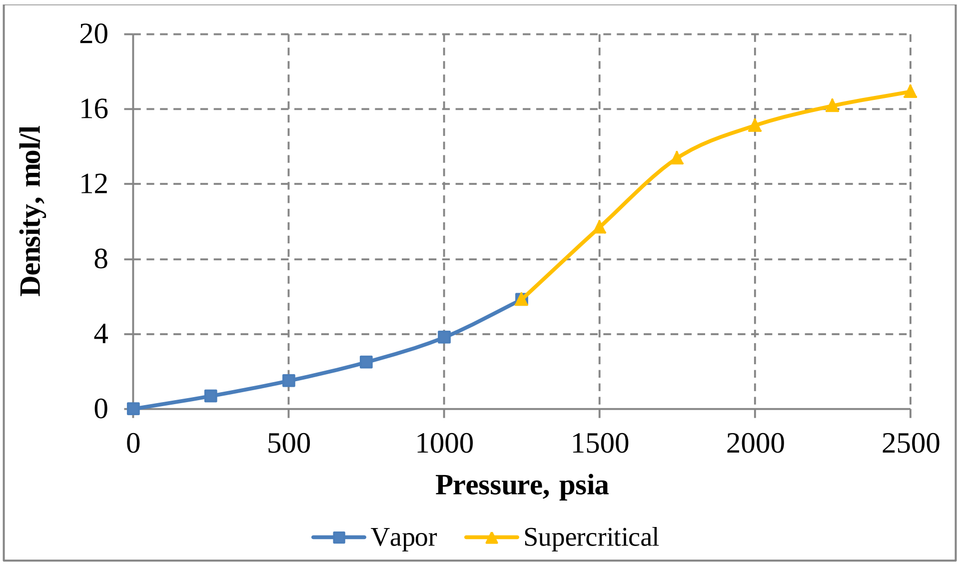

Figure C.5: Density versus pressure graph of carbon dioxide at 50 ^{o}C (NIST)

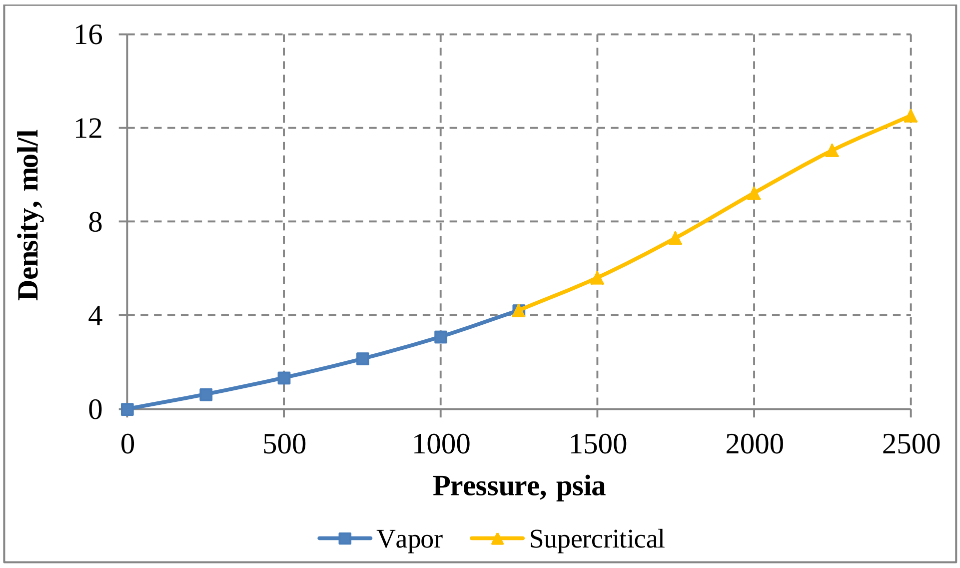

Figure C.6: Density versus pressure graph of carbon dioxide at 75 ^{o}C (NIST)